Ulm University

Institute of Orthopaedic Research and Biomechanics

Director: Prof. Dr. med. vet. Anita Ignatius

Effect of MSC-Administration on Bone Formation and Repair

Dissertation
for the Doctoral Degree in Human Biology
(Dr. biol. hum.)
from the Medical Faculty, Ulm University

Anna Elise Rapp
Born in Ulm

Ulm 2014

Acting Dean: Prof. Dr. rer. nat. Thomas Wirth

1st reviewer: Prof. Dr. med. vet. Anita Ignatius

2nd reviewer: Prof. Dr. med. Rolf Brenner

Day of defence: November 28, 2014

Science is not only a disciple of reason but, also, one of romance and passion.

Stephen Hawking

Table of Contents

1 Introduction 1
I Bone Modelling and Remodelling 1
1.1 Physiological Bone Remodelling 2
1.2 Load Induced Bone Modelling and Mechanotransduction 4
II Fracture Healing and Regenerative Medicine 7
1.3 Regular and Delayed Fracture Healing 8
1.3.1 Regular Fracture Healing 8
1.3.2 Impaired Fracture Healing 10
1.3.3 Osteoprogenitor Cells in Fracture Repair 13
1.4 Mesenchymal Stem Cells in Regenerative Medicine 16
1.4.1 Local Delivery of Stem Cells for Regenerative Medicine 18
1.4.2 Systemic Delivery of Stem Cells for Regenerative Medicine 18
1.5 Stem Cells in Experimental Approaches for Bone Regeneration 20
1.6 Aim of the Study 23

2 Material and Methods 24
2.1 Material 24
2.1.1 Reagents 24
2.1.2 Consumable Supplies 26
2.1.3 Solutions 26
2.1.4 Primer 27
2.1.5 Antibodies 27
2.1.6 Media 28
2.1.7 Kits 28
2.1.8 Equipment 29
2.2 Methods 30
2.2.1 Isolation/Preparation of Mesenchymal Stem Cells 30
2.2.2 In Vitro Analysis of Human Mesenchymal Stem Cells 32
2.2.3 In Vivo Experiments 34
2.2.4 Assessment of the In Vivo Studies 40

3 Results 45
3.1 Contribution of Systemically Administered MSC to Bone Formation in Load-Induced Bone Modelling and Fracture Healing 45
3.1.1 Contribution of Systemically Administered MSC to Load-induced Bone Formation 46
3.1.2 Contribution of Systemically Applied Mesenchymal Stem Cells to Fracture Healing 49
3.2 Local Application of Autogenic and Allogeneic Mesenchymal Stem Cells for Large Bone Defect Repair 56

4 Discussion 66
4.1 Contribution of Systemically Administered MSC to Bone Formation in Load-Induced Bone Modelling and Fracture Healing 66
4.1.1 Contribution of Systemically Administered MSC to Load-induced Bone Formation 66
4.1.2 Contribution of Systemically Applied Mesenchymal Stem Cells to Fracture Healing 67
4.2 Local Application of Autogenic and Allogeneic Mesenchymal Stem Cells for Large Bone Defect Regeneration 70

5 Summary 74

6 References 76

List of Abbreviations

AEC	3-Amino-9-ethylcarbazole
AP	Alkaline phosphatase
BMD	Bone mineral density
BMP	Bone morphogenetic protein(s)
BRC	Bone remodelling compartment
BSA	Bovine serum albumin
BSP	Bone sialo protein
BV	Bone volume, absolute
BV/TV	Ratio bone volume/tissue volume
CD	Cluster of differentiation
CFU-F	Colony forming unit fibroblast
CO_2	Carbon dioxide
Ct.Wi.	Cortical width
DMEM	Dulbecco's Modified Eagle Medium
DMSO	Dimethyl sulfoxide
DNA	Desoxyribonucleic acid
E	Modulus of elasticity (Young's modulus)
EDTA	Ethylenediamine tetraacetic acid
EGFP	Enhanced green fluorescent protein
EMA	European Medicines Agency
FACS	Fluorescence-activated cell sorting
FBS	Foetal bovine serum
FDA	Food and Drug Administration
GAPDH	Glyceraldehyde-3-phosphatase dehydrogenase
GFP/EGFP	Green fluorescent protein/enhanced green fluorescent protein
HCl	Hydrochloric acid
HRP	Horseradish peroxidase
HSC	Haematopoietic stem cell(s)
I or MMI	Moment of inertia
i.p.	Intraperitoneal(ly)
i.v.	Intravenous(ly)
IL	Interleukin
IU	International units
MCP-1/CCL2	Monocyte chemotactic protein-1, CC-motif chemokine ligand 2
MCSF/CSF-1	Macrophage colony stimulation factor, colony stimulating factor 1
MIP-1α/CCL3	Macrophage inflammatory protein-1α, CC-motif chemokine ligand 3
MMA	Methyl methacrylate
mRNA	Messenger ribonucleic acid
MSC	Mesenchymal stem/stromal cell(s)

Na_2HPO_4	Disodium hydrogen phosphate
NaCl	Sodium chloride
NaH_2PO_4	Sodium dihydrogen phosphate
O_2	Oxygen
OB	Osteoblast(s)
OC	Osteoclast(s)
OCA	Osteocalcin
PBS	Phosphate buffered saline
PDGF	Platelet-derived growth factor
PECAM (CD31)	Platelet endothelial cell adhesion molecule
PMN	Polymorphonuclear neutrophil
rh	Recombinant human
RNA	Ribonucleic acid
ROI	Region of interest
Runx2	Runt-related transcription factor 2
siRNA	Small interfering RNA
TAE	Tris-acetate-EDTA
TGF	Transforming growth factor(s)
TNF	Tumour necrosis factor
TNFAIP6/TSG-6	Tumour necrosis factor α induced protein/gene-6
TRAP	Tartrat-resistant acid phosphatase
Tris	Tris(hydroxymethyl)aminomethan
TV	Tissue volume, absolute
VEGF	Vascular endothelial growth factor
VOI	Volume of interest
µCT	Micro-computed tomography

List of Figures

Fig. *1: Regulation of skeletal homeostasis and bone mass.* *2*
Fig. 2: Basic multicellular unit of bone remodelling. *3*
Fig. 3: Model of bone remodelling. *3*
Fig. 4: Loading of the ulna leads to a distinct strain distribution within the bone. *5*
Fig. 5: Mechanotransduction in bone. *6*
Fig. 6: Active osteoblasts and osteoid apposition appear within 4 days on the medial periosteal surface of loaded ulnae [76]. *7*
Fig. 7: Stages of secondary fracture healing. *9*
Fig. 8: Classification of non-unions.. ..... *11*
Fig. 9: Cells with osteogenic potential are recruited out of the circulation during fracture healing… *15*
Fig. 10: The mesengenic process according to Caplan et al. [19]. *17*
Fig. 11: Post-surgical X-ray of an ostetomised femur with mounted external fixator (A) and a mouse one week after surgery wearing a fixator (B). *38*
Fig. 12: Critical-size defect in the femur of a NOD/scid-Il2rγ^{0} mouse before (A) and after (B) filling of the defect with collagen gel. *39*
Fig. 13: Scheme of three-point bending test (A) and femur mounted to the three-point bending device (B). *41*
Fig. 14: Representative PCR results of lung lysates analysed for the EGFP-transgene of MSC- and vehicle-treated mice. *45*
Fig. 15: Immunohistochmical staining for SDF-1 in the stroma (A, B) and cortex (C, D) of loaded ulnae of mice treated with vehicle (A, C) or MSC (B, D), day 16. ..... *46*
Fig. 16: Immunohistochemical staining of EGFP in loaded ulnae of mice treated with vehicle (A) and EGFP-transgenic MSC (B) on day 16. ..... *47*
Fig. 17: µCT analysis of bone formation in ulnae after mechanical loading. *48*
Fig. 18: Analysis of bone formation rate in ulnae after mechanical loading by dynamic histomorphometry. *49*
Fig. 19: Staining for SDF-1 (CXCL-12) in animals treated with vehicle (A, C) and EGFP-transgenic MSC (B, D) three days after surgery. *50*
Fig. 20: Immunhistochemical staining of EGFP in MSC-treated mice after 10 days. *51*
Fig. 21: Immunohistochemical staining of EGFP in longitudinal sections of fracture calli of vehicle (A, C, E and G) and EGFP-transgenic MSC-treated (B, D, F and H) mice 21 days after fracture… *53*
Fig. 22: Assessment of the healing outcome after 21 days by µCT-analysis of the former fracture gap and biomechanical testing. *54*
Fig. 23: Histomorphometric analysis fracture calli 10 days (A, C, E) and 21 days (B, D, F) after surgery. *55*
Fig. 24: Representative staining of the viability of human mesenchymal stem cells seeded in a collagen matrix using Hoechst 33342 dye and propidium iodine 1 h (A) and 24 h (B) after seeding. *57*
Fig. 25: Qualitative analysis of osteogenic MSC differentiation. *58*

Fig. 26: Safranin-O stained sections of the defect region in animals with empty defect (A), and defects treated filled with collagen gel (B), allogeneic MSC (C) and autogenic MSC (D).....59
Fig. 27: Histomorphometric analyses of the defect region in animals with empty defect or treated with autogenic and allogeneic MSC, respectively, after 35 days. 60
Fig. 28: µCT analyses of the defect region (A) and the bone per tissue volume ratio (B) in animals with empty defects and defects filled with cell-free collagen gel, collagen gel seeded with autogenic cells or collagen gel with allogeneic cells on day 35 after implantation. 61
Fig. 29: Immunohistochemical staining for human β2-microglobulin in mice treated with allogeneic (A, C, E) and autogenic (B, D, F) human MSC on day 10 (A, B) and 35 (C-F) after implantation. ..62
Fig. 30: Staining of human CD8 3 and 10 days after implantation of allogeneic (A, C) and autogenic (B, D) MSC.....63
Fig. 31: Immunohistochemical staining for CD31 10 (A, B) and 35 (C - F) days after implantation of allogeneic (A, C, E) or autogenic (B, D, F) MSC.....64
Fig. 32: Immunohistochemical staining for Runx2 in mice treated with allogeneic (A) or autogenic (B) MSC on day 10 after implantation.....65
Fig. 33: Immunohistochemic staining for osteocalcin in mice treated with allogeneic (A, C) and autogenic (B, D) MSC. 65

List of Tables

Tab. 1: Reagents *24*
Tab. 2: Consumable supplies *26*
Tab. 3: Solutions *26*
Tab. 4: Antibodies *27*
Tab. 5: Media *28*
Tab. 6: Kits *28*
Tab. 7: Equipment *29*

1 Introduction

Over the last decade, huge interest in cell-based approaches in regenerative medicine evolved. A cell in focus for bone tissue engineering in the wider sense of meaning is the mesenchymal stem cell (MSC), as these cells are the natural progenitors of bone cells and they have intriguing features making them a promising tool for bone (re-)generation.

In the field of fracture healing, there is still the problem that despite enormous progress in therapies over the last decades, 5 to 10% of all fracture healing events show poor healing due to biological or mechanical reasons [34].

In the present study, the potential for systemically administered cells to promote bone formation in inflammatory and non-inflammatory environments was investigated on the one hand; on the other hand, the efficacy of locally implanted MSC form allogeneic and autogenic sources to consolidate large bone defects was addressed.

I Bone Modelling and Remodelling

To maintain the health and integrity of bone, a constant cycle of resorption and formation, the so-called bone remodelling occurs. About 5 - 10% of the skeletal mass are remodelled per year in healthy adult humans. The steady state between resorption and formation is intricately regulated and influenced by various internal and extrinsic effectors (Fig. 1) [52].

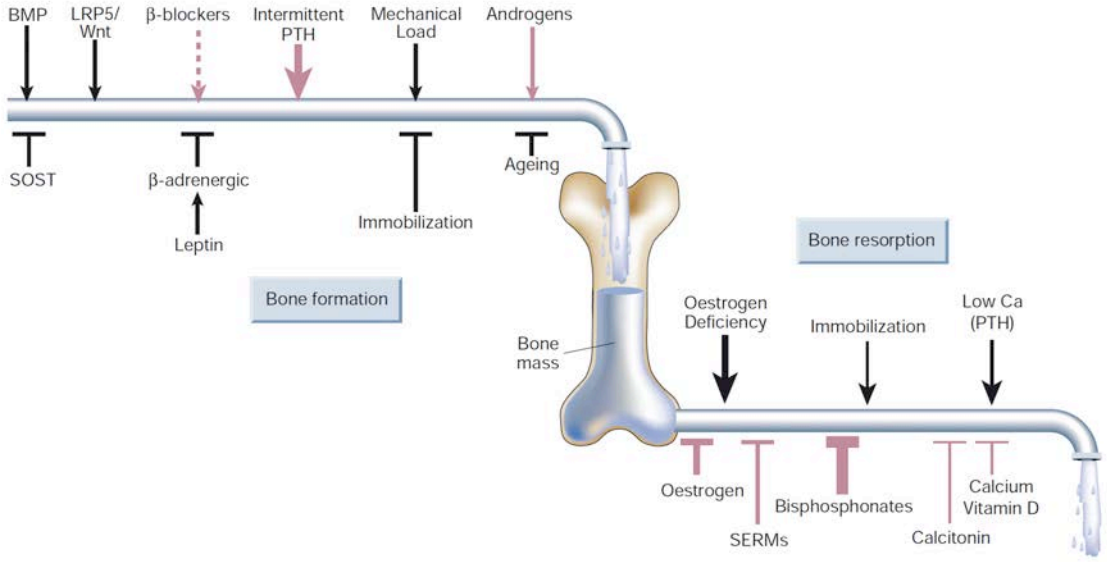

Fig. 1: Regulation of skeletal homeostasis and bone mass. Bone homeostasis is influenced by numerous intrinsic and extrinsic factors. Adapted by permission from Macmillan Publishers Ltd from [52, page 350].

1.1 Physiological Bone Remodelling

The physiological bone remodelling requires tight spatio-temporal collaboration of osteoclasts, osteoblasts, which form the so-called basic multicellular unit (BMU, Fig. 2) and their respective precursor cells [110]. It is anticipated, that remodelling occurs within the so-called bone remodelling compartment (BRC), a highly vascularized compartment that is sealed from its surrounding by bone lining cells forming a canopy [54]. How the precursor cells invade into the BRC is not fully elucidated; both crossing the bone lining cell monolayer and recruitment out of the microvasculature of the BRC is plausible [37].

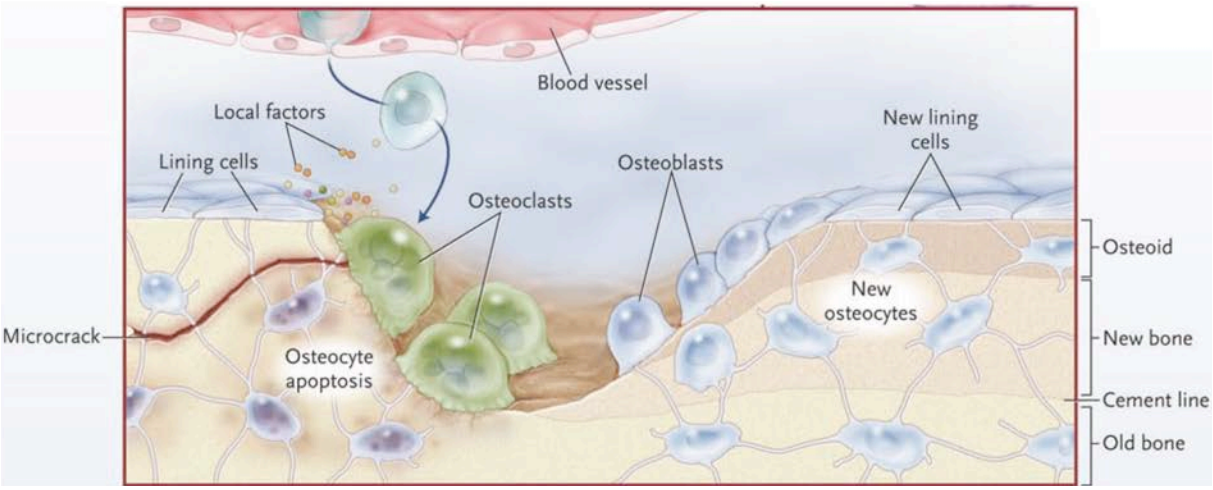

Fig. 2: Basic multicellular unit of bone remodelling. To maintain bone homeostasis, physiological bone remodelling requires highly regulated coupling of bone resorbing osteoclasts and bone forming osteoblasts. Reproduced with permission from [16, page 907], Copyright Massachusetts Medical Society.

The process of bone remodelling can be distinguished into sequential phases: activation, resorption, reversal, formation and termination (Fig. 3) [96].

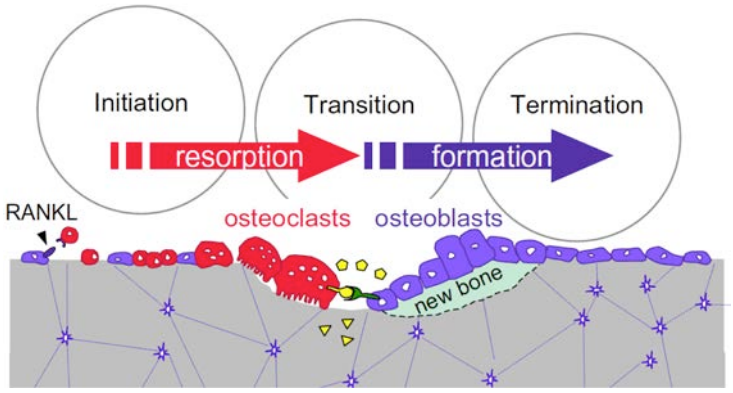

Fig. 3: Model of bone remodelling. The process of bone remodelling can be divided into sequential phases: Initiation, transition and termination. During the initiation phase, bone is resorbed by osteoclasts. During the transition phase, osteoclasts undergo apoptosis and osteoblasts are recruited. These osteoblasts form bone during the formation phase. Reprinted from [78, page 202] with permission from Elsevier.

Bone remodelling has to be initiated by an initiation signal. There is no unique signal but a variety of them, like the bones age, mechanical signals or micro-cracks within the bone. Micro-cracks for example disrupt the dense lacuno-canalicular network, leading to osteocyte apoptosis. Soluble factors released by

the decaying osteocytes or by macrophages removing the dead cells induce osteoclastogenesis from monocytic precursors. Essential for the fusion and function of osteoclasts are the osteoblastic factors receptor activator for nuclear factor κB ligand (RANKL) and macrophage colony stimulating factor (M-CSF). After fusion, the osteoclasts adhere to the bones surface [14], where they polarize and form an isolated, extracellular microenvironment by formation of the so-called sealing zone [118]. To resorb the mineralized bone, the lumen between the osteoclast and the bone is acidified by secretion of hydrochloric acid. Various proteinases are involved in the degradation of the organic matrix, but the predominant enzyme is the thiol-proteinase cathepsin K [14]. In the formation phase, the resorption lacunae are filled with new bone deposited by osteoblasts. During this process, some osteoblasts are embedded into the new bone matrix, where they terminally differentiate into osteocytes, thus re-establishing the lacuno-canalicular network.

Bone formation and resorption can also occur uncoupled. *In vivo*, uncoupling leads to osteopenic disorders like osteoporosis when resorption outbalances formation or to osteopetrosis if reversed.

1.2 Load-Induced Bone Modelling and Mechanotransduction

One of the factors that influences the intricate steady state of bone homeostasis is mechanical loading [32]. In 1892, Julius Wolff postulated that bone adapts to its mechanical demands [127]. Observational studies show a considerable bone loss after prolonged bed-rest, immobilization or space flight [115]. On the other hand, exercise induced bone gain is observed e.g. in the playing arm of tennis players [51]. Based on observations in humans, there are various animal models to study the adaption of bone to altered load situations. To model bone loss, cast-immobilization, hind limb unloading e.g. by tail suspension or sciatic neurectomy are used [50, 123-125]. To model bone formation, in rodents usually load is applied to one ulna or tibia. Externally applied mechanical strain was shown to significantly increase bone apposition in the ulnae of rats [99] and mice [71].

By externally applied axial compression of the ulna and thus stretching of the normal curvature of the bone, strain occurs inside the bone matrix and cells. Depending on the resulting strain, bone apposition occurs (Fig. 4).

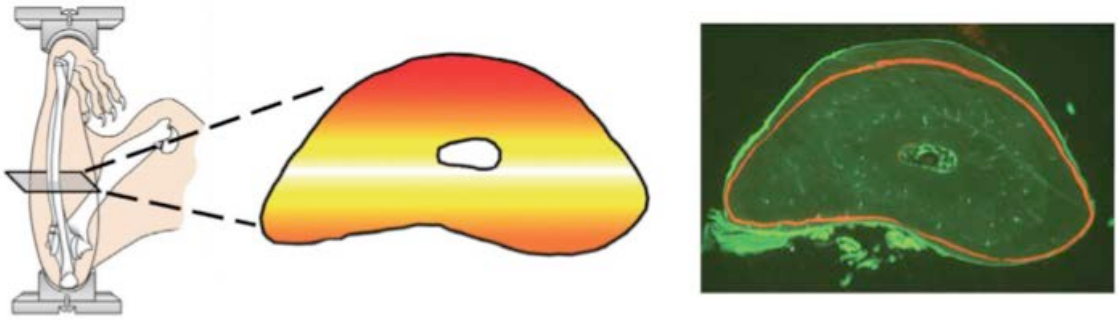

Fig. 4: Loading of the ulna leads to a distinct strain distribution within the bone. The highest strain is shown in red, the lowest in white. Bone apposition corresponds to the strain distribution. The red line indicates the bone surface at the beginning of the loading experiment [100, page 324].

Osteoblasts and Osteocytes have been identified as the bone's mechanosensors [15, 105]. Within the bone, strain is translated into fluid flow in the lacuno-canalicular system (Fig. 5). The flow is perceived by the osteocyte processes in the pericellular matrix and transduced into intracellular biochemical processes [22, 83].

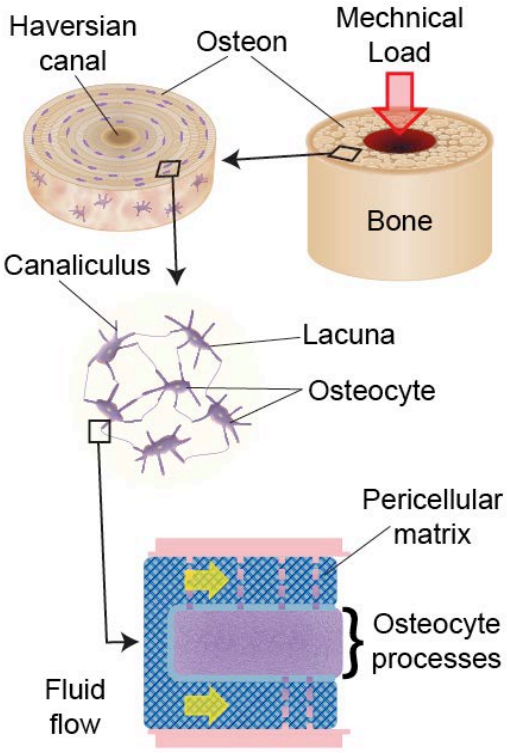

Fig. 5: Mechanotransduction in bone. Mechanical loading of bone results in fluid flow in the lacuno-canalicular system formed by osteocytes. The osteocytes perceive the fluid flow via their processes. Inside the osteocytes, the mechanical signal is transduced into biochemical processes. Adapted from [22, page 109].

By shear stress produced by the fluid flow, for instance, mechanosensitive ion channels and receptors and thus subsequent signalling pathways are activated [119]. Among these pathways are mitogen activated protein kinase (MAPK) cascades, which lead to a down-regulation of e.g. RANKL expression *in vitro* [103], inactivation of glycogen synthase kinase 3-β and thus accumulation of β-catenin and activation of downstream gene cascades.

An anabolic response on the cellular level in form of increased osteoblast numbers relative to a non-loaded control [76, 106] and osteoid formation [76] is evident within 4 to 5 days after a single loading bout in rats (Fig. 6). It is unclear, whether this increase in osteoblast number is solely due to proliferation of local cells or if circulating cells are also recruited as it is anticipated in physiological bone remodelling [90].

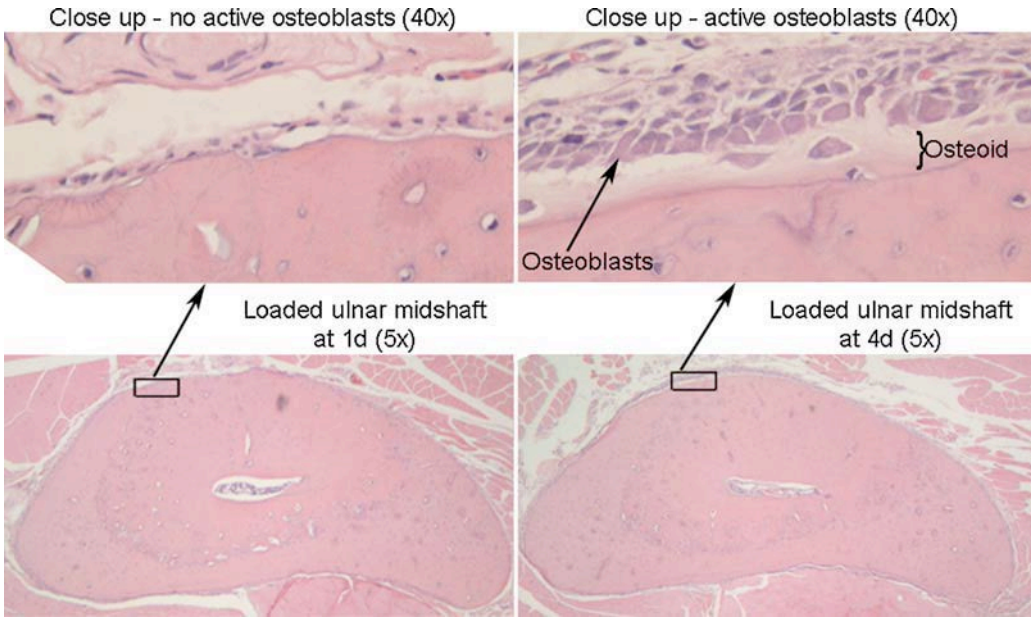

Fig. 6: Active osteoblasts and osteoid apposition appear within 4 days on the medial periosteal surface of loaded ulnae. Reproduced with permission from [76, page 103], Copyright © 2011 American Society for Bone and Mineral Research.

Differential gene analysis in loaded and non-loaded ulnae in rats showed a considerable up-regulation of genes 4 hours after initial loading [76]. Among the early up-regulated genes were the C-C motif chemokines CCL2 (monocyte chemotactic protein-1, MCP-1) and CCL7 (MCP-3). Both cytokines were shown to have a chemo-attractive effect on MSC in migration assays *in vitro* [40] and *in vivo* in rodents [107, 113]. During the time course of loading, platelet-derived growth factor (PDGF) isoforms A and C were up-regulated as well. Expression of genes associated with matrix-formation peaked between 12 to 16 days after first loading. Considering the up-regulation of chemoattractive molecules after mechanical loading, a possible role for systemically administered mesenchymal stem cells (MSC) in load induced bone formation is conceivable.

II Fracture Healing and Regenerative Medicine

Bone formation is not only necessary in bone modelling or remodelling but also to restore the bones integrity after injury.

1.3 Regular and Delayed Fracture Healing

Fractures are among the most frequent injuries of the musculoskeletal system. Fracture healing is a highly dynamic and complex process, that is influenced by various factors and that requires a tight spatio-temporal coordination of various cellular processes.
Giannoudis and colleagues brought up the “diamond concept” of fracture healing, which describes the pillars of regular fracture healing being the mechanical environment, the disposability of osteogenic cells, osteoinduction by growth factors and osteoconduction by an appropriate scaffold [45].

1.3.1 Regular Fracture Healing

In regular healing of fractures, two general principles can be distinguished: primary and secondary healing. Primary fracture healing, also called cortical healing, is a direct attempt of the cortex to re-establish its integrity [35]. This form of fracture healing occurs, when the bone ends are aligned in a correct anatomical way without formation of a gap and fixed rigidly with interfragmentary strain below 2 % [77]. In primary fracture healing, bone-resorbing osteoclasts form cutting cones at the end of the osteon nearest to the fracture site and ream cavities beyond the fracture, which are filled up with new bone by osteoblasts. This process results in union of the bone and formation of new Haversian canals at the same time [77].
As most fractures are mechanically more instable with larger interfragmentary strains, this form of fracture healing is rarely seen in clinics. The more common type of healing is secondary fracture healing.

Processes in secondary fracture healing - or indirect healing - are more complex. Secondary fracture healing can be divided into three consecutive and overlapping stages: The inflammatory phase, the repair stage - uniting the stages of soft and hard callus formation - and the remodelling stage [23, 44, 108] (Fig. 7).

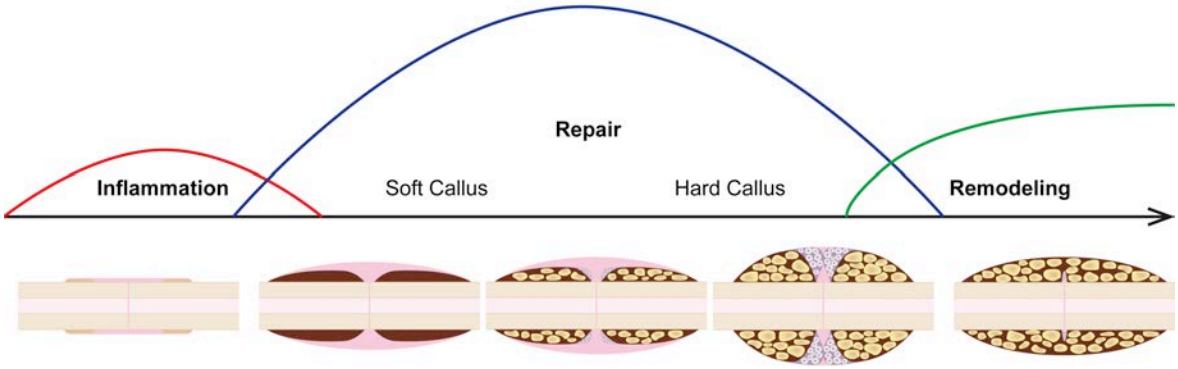

Fig. 7: Stages of secondary fracture healing. The process of secondary fracture healing can be divided in three consecutive and overlapping stages: The initial inflammatory stage, the repair stage that can be divided into the stage of soft callus formation and hard callus formation and the remodelling stage. Adapted from [23, page 137].

The initial inflammatory cascade leading to fracture healing is induced by disruption of the bone itself, the surrounding soft tissue and vessels at the fracture site. With blood exuding from damaged vessels, circulating inflammatory cells invade the fracture gap. Almost immediately, the coagulation cascade is activated, leading to formation of a fracture hematoma, being characterized by high lactate, low pH, and hypoxia [63]. The inflammatory cells within the hematoma together with cytokines lead to recruitment of additional immune cells. Degranulating platelets for instance release transforming growth factor (TGF)-β and PDGF, which act as chemotactic agents on macrophages and other inflammatory cells [74]. Additionally, these factors positively influence the migration of MCS [38] and osteoblasts to the injured region. During the first acute inflammatory phase, polymorphonuclear neutrophils (PMNs), which secrete chemo-attractive cytokines and interleukin 6 (IL-6) [23], infiltrate the damaged region. Thereafter, other inflammatory cells like macrophages and lymphocytes invade the hematoma.

Neovascularization is mandatory for the formation of new bone. Due to the activation of hypoxia inducible protein-1α (HIF-1α) by low oxygen tension, angiogenic factors like vascular endothelial growth factor (VEGF) are up-regulated [65], thus leading to formation of new vessels that are mandatory for the formation of new bone [111]. With the new vessels, perivascular cells invade the fracture

site. These pericytes are discussed to be MSC that are necessary for the progress of the healing [18, 27, 112].

Early after fracture, intramembranous ossification occurs in some distance to the fracture gap. This process is initiated by periosteal osteoblasts and precursor cells. Growth of the soft callus is further driven by proliferation and maturation of chondrocytes derived from MSC. Cartilage forms at both sides of the fracture gap and grows towards the fracture line. During callus maturation, the chondrocytes within the callus become hypertrophic and mineralize, thus showing typical characteristics of endochondral ossification. When bridging and thereby mechanical stabilization of the fracture gap by the callus is achieved, blood vessels start to grow into the mineralized cartilage, enabling recruitment of monocytes and MSC from peripheral blood. While monocytes differentiate into cartilage-resorbing cells, MSC differentiate into osteoblasts that fill the resorption cavities with bone [35, 79, 108].

Once the fracture is stabilized by and filled with new bone, resorption of the periosteal callus by osteoclasts begins. In this remodelling process, woven bone is replaced by lamellar bone, thus re-establishing the original geometry and stability of the bone [35, 79, 108].

1.3.2 Impaired Fracture Healing

Poor fracture healing is anticipated to occur in 5 to 10% of all cases [34]. In impaired healing, a delayed healing and the formation of a non-union can be distinguished. A delayed healing is evident, when a fracture lacks bony consolidation within 5 to 6 months after trauma, but a progression of the healing process is evident [91]. The American Food and Drug Administration (FDA) defined a fracture non-union as a fracture existing for more than 9 month without the evidence of a healing progression for more than 3 consecutive months [13]. In Germany, fractures lacking bony consolidation for more than 6 month after trauma are classified as non-union [117].

There are many known risk factors that promote delayed healing or the formation of a non-union. In experimental studies and clinical observations for instance, smoking has been identified as a risk factor for impaired fracture healing [1, 97].

Further systemic factors are e.g. comorbidities like diabetes or peripheral artery occlusion disease, age, the nutritional state, medication with steroids or cytostatic drugs [55, 117].

There is evidence, that a balanced inflammatory stage is essential for a satisfactory healing outcome [77, 85]. In an experimental model in rats using blunt chest trauma to simulate poly-traumatic patients, significantly elevated levels of the pro-inflammatory cytokine IL-6 during the early inflammatory phase and impaired fracture healing outcome could be detected [98]. Other reasons for impairment of the healing of bone defects can be found in high biomechanical instability, extensive periosteal injuries, infection, or the sheer size of the defect itself [55, 117].

Fracture non-union

According to their appearance in radiographies, non-unions can be classified as hypertrophic, oligo- or normotrophic and atrophic [68] (Fig. 8).

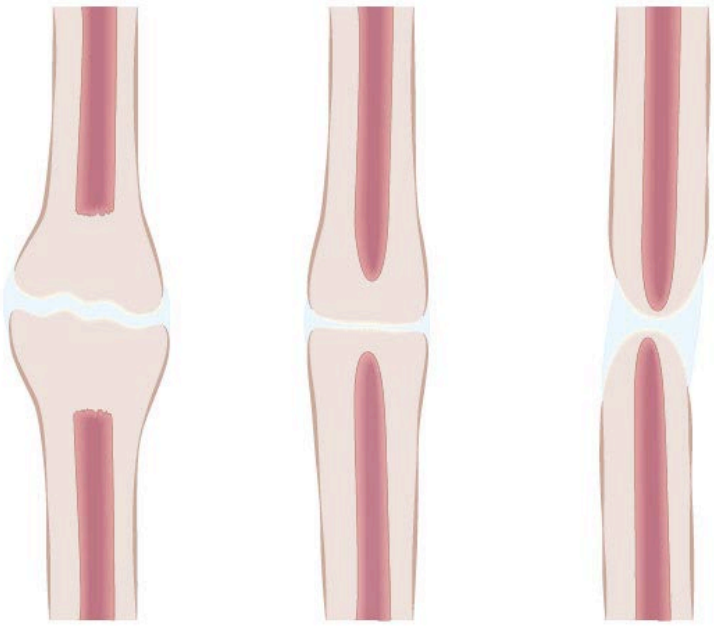

Fig. 8: Classification of non-unions. From left to right side: Hypertrophic non-union with excessive callus formation, normo- or oligothrophic non-union with normal callus formation but lack of bridging, atrophic non-union without callus formation. Adapted from [68].

Hypertrophic non-unions show extensive callus formation - often in the typical elephant foot form - which indicates adequate supply with blood and nutrients. The reason for the lack of healing can be found in poor mechanical stability of the fracture region, leading to continually disruption of newly formed tissue. In most cases of hypertrophic non-unions, a more rigid stabilization of the fracture is sufficient to stimulate healing [120]. This can be achieved by surgical means like the exchange of an existing osteosynthesis to a more rigid one or by non-surgical stabilization by casting or bracing.
In the most severe type of non-unions, the atrophic non-union, no or little callus formation is observed. Characteristic for atrophic non-unions is the resorption of the bone ends adjacent to the fracture gap. In general, atrophic non-unions are the result of deficiencies in biological processes [91] or high mechanical instability combined with insufficient perfusion. [80]

Treatment of atrophic non-unions aims to restore the biological potential for healing of the fracture or defect region. The gold standard in treatment of atrophic non-unions still is the transplantation of autologous bone grafts [111]. This type of graft is the only one that combines osteogenic, osteoinductive and osteoconductive properties [117]. Furthermore, there is no risk of graft rejection and transmission of diseases, as it is with allogeneic grafts. Within autologous bone grafts, cancellous, cortico-cancellous or vascularized grafts can be distinguished, but the most commonly used is the cancellous graft [111]. Mostly, autologous grafts are harvested from the iliac crest due to the large quantity of progenitor cells and growth factors at this site as well as the bone quality and the relative ease of the surgical approach [111]. Due to the limited availability of autologous grafts, other methods for the treatment of atrophic non-unions are desirable.

The application of osteoanabolic growth factors like BMP-2 or BMP-7 is another option in treatment of delayed healing fractures or non-unions. In preclinical studies, the efficacy of recombinant human (rh) BMPs to promote healing has been assessed using models of critical and non-critical sized bone defects [74]. In general, treatment with rhBMP led to improved biomechanical properties and faster bony bridging of defects. In clinical studies comparing the healing outcome

of acute tibial shaft fractures treated with standard procedures - autologous bone graft and intramedullary nailing - or rhBPM-7 and rhBMP-2 respectively, the recombinant BMPs have been shown to be equivalent to the respective standard but not superior [42, 47]. In 2001 and 2002 respectively, the use of rhBMP-7 and rhBMP-2 on non-unions or pseudarthroses has been approved by the European Medicines Agency (EMA). In humans, a retrospective study on the off-label use of BMP-2 for treatment of acute fractures at other sites than the tibia and non-unions showed a success rate of 66% [116].

A recent approach in treatment of manifest non-unions is the local application of osteogenic precursor cells. The effectiveness of the application of bone marrow aspirates for treatment of tibial non-unions could be shown in a clinical study in the early 1990 [56]. A further clinical study with sixty patients enrolled could draw a positive correlation between the number of progenitors injected percutaneously into the non-union site and the volume of the newly formed bone [57]. This indicates that an increase in the number of osteoprogenitor cells in fracture healing is favourable.

1.3.3 Osteoprogenitor Cells in Fracture Repair

The contribution of local periosteal and stromal osteoprogenitor cells to fracture healing has been investigated quite extensively. Analysis revealed that osteoblasts and osteocytes within the fracture callus originate equally from periosteum, endosteum and bone marrow, while chondrocytes might primarily be derived form periosteal progenitor cells [26]. Of the three compartments, the periosteum seems to be the most important source for osteoprogenitor cells, as stripping of the periosteum leads to reductions in the bone's cortical thickness, cross section area and moment of inertia as well as significantly inferior mechanical properties compared to animals with intact periosteum [81]. The importance of the periosteum as a source for osteoprogenitors is further emphasized by fact that periosteal stripping is often used to create delayed or non-unions experimentally.
While the contribution of local periosteal and stromal osteoprogenitors to fracture healing is well known [25, 26], the role of circulating osteoprogenitor cells is less clear. In 2001, first evidences for physiologically circulating skeletal stem cells in

healthy individuals were provided [67]. The authors were able to isolate cells with osteogenic potential by plastic adherence out of the peripheral blood from humans, mice, rabbits and guinea pigs; however the colony forming efficiency ranged between 2.7 and 0.18 CFU-F per 10^6 plated cells and below.

Another study used flow cytometry to investigate, if the number of circulating osteoprogenitor cells is increased in states of increased bone formation like the gain in bone mass during adolescence or during fracture healing [33]. The authors found a significantly higher number of circulating, osteocalcin positive osteogenic cells in adolescent individuals relative to adults. Furthermore, they could correlate the abundance of the cells to serum levels of the bone formation markers osteocalcin and bone specific alkaline phosphatase. The authors could also demonstrate an increase in the number of circulating cells positive for osteocalcin and alkaline phosphatase, respectively, in individuals with fractures relative to healthy individuals. Taken together, this study gives evidence for a significant number of physiologically circulating bone precursors and indicates a possible role for circulating precursors in fracture healing [33].

The role of circulating osteoprogenitor cells is further emphasized by a study comparing the abundance of circulating plastic adherent MSC after hip fracture and total hip arthroplasty in elderly women, respectively [5]. Here, circulating MSC appeared in 22 % of the cases in the blood within 39 to 101 h after fracture, whereas no circulating cells were detected in arthroplasty-patients. In a control group of surgically treated fractures of the lower limbs in young people, the same observation as in the elderly hip fracture patients was made with even higher appearance rates of circulating osteoprogenitor cells [5].

The question, if circulating osteoprogenitor cells are physiologically recruited to sites of skeletal injuries has been addressed by Kumagai et al. [66]. The authors established a parabiosis model of a GFP-transgenic mouse and a wild type mouse by conjunction of the circulation, so cells of one mouse circulate through the other one. After a fibular fracture in the wild type mouse, GFP-positive cells from the transgenic parabiosis-partner could be detected in the evolving callus. It was also demonstrated, that the number of GFP-positive cells within the callus increases with parabiosis time (Fig. 9).

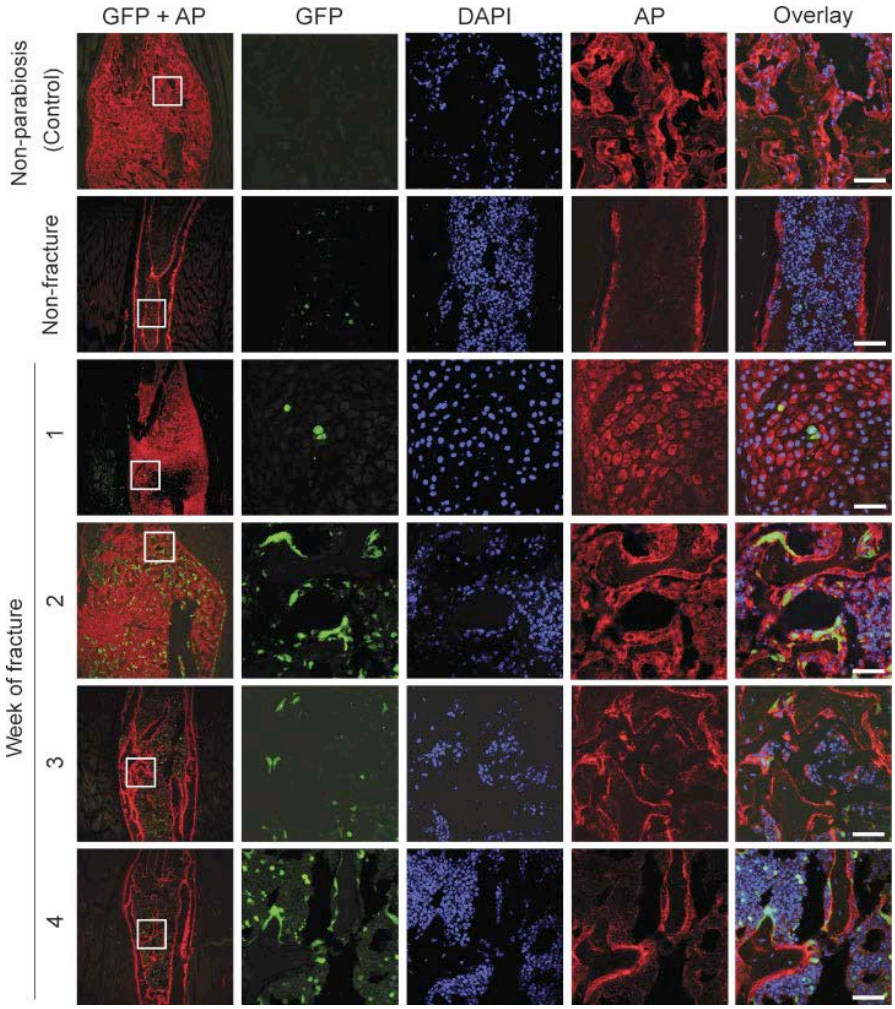

Fig. 9: Cells with osteogenic potential are recruited out of the circulation during fracture healing. Micrographs of fracture calli in parabiosis wild type-partner (GFP-negative) show increasing presence of partner-derived GFP-positive cells with increasing parabiosis time. The GFP+ cells show activity of AP, thus proving contribution to bone formation. Reproduced with permission from [66, page 170], Copyright © 2007 Orthopaedic Research Society.

Staining of alkaline phosphatase revealed a co-localization of AP with GFP^+-cells, thus providing evidence for a contribution to bone formation, as AP is essential for the mineralization process and a marker for active bone formation.

Taken together these aforementioned studies give strong evidence for a role and possible contribution of circulating cells to bone regeneration, thus making an artificial increase of their number a promising treatment option for impaired fracture healing.

1.4 Mesenchymal Stem Cells in Regenerative Medicine

MSC are in focus for regenerative approaches for several decades now due to their high proliferation capacity and differentiation potential. Besides, MSC are able to secrete a broad spectrum of biologically active factors with regenerative and anti-inflammatory effects [94].

In the 1970th, Friedenstein and colleagues were the first to describe cells grown out of the stroma of bone marrow from guinea pigs [41], forming colonies of fibroblastic cells referred to as colony forming unit-fibroblasts (CFU-F). The number of MSC in bone marrow declines with age: in new-borns, one cell in 10,000 bone marrow cells is a MSC, while in middle aged people the ratio declines to 1:250,000 to 1:400,000 [17].

Nowadays, various sources are routinely used for the isolation of MSC, e.g. adipose tissue, umbilical cord and dermis [122, 129], but bone marrow remains the most frequently used source for MSC for bone regeneration.

Due to different sources used for isolation as well as differing isolation and expansion protocols, the term “mesenchymal stem/stromal cell” refers not to a sole cell type but to a highly heterogeneous population. Even if the same source, e.g. bone marrow, is used, growth rates and morphology of the cells can vary considerably [12]. To enable the comparison of MSC-related studies despite the differing approaches, minimal criteria have been defined to reproducibly identify human MSC [31, 58]. These criteria include plastic adherence, expression of a specific pattern of cluster of differentiation (CD) surface antigens comprising of CD105, CD73 and CD90, the lack of expression of CD34, CD45 and CD11b and the potential to differentiate into osteoblasts, chondrocytes and adipocytes [31]. Besides these three traditional lines, MSC could be differentiated *in vitro* into myocytes and tenocytes as well [17] (Fig. 10).

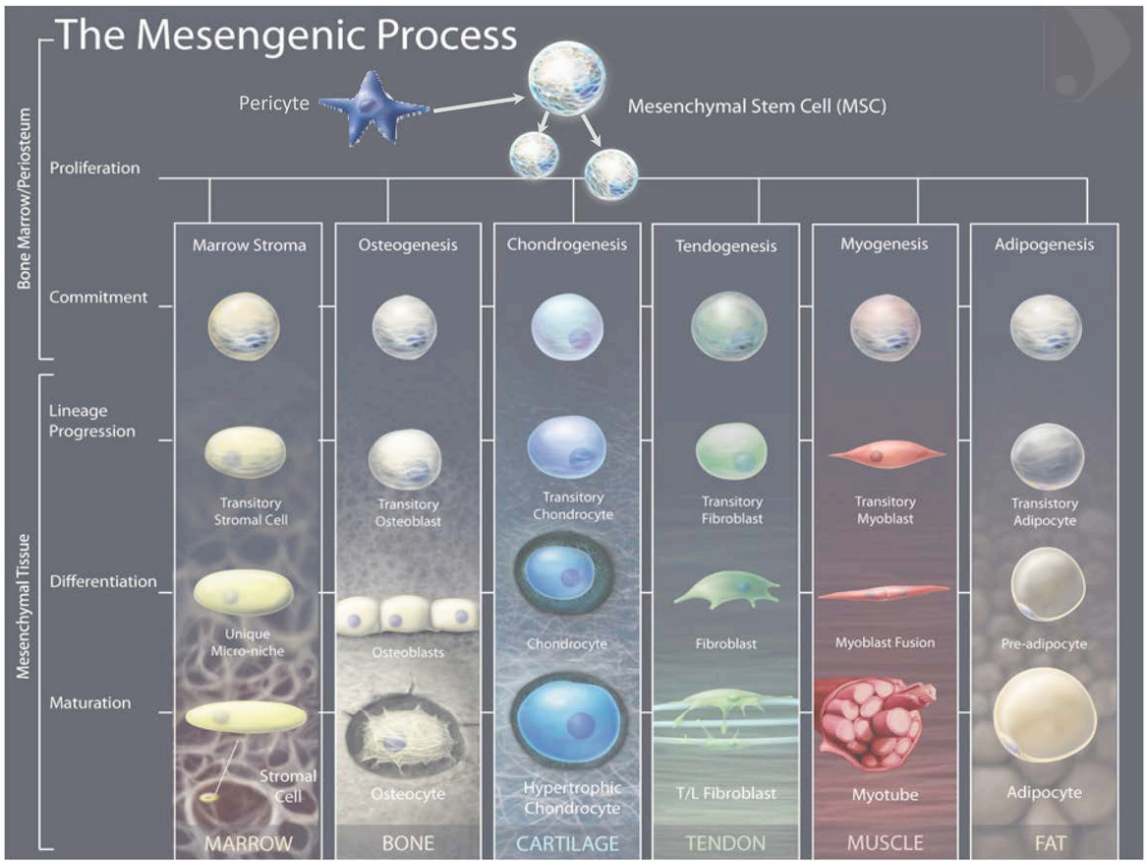

Fig. 10: The mesengenic process according to Caplan et al. Mesenchymal Stem Cells are able to differentiate into a multitude of mesenchyme-derived tissues, among those bone, cartilage and fat but also tendon and muscle. Reprinted from [19, page 12] with permission from Elsevier.

Other promising attributes of MSC for regenerative approaches are their low immunogenicity and their immunomodulatory capacity. [10] *In vitro*, MSC were shown to be able to inhibit the proliferation of mitogen activated T-lymphocytes in mixed lymphocyte reaction [29], thus indicating immunomodulation *in vivo*. The exact mechanism of immunomodulation is still under investigation. A recent publication could demonstrate the involvement of Fas/Fas-ligand induced T-cell apoptosis in MSC-mediated immunoregulation in mice [3]. Furthermore, a number of recent studies suggest a role for the anti-inflammatory cytokine TNFα induced protein/gene 6 (TNFAIP6/TSG-6) that is released by hMSC after activation by tumour necrosis factor α. [72, 101].

1.4.1 Local Delivery of Stem Cells for Regenerative Medicine

The local application of stem cells for regenerative approaches is predominantly limited to bone or musculoskeletal injuries. Generally, a local application is coupled to the use of an appropriate scaffold material to hold the cells in place.

1.4.2 Systemic Delivery of Stem Cells for Regenerative Medicine

Trafficking and Homing of Stem Cells after Systemic Administration

Trafficking of intravenous injected cells has been investigated in various studies. Gao et al. [43] injected radioactive labelled cells in rats and monitored the distribution of the cells by using a gamma camera for 48 hours. Radioactivity was primarily detected in the lungs and secondary in parenchymal organs like liver, spleen and kidneys. Only a small proportion of the radioactive signal could be detected in bone. In sub-lethally irradiated immunodeficient mice, hMSC administered via different routes could be traced for up to 75 days [82]. The administered cells could be detected in parenchymal organs like lung, liver and spleen consistently. The calculated donor cell frequency was highest in the lung and lowest in skeletal tissues [82].

Homing of stem cells to injured tissues or organs is driven by a variety of cyto- and chemokines. One of the most prominent chemo-attractants for stem cells, both hematopoietic and mesenchymal, is the CXC-motif chemokine ligand 12 (CXCL-12), also known as stromal cell derived factor-1α (SDF-1α). One of the physiological roles of SDF-1 is the retention of hematopoietic stem cells that express one of the receptors for SDF1, the CXC motif chemokine receptor 4 (CXCR4) in the bone marrow. It is known, that also a distinct proportion of mesenchymal stem cells is positive for this receptor [128] and thus able to migrate upon SDF1-gradients. Under hypoxic conditions - as they are in the early fracture healing phase - SDF-1 is up regulated via HIF-1α signalling [21]. Experiments demonstrate a central role for SDF-1 in the recruitment of progenitor cells to sites of bone formation [89] or musculoskeletal injuries [61] and a significant influence on their differentiation [59]. Otsuru and colleagues investigated the recruitment of intravenously injected, GFP-transgenic osteoblast precursors to BMP-2 containing

pellets implanted into nude mice. The *in vivo* migration and ectopic bone formation induced by the injected cells was completely abolished by administration of a specific antibody against the receptor for SDF-1 [89]. The blockade of CXCR4/SDF-1 signalling by a specific antagonist during fracture repair altered the callus composition in means of a significantly reduced hyaline cartilage volume, total callus volume and mineralized bone volume [121]. Furthermore, the expression of genes associated with endochondral ossification was reduced, too. Mechanical properties were not influenced by blocking the CXCR4/SDF-1 axis.
Chemo-attractive properties were also shown for PDGF [38, 92] that is released by platelets during the early phase of fracture healing [18, 74]. Other molecules exerting chemo-attractive action on MSC are MCP-1 and 3 [9, 107]. Local application of MCP-3 in fibular defects lead to an enhanced recruitment of circulating osteoprogenitor cells [113].

Systemically Applied Mesenchymal Stem Cells for Regenerative Approaches

Systemic application of MSC has been used successfully in various models for diseases and also in special cases in clinics. A single intravenous dose of $5x10^5$ MSC was sufficient to compensate hyperglycaemia and to prevent nephropathy in a mouse model for streptozotocin-induced type-1 diabetes [36]. In a model for stroke, application of $3x10^6$ BMSC via the lateral tail significantly enhanced functional recovery [75]. Treatment with MSC was also successful in a model of cisplatin-induced acute kidney injury in rats. Here, injection of MSC lead to reduced apoptosis of renal tubular cells, acceleration of tubular cell regeneration and preservation of renal function [95].
In addition to the experimental studies, there are numerous clinical trials in different phases on MSC-based therapies. Systemic application of allogeneic MSC reverted graft-versus-host disease, a severe complication after bone marrow transplantation [60, 93]. In hematopoietic stem cell transplantation, engraftment could be improved by co-transplantation of MSC [69]. Furthermore, MSC application after myocardial infarction reduced ventricular tachycardia episodes and improved the overall status of the patients [53].

1.5 Stem Cells in Experimental Approaches for Bone Regeneration

The contribution of *ex vivo* expanded osteogenic or epithelial progenitor cells to bone formation and regeneration has been investigated in various experimental studies. There are two general approaches for the delivery of cells: a local application or a systemic one.

Local Application of Progenitor Cells for Bone Regeneration

The effect of locally implanted progenitor cells on fracture or bone defect healing has been addressed by various researchers. The application of syngeneic endothelial progenitor cells seeded on gel foam in segmental bone defects in rats was shown to be superior to a non-cell loaded control [7]. After 10 weeks of healing, the authors found bony bridging of the defect in all EPC-treated animals but in none of the animals without EPC-implantation. Micro-computational analysis revealed amongst others a significant increase in the absolute bone volume and in the relative bone volume per callus volume [7].

Similar effects were detected after the application of human multipotent adipose-derived stem cells (hMADS) in long bone defects in immunodeficient rats [114]. Here the authors found a significantly improved healing after treatment with hMADS compared to treatment with human fibroblastic cells or PBS [114].

As the application of autologous stem cells in bone defects faces the same limitations as autologous bone grafts do – namely the limited availability – a focus has to be drawn to the possibility to use allogeneic stem cells, as such an approach would overcome the major drawbacks of the autologous approach.

The outcome of experimental studies considering the use of allogeneic stem cells is somewhat heterogenic. There are reports of successful use of allogeneic cells for bone regeneration, but other studies report opposite. Recently, a study in sheep reported equal bone formation after implantation of autogenic and allogeneic MSC seeded on polycaprolactone-β-tricalcium phosphate scaffolds into critical size defects [11]. However, new bone formation was considerably inferior to treatment with autologous bone graft. Another study reported no bone formation adjacent to tumour prostheses coated with allogeneic MSC while autologous cells demonstrated sufficient bone formation [24].

The reason for impaired bone formation with allogeneic MSC was addressed in mouse models with different immune deficiencies [30]. The authors suggest T-cells and interferon gamma (IFNγ) being responsible for the impairment.

Systemically Administered Osteoprogenitor Cells for Bone Defect Repair

Only few studies investigated the effect of systemically administered MSC or osteogenic precursor cells to bone defect healing so far. Devine and colleagues injected β-galactosidase transgenic, osteogenic D1 cells into BALB/c mice that received a closed fracture of the femur that was stabilized with an intramedullary needle [28]. They were able to detect the injected cells in the fracture callus from one to 6 weeks post fracture by X-Gal staining. The cells were principally located in areas of woven bone formation. Furthermore, the authors described a peak of the appearance of stained cells between 4 and 6 weeks after fracture. However, the authors could not detect any improvement of fracture healing due to the cells [28]. Another study conducted by Lee et al. investigated the efficacy of intravenous injected adipose-derived multipotent stem cells to consolidate a bone defect by in vivo imaging techniques [73]. They were able to demonstrate an accelerated increase in mineralized tissue in a unicortical drill-hole defect in mice by CT measurement. They also located the injected cells in the defect by in vivo bioluminescence and immunohistochemistry.

Granero-Moltó et al. used a closed tibial fracture model to investigate the regenerative effect of systemically administered MSC [48]. After fracture, the authors infused $1x10^6$ primary MSC depleted from cells positive for the hematopoietic markers CD34, CD45 and CD11b via the lateral tail vein. By using luciferase-transgenic MSC, the distribution of the cells could be monitored by *in vivo* bioluminescence imaging. The authors were able to detect the cells in the lung one day post infusion and fracture. On day three after fracture, the cells started to migrate towards the fractured limb. According to the authors, this process was mainly driven by CXCR4, as MSC negative for this receptor did not show homing to the fracture. After a healing period of 14 days, μCT analysis revealed amongst others a significant increase in callus volume and in new bone volume in MSC-treated mice. Assessment of the callus' mechanical properties revealed a significant increase in toughness and ultimate displacement after MSC-

treatment, while the callus stiffness was not influenced or even tended to be decreased, respectively.

The discrepancy of the results of the aforementioned studies - reaching from no benefit to an improvement of the healing process - clearly demonstrates that further studies investigating the role of systemically applied MSC in fracture healing are needed.

1.6 Aim of the Study

Mesenchymal stem cells represent a promising tool for regeneration of skeletal tissues. Clinicians still face considerable numbers of poor- or non-healing fractures despite the progress in treatment during the last decades. Here, application of MSC might be an interesting approach.

In the present study, different routes of MSC application were investigated, a systemic and a local delivery.

Regarding systemic MSC delivery, the following questions were addressed in C57BL/6 wild-type mice:

- Are the injected MSC recruited to sites of bone formation induced by mechanical loading or injury?
- Is bone formation enhanced after systemic MSC administration?

Regarding local delivery of MSC, the following was investigated in a mouse model with humanized immune system:

- Are MSC from autogenic and allogeneic sources equally effective in the consolidation of large bone defects?

2 Material and Methods

To investigate the contribution of systemically or locally administered mesenchymal stem cells to bone formation and repair, various methods were applied.

2.1 Material

2.1.1 Reagents

Tab. 1: Reagents

Reagent	Company
0.5% Trypsin/0.2% EDTA (10x)	Biochrom AG
2-Mercaptoethanol for cell culture	Gibco®
Accutase	PAA Laboratories GmbH
Acetic acid	Riedel-de Haën
AEC Single Solution	Zytomed Systems GmbH
Agarose for DNA electrophoresis	SERVA Electrophoresis
Alizarin red S	Sigma
AlphaMEM	Lonza
Aquatex®	Merck KGaA
Bovine serum albumin	Sigma-Aldrich®
Calcein green	Sigma
Carbon dioxide	MIT IndustrieGase AG
Citric acid	Sigma
Clindamycin	Ratiopharm
Dako pen	Dako
Dimethyl sulfoxide	Merck KGaA
Disodium hydrogen phosphate	Merck KGaA
Disodium tartrate dihydrate	Sigma-Aldrich
DMEM/F-12 (1:1), liquid	Gibco®
DNA ladder 100 bp	AppliChem GmbH
Dulbecco's MEM	Biochrom AG
Dulbecco's PBS	PAA Laboratories GmbH
Ethanol, absolute	VWR International
Ethidium bromide 0.07%	AppliChem GmbH
Ethylenediamine tetraacetic acid	VWR international

Fast Red Violet LB salt	Sigma
FBS MSC Qualified, USAD Approved regions	Gibco®
Formalin	Merck KGaA
FrekaDerm	Fresenius
Fungizone® Antimycotic, liquid	Gibco®
Gel loading solution, 6x	Sigma-Aldrich®
Giemsa solution	AppliChem GmbH
Hematoxilin	Merck KGaA
Hematoxilin Gill No. 2	Sigma
Heparin, 5,000 IE/0.2 ml	Ratiopharm
Hoechst 33342	Merck KGaA
Hydrochloric acid 2N	AppliChem GmbH
Hydrogen peroxide 30%	Merck KGaA
Isofluran, Forene®	Abbot
L-glutamine	PAA Laboratories GmbH
Methanol	Fluka
Methyl methacrylate	Merck KGaA
N,N-Dimethylformamide	Sigma
Naphthol AS-MX phosphate disodium salt	Sigma-Aldrich
Nitrogen	MIT IndustrieGase AG
Normal Goat Serum	Jackson ImmunoResearch
Octenisept	Schülke
Oxygen, medical grade	MIT IndustrieGase AG
Paraffin Paraplast Plus	McCormick™ SCIENTIFIC
Penicillin-Streptomycin, liquid	invitrogen™
Safranin-O	Sigma
Silver nitrate	Serva
Sodium acetate	Sigma
Sodium carbonate	Merck KGaA
Sodium chloride	Sigma-Aldrich®
Sodium chloride, liquid 0.9% for injection	Fresenius Kabi
Sodium choride, liquid	B. Braun Melsungen AG
Sodium dihydrogen phosphate	Merck KGaA
Sodium thiosulfate	Merck KGaA
Tramal®, liquid	Grünenthal
Trisodium citrate dihydrate	Merck KGaA
Triton X-100	Sigma-Aldrich®
Trizma® base	Sigma-Aldrich®
Trypan blue solution	Merck KGaA
Type-I collagen gel	Amedrix

VECTASTAIN® Elite® ABC Kit	Vector Laboratories
Vector® NovaRED™ Substrate Kit	Vector Laboratories
Vitro-Clud®	Merck KGaA
Weigert's iron hematoxylin	Merck KGaG
Xylene	Riedel-de Haën
β-Glycerophosphate disodium	Sigma-Aldrich®
β-Mercaptoethanol for RNA-isolation	Signa-Aldrich®

2.1.2 Consumable Supplies

Tab. 2: Consumable supplies

Consumable supplies	Company
Cell culture flasks	nunc™
CryoTube™ vials	nunc™
HistoBond® glass slides	Marienfeld GmbH & Co. KG
Microtubes, 1.5 and 2 mL	Eppendorf, Sarstaedt
LD column	Miltenyi
Cell culture plates	Corning, nunc™, TPP

2.1.3 Solutions

Tab. 3: Solutions

Solution	Composition
TAE buffer	40 mM tris, 1 mM EDTA, 40 mM glacial acetic acid, pH 8.5
TTBS buffer	50 mM tris, 0.88 % NaCl, 0.1% Triton X-100, pH 6.7
Citric acid buffer	10 mM citric acid + 10 mM trisodium citrate dihydrate, pH 6.0
Buffered 4% formaldehyde solution	30 mM NaH_2PO_4 + 45 mM Na_2HPO_4 in 4 % formaldehyde, pH 7.0
Injection solution	100 IE heparin/1 mL PBS
Citrate-acetone-formaldehyde fixative for alkaline phophatase staining kit	25 mL citrate solution (supplied with kit) + 65 mL acetone + 8 mL 37 % formaldehyde

2.1.4 Primer

Primers were synthesized by Thermo Fisher Scientific (Germany).

Tab. 1: Primer

mRNA	Primer Sequence 5' - 3'	PCR product size (bp)
EGFP forward	AAG TTC ATC TGC ACC ACC G	173
EGFP reverse	TCC TTG AAG AAG ATG GTG CG	
GAPDH forward (murine)	CCC GTT TGC AAC ATG GCG GC	214
GAPDH reverse (murine)	GCG CCC GTT CAG ACC CAT CC	
p53 forward (human)	GTT CCG AGA GCT GAA TGA GG	159
p53 reverse (human)	TCT GAG TCA GGC CCT TCT GT	
GAPDH forward (human)	GCT CAA CGA CCA CTT TGT	66
GAPDH reverse (human)	CCC TGT TGC TGT AGC CAA AT	

2.1.5 Antibodies

Tab. 4: Antibodies

Antibody	Produced in	Target species	Specificity	Company
CD 11b Microbeads		h, m	CD11b	Miltenyi
Rabbit anti-EGFP antibody	Rabbit	-	EGFP	Abcam
Goat anti-rabbit IgG, F(ab')$_2$-B	Goat	r	IgG, F(ab')$_2$-B	Molecular Probes®
IgG from rabbit serum	Rabbit	-	IgG	Sigma-Aldrich®
Rabbit anti-Runx2 antibody	Rabbit	h, m, r, mk	Runx2	Cell Signalling
Rabbit anti-human CD8 antibody	Rabbit	h	CD8a	Acris
Rabbit anti-human β2-microglobulin	Rabbit	h	β2-microglobulin	DAKO
CD31 (PECAM) monoclonal antibody	Rat	h, m	CD31	DAKO
Rabbit anti-SDF1 antibody	Rabbit		SDF-1	Novus Biologicals

2.1.6 Media

Tab. 5: Media

Medium	Composition
EGFP-MSC growth medium	Dulbecco's MEM/F-12 (1:1) + 10 % FBS MSC Qualified + 1 % L-glutamine + 1 % penicillin-streptomycin + 0.5 % Fungizone® + 50 µM 2-Mercaptoethnol
EGFP osteogenic differentiation medium	EGFP-MSC growth medium + 10 mM β-glycerophosphate, 0.2 mM ascorbate-2-phosphate
Human MSC growth medium 1	DMEM + 8 % platelet lysate + 80 IU heparin sulfate + 1mM L-glutamine + 100 U/mL penicillin + 100 µg/mL streptomycin
Human MSC growth medium 2	AlphaMEM + 10 % platelet lysate + 1 IU/mL sodium-heparin
Human MSC growth medium 3	DMEM + 10 % FCS + 1 % L-glutamine + 1 % penicillin-streptomycin + 0.5 % Fungizone®
Human osteogenic differentiation medium	Human MSC growth medium 2 + 10 mM β-glycerophosphate, 0.2 mM ascorbate-2-phosphate + 0.1 µM dexamethasone

2.1.7 Kits

Tab. 6: Kits

Kit	Company
DNeays™ Kit	QIAGEN GmbH, Hilden, Germany
HotStarTaq® Master Mix Kit	QIAGEN GmbH, Hilden, Germany
Leukocyte Alkaline Phosphatase Kit	Sigma-Aldrich®, Steinheim, Germany
RNeasy MiniKit	QIAGEN GmbH, Hilden, Germany
Omniscript™ RT Kit	Qiagen GmbH, Hilden, Germany
Bio-Plex Pro Cytokine Assay	Bio-Rad, Hercules, CA, USA

2.1.8 Equipment

Tab. 7: Equipment

Equipment	Type	Company
Anaesthesia system		FMI GmbH
Camera	DFC420C	Leica
Camera (monochromatic)	DFC360FX	Leica
Centrifuge	UniCen FR	Herolab GmbH Laborgeräte
Centrifuge, bench top	5417R	Eppendorf
Clean Bench	-	various
Counting chamber	Neubauer double	Jordan Gamma GmbH
External fixator	Stiffness 3 N/mm and 18 N/mm	RISystems AG
Gel documentation system	Fusion-SL 3500.WL	Vilber Lourmat
Gigli wire saw	Ø 0.22 and 0.44 mm	RISystems AG
Image processing software	Metamorph AF, version 14.2	Leica
Incubator	various	Heraeus
Microscope	IX70	Olympus
Microscope (fluorescence)	DMI6000 B	Leica
Microtome, precision	CUT 6062	SLEE
Microtome, sliding	Ultracut S	Leica
Non-invasive ulna loading device		Wissenschaftliche Werkstatt Feinwerktechnik, Ulm University
PCR device	T1 Thermocycler	Biometra GmbH
Photometer	Infinite M200	Tecan
Surgical equipment		various
Water bath	SWB 20	Medigen
µCT	1172	Skyscan

2.2 Methods

2.2.1 Isolation/Preparation of Mesenchymal Stem Cells

2.2.1.1 Murine EGFP-transgenic Mesenchymal Stem Cells

Isolation of Cells

MSC were isolates from mice transgenic for the enhanced green fluorescent protein (EGFP) (Strain C57BL/6-Tg/CAG-EGFP)131Osb/LeySop/J, Jackson Laboratory). Femurs and tibiae from mice aged 8 to 10 weeks were harvested and adjacent muscle was removed under sterile conditions. Bone ends were clipped and bone marrow was flushed into a 40 µm cell strainer with PBS. The bone marrow was minced using a syringe plunger and washed through the cell strainer with PBS. After centrifugation (300xg, 10 min, ambient temperature), the bone marrow cells were resuspended in medium and seeded at a density of 400,000 to 500,000 cells/cm^2 in culture flasks. Cells were cultivated at 37 °C under 8.5 % CO_2, 6 % O_2 and saturated humidity. Medium was replaced twice a week.

To deplete MSC from contaminating hematopoietic cells, magnetic cell sorting was applied (MACS®, Miltenyi Biotech, Bergisch Gladbach, Germany). At subconfluence, the cells were detached by incubation with trypsin/ethylenediamine tetraacetic acid (EDTA) for 5 to 7 min at 37 °C. Medium was added and the cells were centrifuged (300xg, 10 min, 4 °C). The cells were resuspended in 90 µL cold MACS buffer and 10 µL CD11b MicroBeads were added, followed by incubation at 4 °C for 15 min. After incubation, the cells were washed with 2 mL cold MACS buffer (300xg, 10 min, 4 °C). The cells were suspended in 500 µL cold MACS buffer and applied onto a LD-column placed in a MACS separator. Unlabelled cells were collected and the column was washed twice with MACS buffer to remove all unlabelled cells.

The unlabelled cell fraction representing MSC was seeded at 1,000 to 1,500 cells/cm^2 in culture flasks. Cells were grown to subconfluence, trypsinised and cryo-preserved in liquid nitrogen in medium containing 20 % foetal bovine serum (FBS) and 10 % dimethyl sulfoxide (DMSO).

Cultivation of Cells

Cells stored in liquid nitrogen were thawed in a water bath at 37 °C and added to 19 ml medium to dilute DMSO. The cells were centrifuged (250xg, 10 min, ambient temperature) and counted in a counting chamber with trypan blue. For expansion, the cells were seeded at 1,000 to 1,500 cells/cm^2 and cultured at 37 °C under 8.5 % CO_2, 6 % O_2 and saturated humidity. Medium was changed twice a week. At subconfluence, cells were detached and reseeded for further expansion or experiment. Cells in passage 4 to 6 were used for injection.

Cell Preparation for Injection

24 h before injection, serum in the medium was reduced to 5 %. After two washes with PBS, cells were incubated with Accutase (5 mL per 175 cm^2, PAA Laboratories) for 15 min at 37 °C for detachment. The cells were washed with PBS (250 g, 10 min, ambient temperature), resuspended in PBS and counted in a counting chamber with trypsin blue. For injection, $2x10^6$ MSC were calculated per mouse. The suspension volume equating the required cell count was centrifuged (250 g, 10 min, ambient temperature) and the cells were suspended with a concentration of $1x10^6$ MSC per 100 µL injection solution.

2.2.1.2 Human Mesenchymal Stem Cells

Human MSC used for local application in large bone defects were kindly provided by the group of Prof. Dr. med. Ingo Müller, Department of General Paediatrics, Haematology and Oncology, University Children´s Hospital Tübingen, and cultivated by the group of Prof. Dr. med. Hubert Schrezenmeier, Institute for Clinical Transfusion Medicine and Immunogenetics, University Hospital Ulm.

The MSC were isolated from bone marrow aspirates of healthy donors by plastic adherence. The cells were cultivates in human MSC growth medium 1 at 37 °C, under 8.5 % CO_2 and saturated humidity. At 80 % confluence, the cells were trysinised and reseeded. Medium was replaced once a week. Before transfer to Ulm, the cells were frozen in liquid nitrogen.

Cultivation of Cells

The MSC were thawed and cultivated in human MSC growth medium 2 at 37 °C under 5 % CO_2 and saturated humidity. One day before the surgeries, the cells were harvested, resuspended in PBS and transferred to the Institute for Orthopaedic Research and Biomechanics.

Preparation of MSC for Local Delivery

For local delivery, the MSC were seeded in a two-component collagen type-1 gel (Amedrix, Esslingen) in a density of 200,000 MSC/50 µL gel one day before surgery. For this, the cells were harvested using trypsin/EDTA and resuspended in PBS. The amount of cells needed was centrifuged (250 g, 10 min, ambient temperature) and resuspended in neutralization buffer (10 µL/gel). The cell suspension was quickly added to the collagen solution (40 µL/gel) and thoroughly but carefully mixed. The gel solution was quickly filled in the cavities of a 96-well-plate at a volume of 50 µL/cavity. The gel was allowed to polymerize for 15 min on 37 °C, then 150 µL AlphaMEM supplemented with 1 % L-glutamine were added per well.

On the day of the surgery, 2 gels per mouse were selected based on visual examination of the cell distribution and morphology, immersed in PBS for two times 10 min on 37 °C to remove any media, placed in fresh PBS and transferred to the operation facility.

2.2.2 In Vitro Analysis of Human Mesenchymal Stem Cells

2.2.2.1 Mesenchymal Stem Cell Differentiation

To investigate if the MSC are able to differentiate into the osteogenic lineage, human MSC were seeded in cell culture plastic wells at a density of 10,000 cells/cm^2 in human MSC growth medium 3 at 37 °C under 8.5 % CO_2 and saturated humidity. After 24 h, growth medium was replaced by osteogenic differentiation medium. The medium was changed twice a week and cells were cultured for 21 days. The differentiation of the cells was qualitatively assessed using specific staining methods.

Alkaline Phosphatase Staining

The activity of the alkaline phosphatase was analysed using the Leukocyte Alkaline Phosphatase Kit according to the manufacturer's instructions. On day 21, the cells were fixed using citrate-acetone-formaldehyde fixative. Incubation of the cells with an AP substrate-containing solution resulted in the deposition of a red precipitate in cells with AP activity.

Von Kossa Staining

The deposition of calcium phosphate was analysed by von Kossa staining. Briefly, by incubation with silver nitrate, calcium ions are exchanged with silver ions. By reduction of the silver ions, a dark staining develops, showing places of mineral deposits.

On day 21 cells were fixed with 4 % formalin solution, washed with demineralized water and incubated with silver nitrate (0.05 g/mL) for 60 min. After washing with demineralized water, the cells were incubated with pyrogallol (0.01 g/mL) for 10 min, fixed with sodium thioslufate (0.05 g/mL), rinsed and air-dried.

2.2.2.2 Analyses of Human MSC Seeded in Collagen Gel

Cell Viability

One hour after seeding and on the day of the surgery, two gels each were stained with 5 ng/mL Hoechst 33342 dye and 10 µg/mL propidium iodine for 20 min. The viability was qualitatively assessed using fluorescence microscopy.

Two further gels each were lysed in RLT buffer to analyse the expression of p53. RNA-isolation, cDNA synthesis and PCR were performed as described above and stored at -80 °C until RNA isolation. Lysates were homogenized using QIAshredder™ columns and RNA was isolated using RNeasy™ Mini Kit and RNAse-Free DNAse Set according to the manufacturer. RNA concentration was determined photometrically.

- cDNA-Synthesis

1 µg RNA was transcribed into cDNA using Omniscript^{TM} RT Kit according to the manufacturer instructions. The obtained cDNA was diluted 1:4 and used for PCR.

- Qualitative Reverse Transcriptase Polymerase Chain Reaction

Reverse transcriptase PCR was performed in a total volume of 20 µL using 10 µL HotStarTaq® Master Mix completed with 0.5 µM of the specific primer and 1µL cDNA. Specific primer pairs were designed using published gene sequences (PubMed, NCBI Entrez Nucleotide Database).

The amplification products were mixed with gel loading solution at a ration of 6:1 and separated on a 2 % agarose gel in tris-acetate-EDTA (TAE) buffer. The separated amplicons and DNA ladder were visualized using ethidium bromide staining (0.9 µM) and documented with a gel documentation system.

2.2.3 In Vivo Experiments

All experimental procedures were performed according to the national and international regulations for the care and use of laboratory animals and were approved by the national ethics committee (Germany, Regierungspräsidium Tübingen, No. 1000 and 1029)

2.2.3.1 Systemic Delivery of EGFP-Transgenic MSC in Load Induced Bone Modelling and Fracture Healing

Animal Model and Husbandry

For the fracture healing study, male C57BL/6J mice aged 12 weeks were used. The study regarding load induced bone formation was conducted with male C57BL/6J mice aged 18 weeks. All mice were purchased from Charles River.

The animals were housed in groups of 3 to 4 mice in Macrolon-Type II cages (370 cm^2) at 14 h light and 10 h dark rhythm. Chow and water were offered ad *libitum*. Temperature in the animal room was maintained at 23 °C with 55 ± 10% humidity.

2.2.3.1.1 Load Induced Bone Formation

The following experimental groups were investigated in the study:

Experimental group	Euthanasia (day of regimen) 16 (immunohistochemistry)	16 (histomorphometry)
Mechanical loading	5 mice	7 mice
Mechanical loading + EGFP-MSC	5 mice	7 mice

Anaesthesia

The non-invasive loading of the right ulnae was carried out under general anaesthesia using 7 % isofluran/oxygen for anaesthetization and 2 - 2.5 % for anaesthesia sustainment using a unit from FMI GmbH.

In Vivo Loading

Right ulnae of male C57BL/6J mice aged 18 weeks were loaded with 1,5 N in a 2 Hz trapezoidal wave for 1 min per day on 5 consecutive days per week for two weeks. Left ulnae served as internal non-loaded control.

The anaesthetized mouse was placed into the ulna-loading machine in a supine position. The right ulna was positioned between two silicon-padded cylinders with flexed carpus and flexed *Articulatio cubiti*. Then, the cyclic axial compression of the ulna was performed. On day two and eight of the loading regimen, $1x10^6$ MSC in injection solution or injection solution as control were administered via lateral tail vein before loading. For histomorphometric analysis, mice received an intraperitoneal injection of calcein green (0.03 g/kg, Sigma) and alizarin red S (0.045 g/kg) on day 3 and 12, respectively. Mice were housed in the original groups during the experiment until euthanasia after 16 days.

Euthanasia and Sample Recovery

Mice were euthanized by cervical dislocation under general anaesthesia. From all mice the organs brain, lung, liver, spleen, heart and both kidneys were harvested

and fixed in 4 % formaldehyde or snap frozen in liquid nitrogen, depending on the further processing.
Left and right ulnae were harvested and immediately fixed in 4% formaldehyde.

2.2.3.1.2 Fracture Healing Study

The following experimental groups were investigated in the fracture healing study.

Experimental group	Euthanasia (days after surgery)		
	3	10	21
Osteotomy	6 mice	5 mice	6 mice
Osteotomy + EGFP-MSC	6 mice	6 mice	6 mice

Medication and Anaesthesia

All mice received pain medication one day before and three days after surgery in form of 25 mg/L Tramadol hydrochloride (Tramal®) in drinking water. Surgery was performed under inhalation anaesthesia using a unit from FMI GmbH. Anaesthetization was done in a tube flown through with 7 % isolurane/oxygen. At absence of labyrinthine postural reflexes, mice were withdrawn from the tube and positioned in an inhalation mask for spontaneously breathing small animal. Anaesthesia was sustained with 2 – 2.5 % isoflurane/oxygen. As anaesthetized rodent don't show eyelid closure reflex, Vidisic® eye ointment was administered to prevent drying-out. To prevent fluid loss during surgery, 500 µL isotonic sodium chloride solution were injected subcutaneously. For prophylaxis, 45 mg/kg antibiotics (Clindamycin) were injected subcutaneously. Body temperature was held at 37 °C by using heating plates.

Preparations for Surgery

The surgical procedures were conducted as described previously [102]. For surgery, the right hind limb of an anaesthetized mouse was shaved and disinfected using a disinfection solution for skin (FrekaDerm). The mouse was placed in prone position on a sterile covered heating plate and fixed with plaster stripes. The right hind limb remained freely movable. The eyes were covered with gauze. The mouse was covered with a transparent, sterile foil and the right hind

limb was lifted through a cut-out using forceps. The free paw was covered. The free part of the limb was disinfected again with disinfection solution for wounds and mucosa (Octenisept).

Surgical Procedure

The surgery was carried out under sterile conditions. After lateral incision of the skin and blunt preparation of the fasciae between *M. biceps femoralis* and *M. vastus lateralis* of *M. quadriceps femoris*, the femur of the right hind limb was exposed. The external fixator was fixed to the cranio-lateral side of the femur with 4 mini-Schanz screws (ø 0.5 mm). The *Trochanter tertius* served as orientation point for the position of the most proximal screw. After drilling the first hole with a hand drill (ø 0.45 mm) orthogonal to the bone, the fixator was mounted with the first screw parallel to the longitudinal orientation of the femur. Next, the most distal drill hole was drilled and the fixator was fixed securely to the bone with the second screw. The position of the inner holes was dictated from the fit of the fixator. After all screws were mounted to the femur, the femur was osteotomised in the middle between the inner screws using a Gigli wire saw (ø 0.44 mm). Subsequently, the muscle was adapted by running stiches with absorbable suture (Vicryl 5-0). The skin incision was closed with non-absorbable sutures (Resolon 5-0). The wound was cleaned and disinfected with Octenisept.
To assess the position of the fixator and the osteotomy, radiographs were taken from the still anaesthetized mice.

During the recovery phase after anaesthesia, mice were irradiated with red light and the cages were heated via underlying heat plates. Two hours after the osteotomy was performed, all mice were anaesthetized again to administer either $1x10^6$ MSC in 100 µL injection solution or 100 µL injection solution as control via lateral tail vein.
After the surgery, the mice were housed in the original groups until euthanasia.

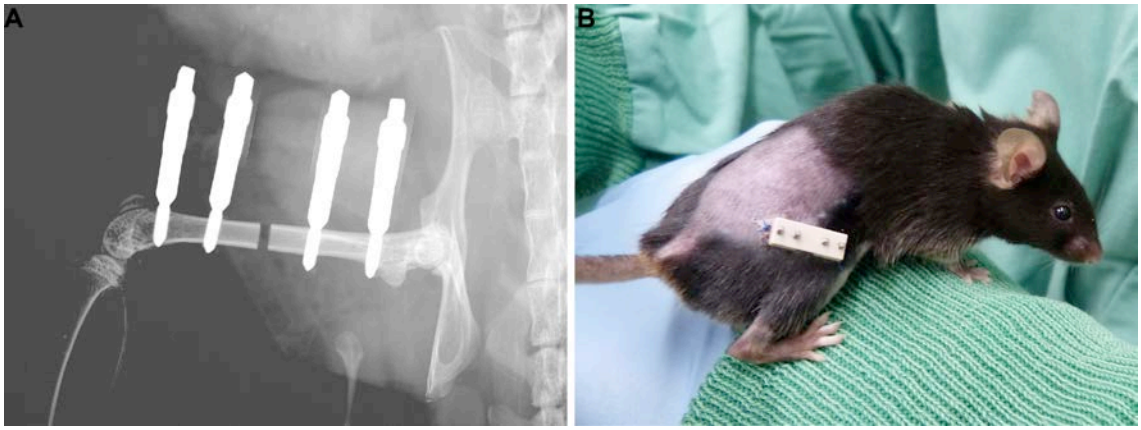

Fig. 11: Post-surgical X-ray of an ostetomised femur with mounted external fixator (A) and a mouse one week after surgery wearing a fixator (B).

Euthanasia and Sample Recovery

The mice were euthanized at after 3, 10 or 21 days by cervical dislocation under general anaesthesia after blood withdrawal.

From all mice the organs brain, lung, liver, spleen, heart and both kidneys were harvested and fixed in 4 % formalin or snap frozen in liquid nitrogen, depending on the further processing. From snap-frozen organs, DNA was isolated using DNeasy^{TM} kit according to the manufacturer. 1 µg DNA was applied in PCR as described above.

After harvesting, the femurs designated to biomechanical testing were immersed in 0.9 % sodium chloride solution until testing and afterwards fixed in 4 % formaldehyde. Femurs designated to (immuno-)histochemical analysis were fixed in 4 % formaldehyde immediately after being harvested.

2.2.3.2 Local Delivery of Autogenic and Allogeneic Mesenchymal Stem Cells for Bone Defect Repair

Animal Model and Husbandry

For this study, mice with a humanized immune system were used. The mice were kindly provided by the group of Prof. Dr. med I. Müller, Department of General Paediatrics, Haematology and Oncology, University Children´s Hospital Tübingen, Germany. Briefly, mice of the strain NOD.Cg-Prkdc^{scid} Il2rg^{tm1Wjl}/SzJ (common name NOD/scid IL2rγ^{0}) were irradiated with 250 cGy. Within 24 h, 1x10^{6} human

haematopoietic stem cells in 100 µL PBS were administered intravenously. The mice received X mg/mL antibiotics (CotrimE-ratiopharm) via drinking water for four weeks to prevent opportunistic infections. To ensure optimal conditions for the human cells, 20 µg IL-7 were administered once a week until the mice were transferred to Ulm. 18 weeks after transplantation, the human engraftment was assessed by FACS analysis for CD45 in the peripheral blood. Animals displaying more than 5 % human cells in peripheral blood were transferred to Ulm and operated after two further weeks. The mice were housed in isolated ventilation cages to ensure a pathogen free environment.

Medication, Anaesthesia and Preparation for Surgery

Additional to the above-mentioned procedure, the mice received an s.c. injection of 15 mg/kg tramadol hydrochloride before surgery to achieve appropriate anaesthesia. The mice were prepared for surgery as described above.

Surgical Procedure

In general, the surgical procedure was similar to the procedure described above. After fixing the external fixator (stiffness 18 N/mm), a 1 mm large defect was created in the mid diaphysis by sawing two times using 0.22 mm Gigli wire-saw. After thoroughly flushing the defect, either the respective collagen gel was inserted into the defect or the defect was left empty (Fig. 12).

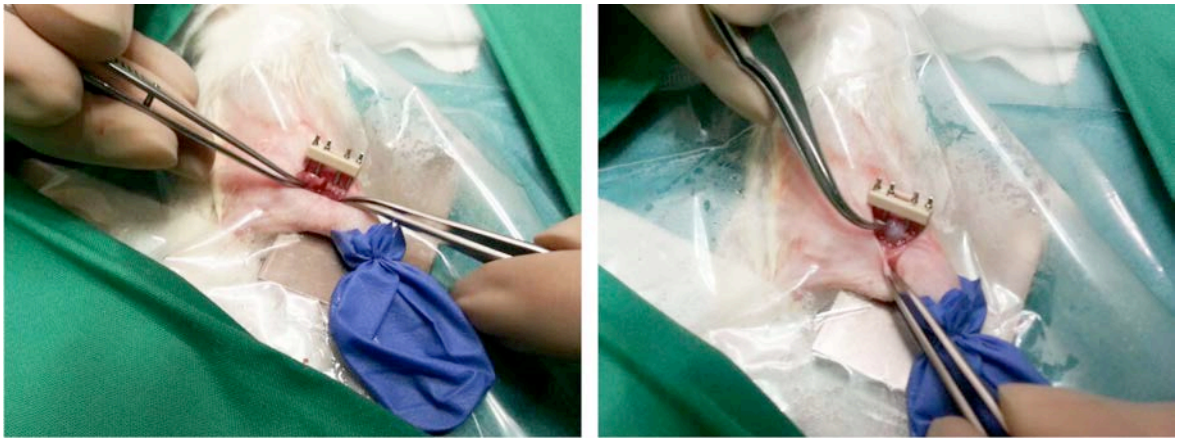

Fig. 12: Critical-size defect in the femur of a NOD/scid-Il2rγ^{0} mouse before (A) and after (B) filling of the defect with collagen gel.

After surgery the mice were housed in the original groups and received tramadol hydrochloride via the drinking water for three days.

Euthanasia and Sample Recovery

The mice were sacrificed after three, 10 or 35 days by blood withdrawal from the *Vena cava inferior* under general anaesthesia. Before, about 50 µL whole blood were withdrawn form the lateral tail vein for FACS analysis to investigate the percentage of human cells in the peripheral blood.

Right femurs were immediately fixed in 4 % formaldehyde solution for at least 24 h and applied to further histological processing. Spleen, humeri and tibiae were harvested for analysis of the human engraftment.

2.2.4 Assessment of the In Vivo Studies

2.2.4.1 Biomechanical Testing

The healing outcome 21 days after osteotomy was assessed by three-point bending. For testing, the femoral heads were fixed to aluminium cylinders (ø 8mm) using UV-curing, two-component adhesive (iCEM® Adhesive; Heraeus-Kulzer, Hanau, Germany). The cylinder was fixed into a material testing machine (Z10, Zwick Roell, Ulm, Germany), serving as proximal support for the bending test. The condyles of the femur were placed on the distal bending support so that 20 mm free length (Lv) between the supports remained. The bending load F was applied on top of the callus and a force-displacement curve was recorded up to a maximum load of 4 N with a crosshead speed 2 mm/min. The flexural rigidity E*I was calculated from the slope k of the linear region of the force-displacement curve, the distance between the force vector and the proximal support (a) and the distal support (b) respectively according to $E*I = k(a^2b^2/3Lv)$ in N/mm^2 [102].

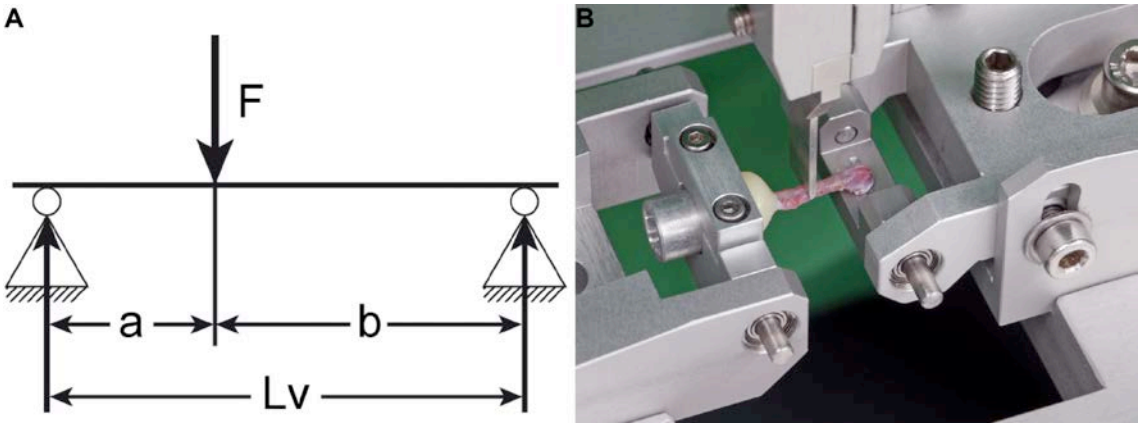

Fig. 13: Scheme of three-point bending test (A) and femur mounted to the three-point bending device (B).

2.2.4.2 µCT Analysis

Femurs and ulnae were scanned in a SkyScan 1172 µCT device with a resolution of 8 µm/pixel. The peak voltage used for scanning is listed below. Dataset reconstruction was done using NRecon, the analysis itself was performed using CtAnalyser (CtAn). For analysis, the former osteotomy gap was defined as region of interest. To dissect bone from non-mineralized tissue, a threshold for bone was defined at 641.9 mg HA/cm^3 [84]. Bone mineral density and moment of inertia were determined without threshold.

Experiment	kV	µA
Systemic application of MSC in load induced modelling	50	200
Systemic application of MSC in fracture healing	50	200
Local delivery of autogenic and allogeneic MSC	100	100

The following ASBMR parameters were analysed:

ASBMR parameter		Unit
BMD	bone mineral density	mg HA/cm^3
BV	bone volume	mm^3
TV	tissue volume	mm^3
BV/TV	Ratio bone volume to tissue volume	mm^2

To investigate the load induced bone formation a 1 mm volume of interest (VOI) starting 3.5 mm distal from ulna-middle was analysed for the following ASBMR standard parameters:

ASBMR parameter		Unit
BMD	bone mineral density	mg HA/cm^3
BV	bone volume	mm^3
BS	bone surface	mm^2
MMI(x)	moment of inertia (x-axis)	mm^4
Ct.Wi.	cortical width	mm

2.2.4.3 Histological Analyses

Sample Preparation

Decalcified Histology

The specimens for decalcified histology/immunohistochemistry were immersed in 4 % formaldehyde for three to four days and subjected to decalcification with 20 % EDTA for 10 to 11 days. After decalcification, the specimens were dehydrated in a series of ethanol, infiltrated with paraffin and embedded in paraffin blocks for cutting with a precision microtome (CUT 6062, SLEE). From embedded bones, 6 µm thick longitudinally sections were cut.

Undecalcified Histology

Specimens for undecalcified histology were immersed in 4 % formalin for at least three days, subsequently dehydrated in an increasing ethanol series over two weeks and degreased in xylene. After this, the specimens were infiltrated with methyl methacrylate (MMA) solution for 2 to 4 days, followed by a second infiltration step for 7 to 10 days. Subsequently, the specimens were immersed in destabilized MMA in glass vials. For polymerization, the vials were incubated at 4 °C under air exclusion over night.

Using a sliding microtome, the MMA-embedded femurs were cut longitudinally with 6 µm thickness. From ulnae, 10 µm thick cross-sections were cut 4 mm distal of the ulna-middle.

Histological staining

Safranin-O Staining

Paraffin-embedded sections were deparaffinised and rehydrated. Then, sections were immersed in Weigert's iron haematoxylin for 4 min and subsequently briefly immersed in acidified ethanol and rinsed with tap water for 5 min. Then, sections were stained with 0.02 % light-green for 3 min and rinsed with 1 % acetic acid. After that, sections were immersed in safranin-O solution for 5 min, dehydrated in an increasing series of ethanol and covered.

After staining, cartilage is stained bright orange-red, mature bone develops turquoise-greenish and newly mineralized bone develops light green to turquoise.

Giemsa Staining

Methacrylate-embedded sections were recovered and rehydrated. The sections were immersed in Giemsa-solution in phosphate buffer for 45 min at ambient temperature. Subsequently, the staining was developed by immersion of the sections in 0.4 % acetic acid and ethanol. Then sections were dehydrated and mounted using Vitro-Clud®.

After staining, mature bone develops blue-greyish, new mineralized bone develops light grey-violet and cartilage is stained dark purple.

Immunohistological Staining

In general, sections were deparaffinised in xylene and rehydrated in decreasing series of ethanol. Antigen retrieval was performed by immersion in citric acid buffer pH 6 at 95 °C for 20 min. Nonspecific binding sites were blocked with the respective blocking solution 1 h at room temperature. Sections were incubated over night at 4 °C with primary antibody and isotype control, respectively. Incubation with the matching biotinylated secondary antibody was performed at room temperature for 45 min. For signal amplification and detection, either HRP-linked Streptavidin and subsequent ACE single solution were applied or VECTASTAIN® Elite® ABC kit and NovaRED™ substrate were used. The sections were counterstained with haematoxylin and mounted.

2.2.4.4 Histomorphometric Analysis

Stained sections from ostetomised femurs were scanned at 50-fold magnification using a light microscope (Leica DMI6000 B). Amounts of fibrous tissue, cartilage and bone were determined by tracing the circumference of the regarding tissue area using image analysis software (Leica MMAF 1.4.0 Imaging System).

Sections from ulnae were scanned at 200-fold magnification using a fluorescence microscope (Leica DMI6000 B) with double filter for red and green fluorescence. Using image analysis software (Leica MMAF 1.4.0 Imaging System), the endocortical and periosteal bone surface (BS, circumference), single (sLS) and double (dLS) label surface and inter label width (Ir.L.Wi) were determined. Using these parameters, mineralizing surface per bone surface (MS; (dLS+(sLS/2))/BS), mineral apposition rate (MAR; Ir.L.Wi/Ir.L.t, inter label time: 9 days) and bone formation rate (MARxMS/BS; $\mu m^2/\mu m/d$) were calculated

2.2.4.5 Statistics

Results are depicted as box-whiskers-plots. Statistical analyses were performed using SPSS statistics software (Version 19, IBM Corp, Chicago, USA). For comparison of MSC and vehicle-treated groups, Mann-Whitney-U-test was applied. To compare results within one treatment group, a paired Mann-Whitney-U-test was used. For comparison of multiple groups, one-way ANOVA with post-hoc Bonferroni correction for multiple testing was applied. $p \leq 0.05$ was assumed as significant.

3 Results

3.1 Contribution of Systemically Administered MSC to Bone Formation in Load-Induced Bone Modelling and Fracture Healing

Confirmation of Successful Systemic MSC Administration

To confirm the successful intravenous injection of the EGFP-transgenic MSC and their distribution, DNA isolated from lung, brain, kidney, heart, liver and spleen on the various time points was applied to PCR. On all time points, we were able to detect the EGFP-transgene in the lung. Representative PCR results of lung lysates of mice sacrificed after 21 days are depicted in Fig. 14. On day 10 and 16, respectively, the transgene could also be detected in heart, liver and kidney in isolated cases. A positive signal in the lung was also used as inclusion criterion for further investigations.

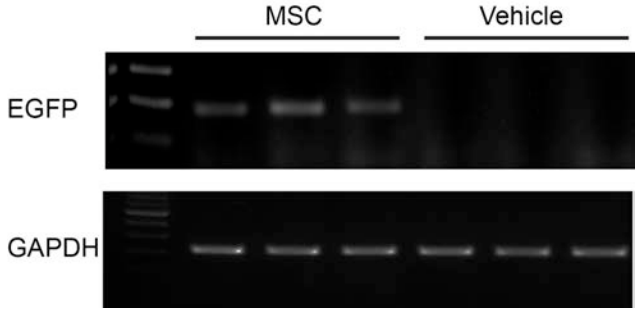

Fig. 14: Representative PCR results of lung lysates analysed for the EGFP-transgene of MSC- and vehicle-treated mice.

3.1.1 Contribution of Systemically Administered MSC to Load-Induced Bone Formation

In Vivo Loading

The non-invasive ulna loading was well tolerated by the mice. No sign of pain or pain related behaviour was observed. The body weight remained stable over the investigation period.

Recruitment and Localization of the Injected MSC

Immunohistochemistry for the chemo-attractive SDF-1 in ulnae of vehicle and MSC-treated mice revealed positive stained cells in the stroma in both treatment groups (Fig. 15 A and B). On day 16 of the loading regimen, there was no evidence for a regulation of SDF-1 by mechanical loading. Osteocytes in the cortex did not stain positive for SDF-1 (Fig. 15 C and D).

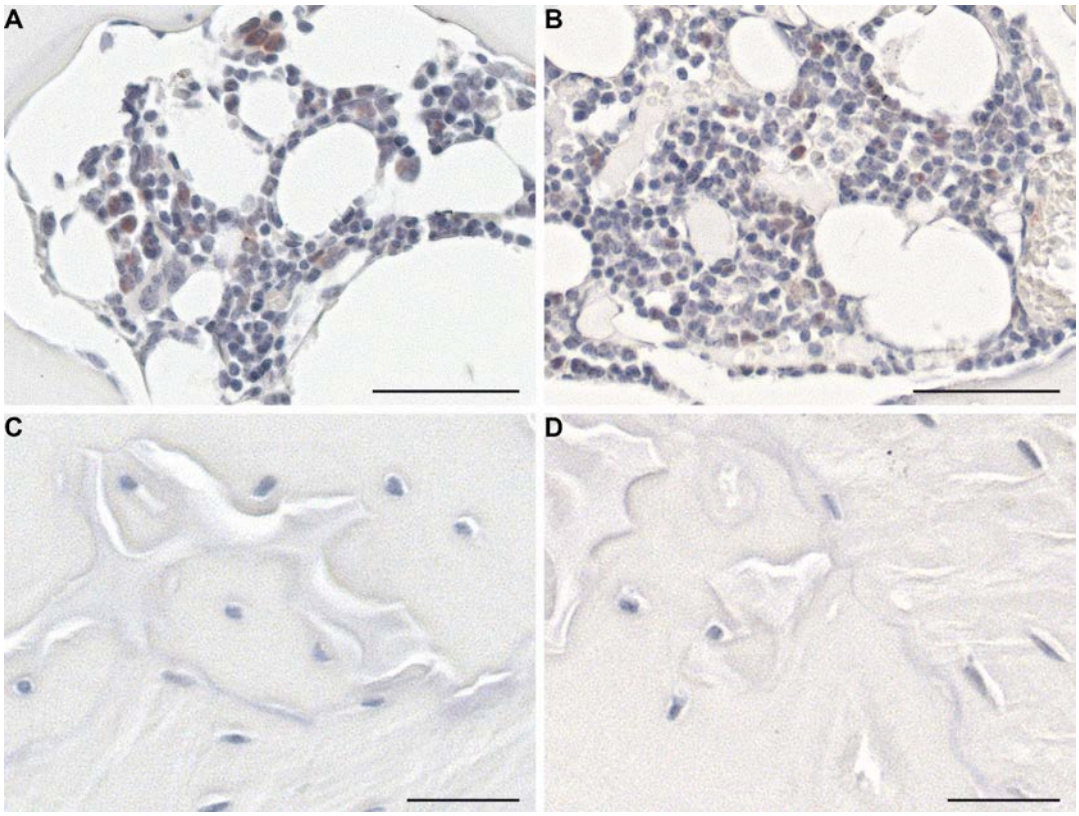

Fig. 15: Immunohistochmical staining for SDF-1 in the stroma (A, B) and cortex (C, D) of loaded ulnae of mice treated with vehicle (A, C) or MSC (B, D), day 16. Positive stained cells were detect in the stroma. Calibration bar = 50 µm.

Staining for EGFP in ulnae of vehicle and MSC-treated animals revealed no engraftment of the injected cells (Fig. 16).

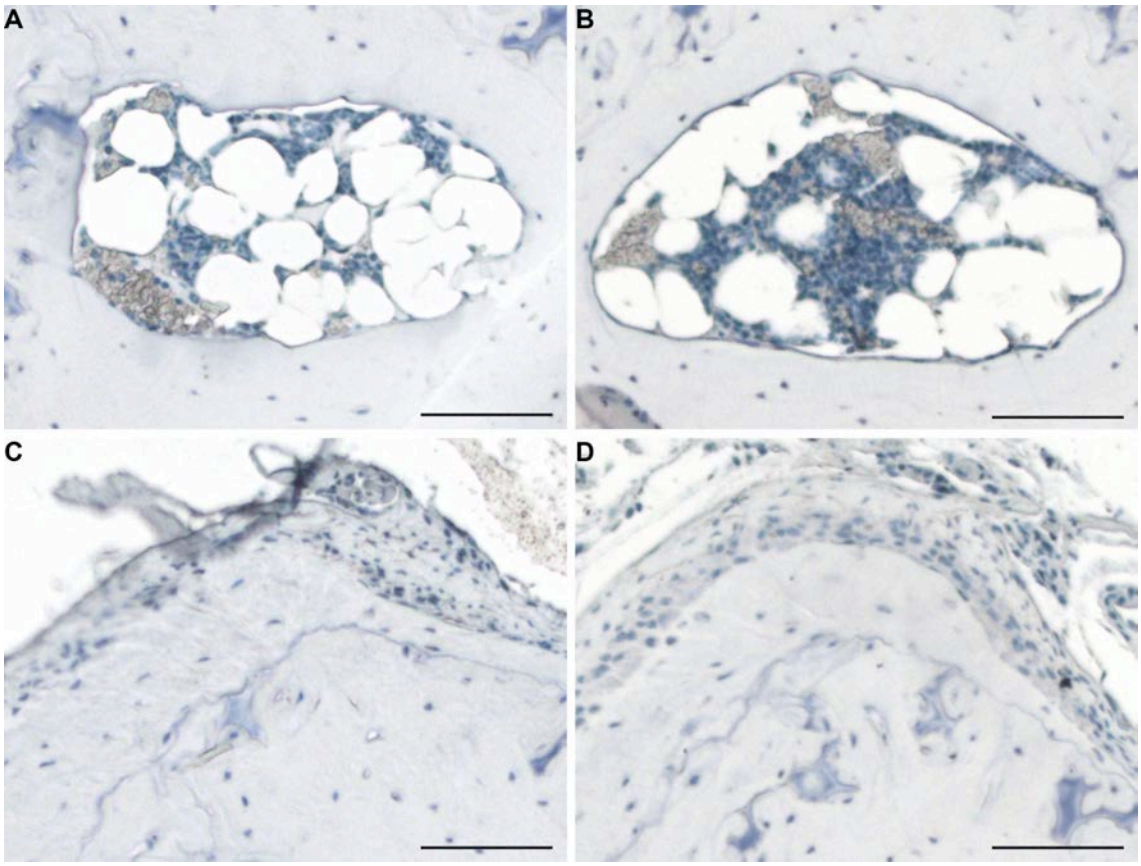

Fig. 16: Immunohistochemical staining of EGFP in loaded ulnae of mice treated with vehicle (A) and EGFP-transgenic MSC (B) on day 16. A, B: marrow cavity; C, D: cortex and periosteum. No positively stained cells were detected. Calibration bar = 200 µm

µCt Analysis of the Ulnae

To assess structural alteration caused by mechanical loading, left and right ulnae from vehicle and MSC-treated mice were scanned at a resolution of 8 µm per pixel using a µCT device. Assessment of a VOI of 1 mm height located 4 mm distally of the mid-shaft (highlighted in red in Fig. 17 A) showed a significant increase in BV, Ct.Wi. and MMIx in the vehicle and MSC-treatment groups (Fig. 17). Inter group comparison revealed no significant differences between vehicle and MSC treated animals.

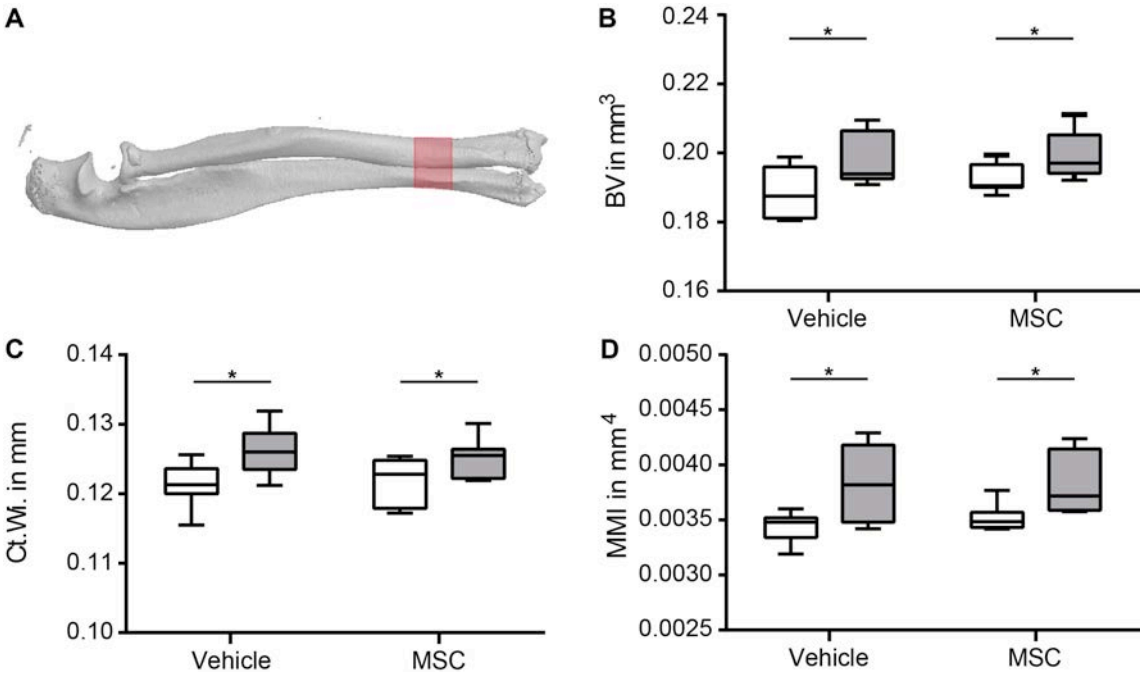

Fig. 17: µCT analysis of bone formation in ulnae after mechanical loading. The region assessed is highlighted red in the 3D-reconstruction (A). In this area, bone volume (B), cortical width (C) and moment of inertia (D) were assessed. Results are depicted as box plots; n=7 per group; asterisk denotes significant differences, $p \leq 0.05$.

Assessment of Dynamic Histomorphometric Parameters

To investigate load induced bone apposition, the mice received intraperitoneal injections of calcein green on day 3 and alizarin red S on day 12. Assessment of the bone formation rate revealed a significant increase after loading in both the endosteal (Fig. 18 E) and periosteal (Fig. 18 F) region. Again, no significant differences were detected between vehicle and MSC treated animals.

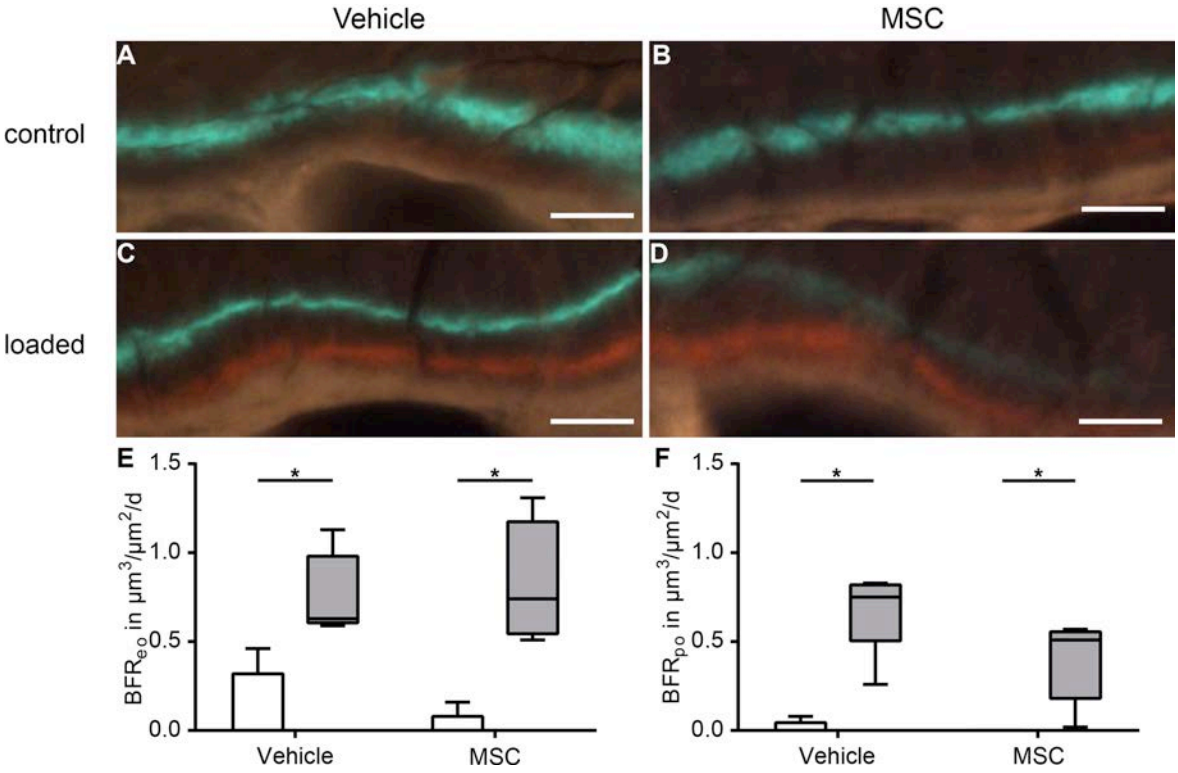

Fig. 18: Analysis of bone formation rate in ulnae after mechanical loading by dynamic histomorphometry. For assessment of dynamic histomorphometric parameters, calcein green and alizarin red S were administered on day 3 and 12 of the loading regimen, respectively. Representative fluorescent micrographs are depicted in A-D. Calibration bar = 10 µm. Bone formation rate was evaluated in the endosteal (E) and periosteal (F) location. Results are presented as box plots. n=5 per group; asterisk denotes significant differences, $p \leq 0.05$.

3.1.2 Contribution of Systemically Applied Mesenchymal Stem Cells to Fracture Healing

The contribution of systemically applied MSC to fracture healing was assessed by immuno-histology, µCT-analysis, histomorphometry and biomechanical testing.

Recruitment and Localization of the Injected MSC

Three days after osteotomy, positive staining for SDF-1 was detected in the stroma and periosteum of ostetomised femurs (Fig. 19). There were no obvious differences between vehicle and MSC treated animals visible.

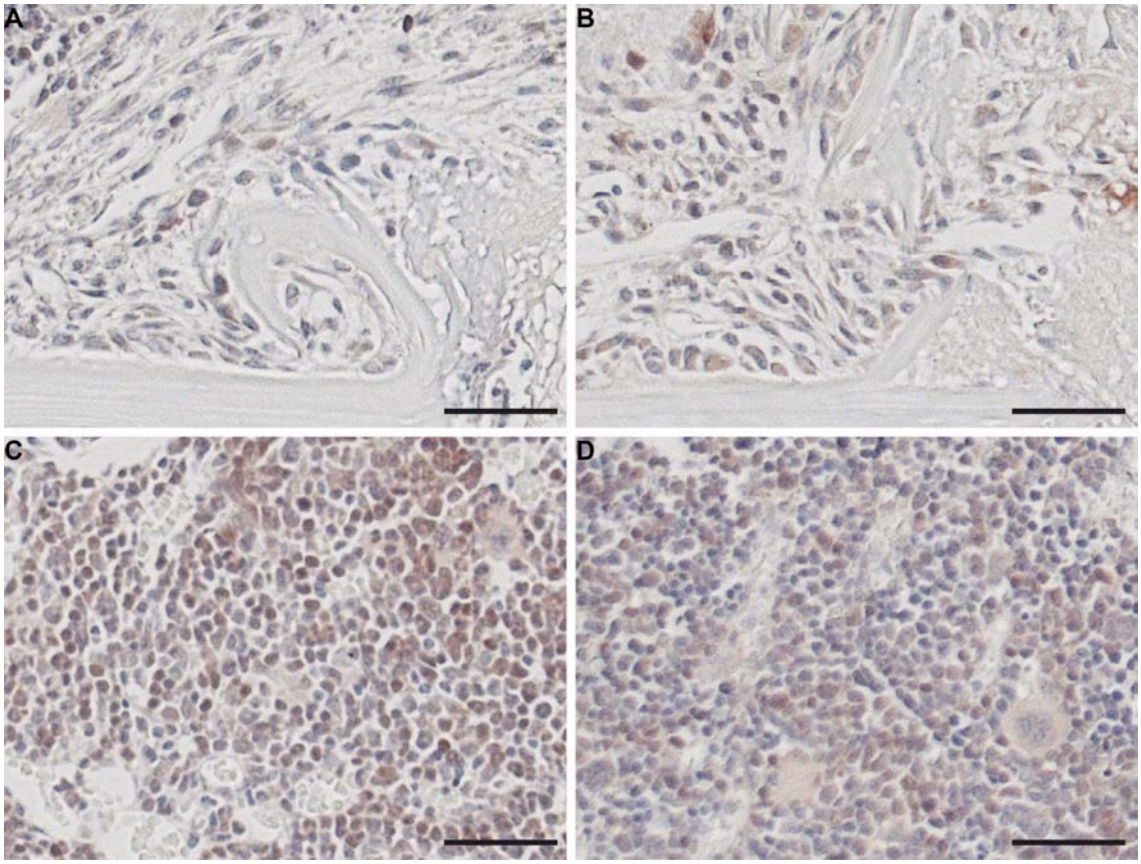

Fig. 19: Staining for SDF-1 (CXCL-12) in animals treated with vehicle (A, C) and EGFP-transgenic MSC (B, D) three days after surgery. In both the osteotomy region (A, B) and the stroma (C, D) positive staining for SDF-1 were observed in both treatment groups. Calibration bar = 50 µm.

By immunohistochemical staining for EGFP, some EGFP-positive cells could be detected in the bone marrow of the osteotomised femurs of MSC-treated mice three days after injection, but not in the osteotomy itself. Staining for EGFP in right femurs of MSC-treated mice on day 10 revealed few cells in the bone marrow and engraftment of MSC in the evolving callus (Fig. 20), where they persisted until sacrification on day 21 (Fig. 21).

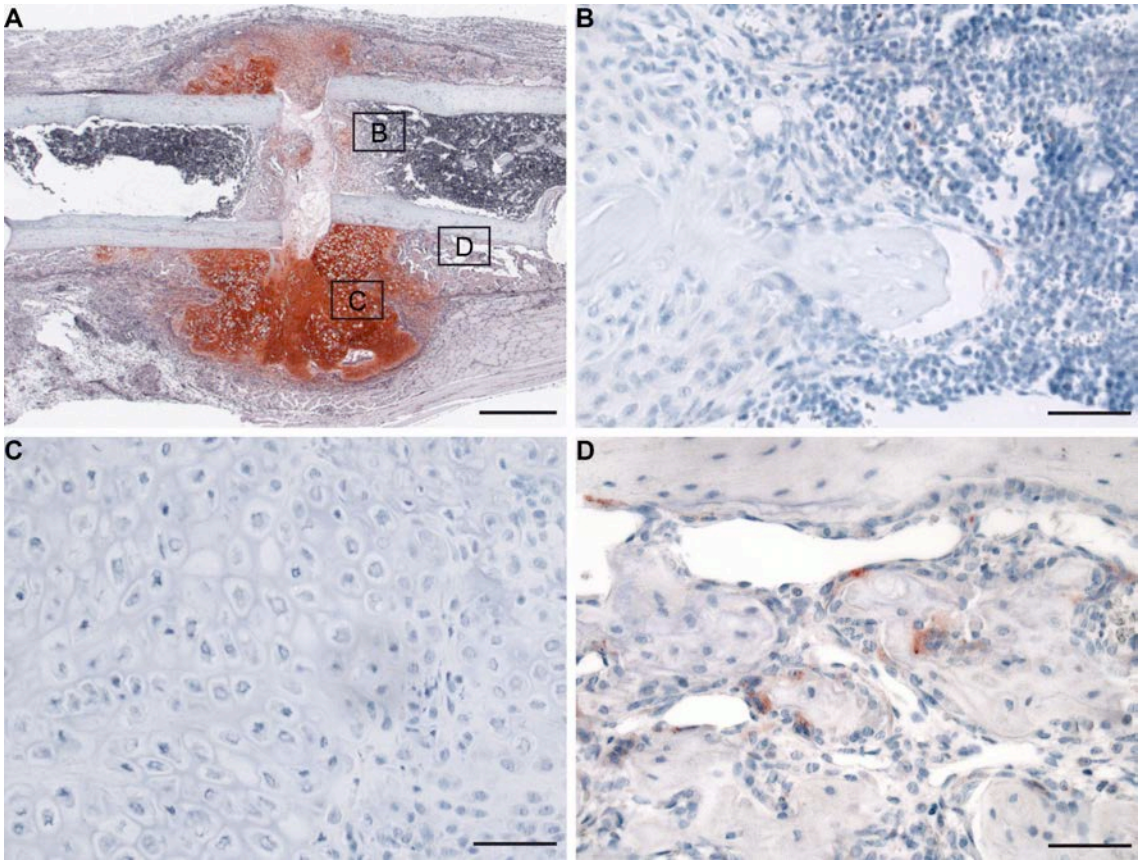

Fig. 20: Immunhistochemical staining of EGFP in MSC-treated mice after 10 days. A: Overview of the whole callus stained with safranin-O; calibration bar = 500 µm. B-D: magnifications of the transition zone of endosteal callus and bone marrow (B), the cartilaginous partition of the callus (C) and zones of woven bone formation (D). B-D calibration bar = 50 µm.

MSC present in fracture calli on day 21 were predominantly located at the margin of newly formed woven bone (Fig. 21 H). No or only few positive cells were detected in the cartilaginous part of the calli or in the bone marrow on day 10 and 21 (Fig. 21). No positive signals could be detected in the left, intact femurs of mice that received an osteotomy of the right femur or in uninjured mice. In vehicle-treated animals, no positive stained cells were detected (Fig. 21 C, E, G).

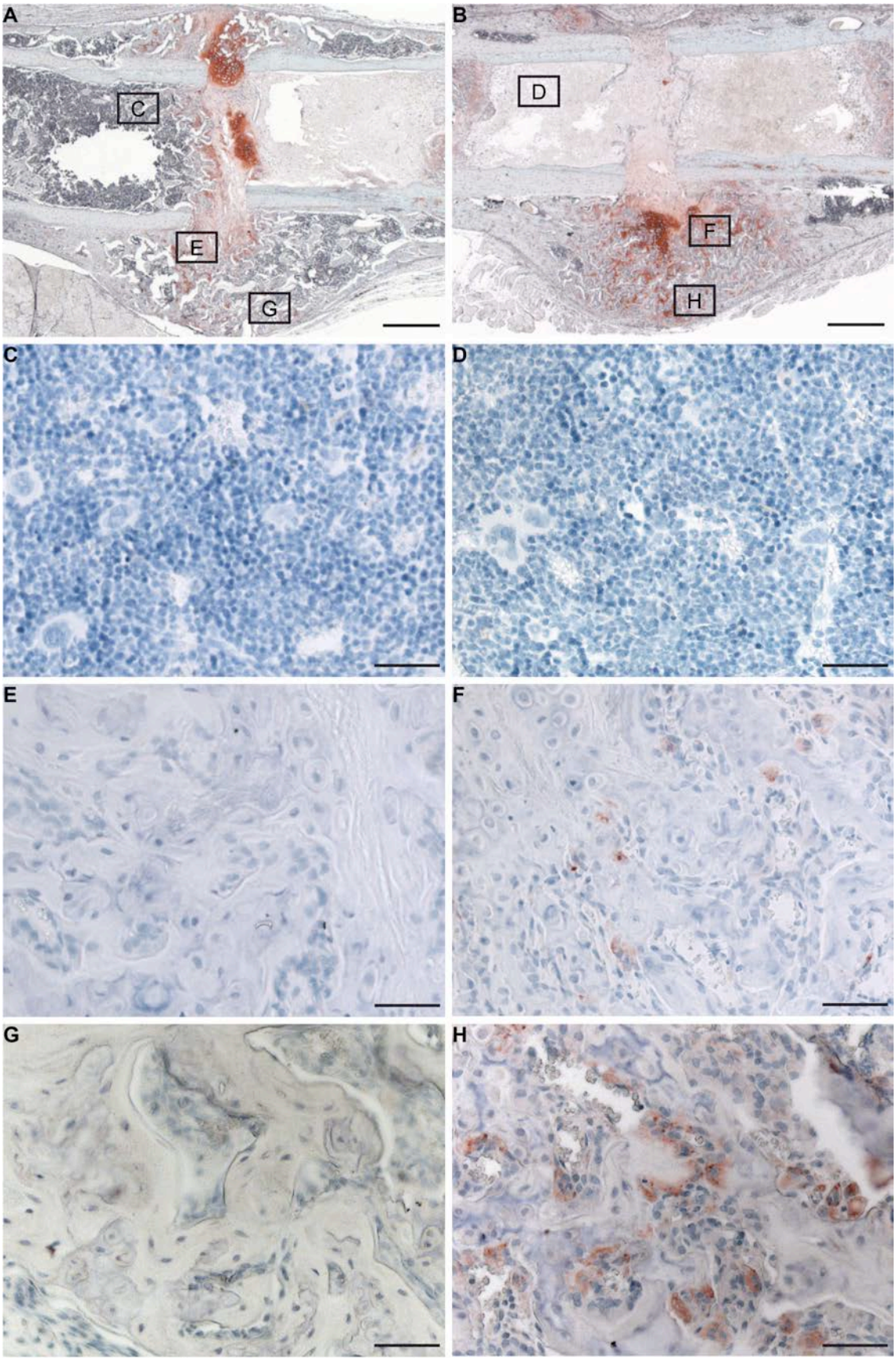
A
C
E
G
B
D
F
H
C
D
E
F
G
H

Fig. 21: Immunohistochemical staining of EGFP in longitudinal sections of fracture calli of vehicle (A, C, E and G) and EGFP-transgenic MSC-treated (B, D, F and H) mice 21 days after fracture. A+B: Overview over the whole callus of vehicle (A) and MSC-treated mice (B), calibration bar = 500 µm. C-H: magnifications of the bone marrow (C, D), the cartilaginous partition of the callus (E, F) and zones of woven bone (G, H). C-F calibration bar = 50 µm.

µCT-Analysis of the Osteotomised Femurs

To investigate the callus micro-architecture after 21 days in vehicle or MSC-treated mice, the calli were scanned with a resolution of 8 µm per pixel using a µCT-device. Comparative analysis revealed a significant increase by 49 % ($p=0.026$) in the bone volume in the former osteotomy gap in mice of the MSC-treatment group relative to the vehicle group. The parameters TV and BV/TV were not significantly altered but elevated in the MSC-group by 21 and 24 %, respectively. Analysis of the biomechanical properties of the fracture calli of vehicle and MSC-treated mice via three-point bending showed no significant differences between the treatment groups (Fig. 22).

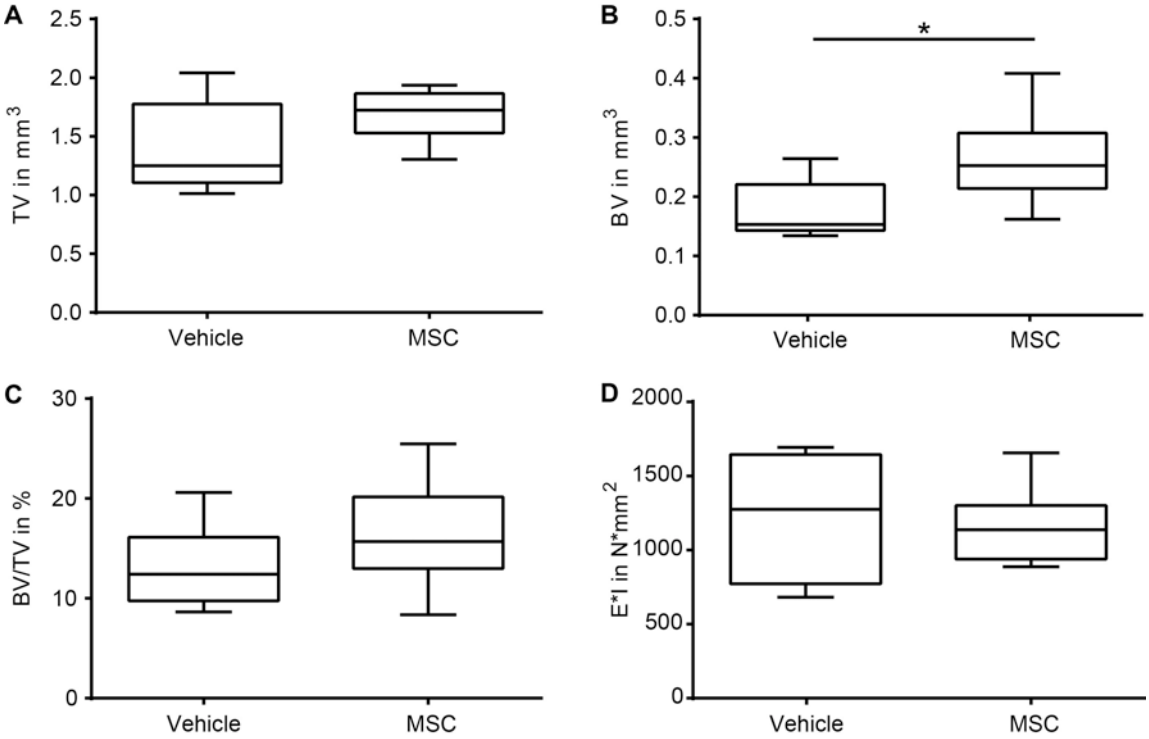

Fig. 22: Assessment of the healing outcome after 21 days by µCT-analysis of the former fracture gap and biomechanical testing. No significant differences could be detected in the whole callus volume (TV) (A), but the bone volume (BV) is significantly elevated in the MSC treatment group (B). The relative proportion of bone in the callus (BV/TV) is also increased in the MSC treatment group, but not significantly (C). Biomechanical testing of the fracture calli showed no differences (D). Results are depicted as box plots; n=6 per group. Asterisk denotes significant differences, $p \leq 0.05$.

Histological Assessment of the Osteotomized Femurs

For histomorphometric analyses, paraffin-embedded sections of femurs harvested on day 3, 10 and 21 were stained with safranin-O and light green. Using image analysis software, the sections were analysed for cartilage, fibrous tissue and bone. On day 3, no differences in callus composition were evident (not shown). On day 10, analyses revealed a 20 % higher content of cartilage in the calli of the MSC-treatment group (Fig. 23 E). Assessment of the fracture gap on 21 days after osteotomy analogously to µCT analysis revealed a slightly larger callus with more fibrous tissue (+ 22 %) and bone (+ 60 %) in the MSC treatment group (Fig. 23 F). The differences in callus composition did not reach significance.

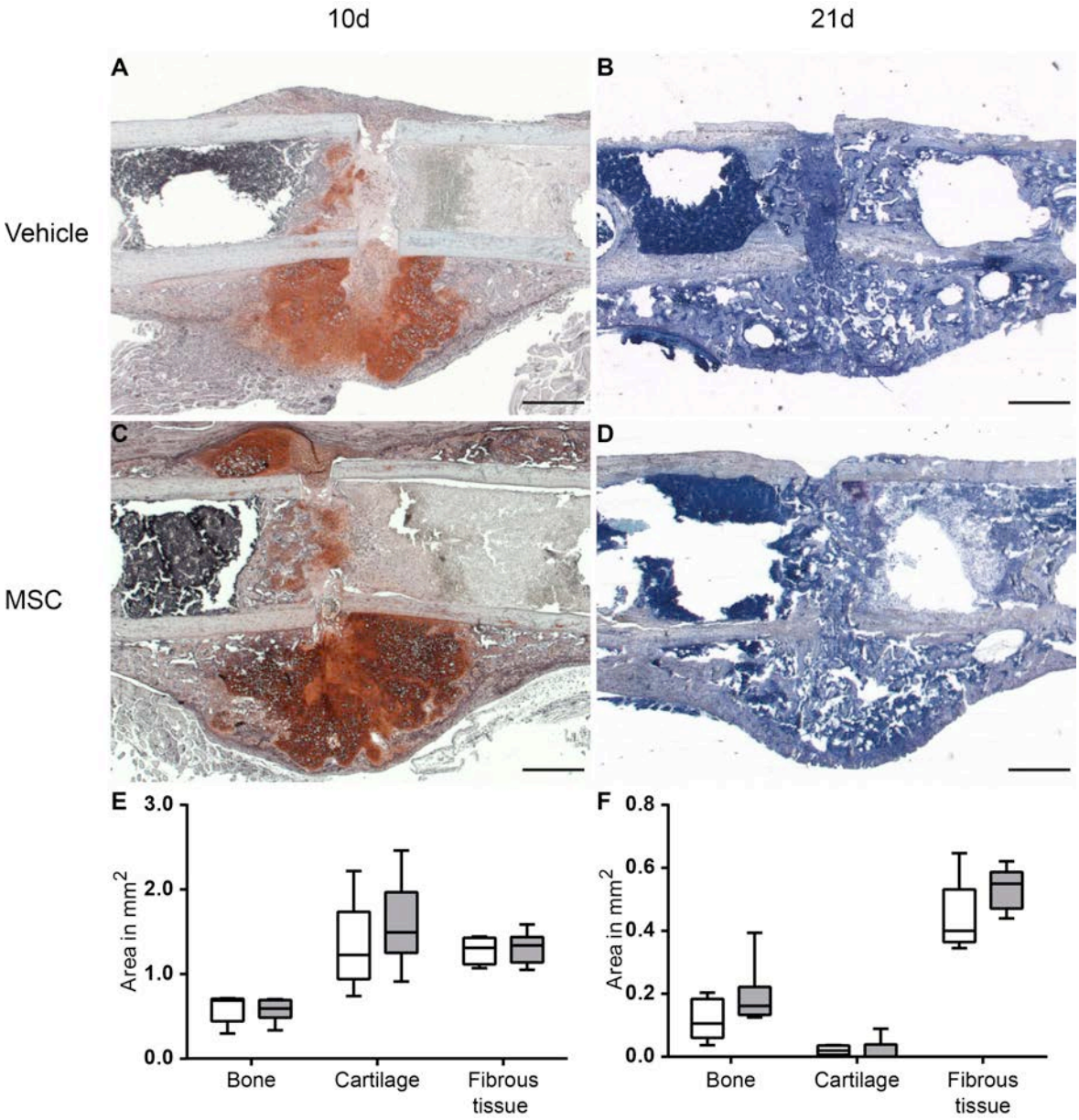

Fig. 23: Histomorphometric analysis fracture calli 10 days (A, C, E) and 21 days (B, D, F) after surgery. The histomorphometric assessment of the whole callus on day 10 (E) and the former osteotomy gap on day 21 (F) revealed no significant alterations in the callus composition between vehicle (white bars) and MSC treated (grey bars) mice. Contents of bone and cartilage were increased in MSC-treated mice relative to the vehicle treatment group on day 10 and 21, respectively, but not significantly. A+C: safranin-O-stained calli from mice sacrificed after 10 days. Scale bar represents 500 µm. E+F: Histomorphometric analysis. White bars: vehicle group, grey bars: MSC-treatment. Results are depicted as box plots; n=6 per group.

Analysis of Serum Cytokine Levels

To investigate, if the systemically administered MSC exert immunomodulatory action, serum of mice treated with vehicle or MSC solution obtained three days after osteotomy was analysed for the cytokines IL-1β, IL-6, IL-10, TNFα and MCP-1. Multiplex analysis demonstrated no significant differences in the respective serum levels. The values obtained were largely in the physiological range [62], while only TNFα appeared to be slightly elevated (data not shown).

3.2 Local Application of Autogenic and Allogeneic Mesenchymal Stem Cells for Large Bone Defect Repair

In Vitro Characterization of MSC in Collagen Gel

To assess the cell viability in the gel matrix, the cells were stained with propidium iodine and Hoechst 33342 dye one and 24 h after seeding. One hour after seeding, the cells in the gel matrix appeared rounded. Furthermore, the cells were stained double positive for PI and Hoechst dye, indicating reduced viability (Fig. 24 A). 24 hours after seeding, most cells displayed a stretched, fibroblast-like cell morphology (Fig 24 C) and reduced double staining (Fig. 24 B). Cells embedded in the collagen matrix were also analysed for the apoptosis marker p53 one and 24 h after seeding. Qualitative PCR revealed no noticeable increase in p53. These observations were consistent for all donors.

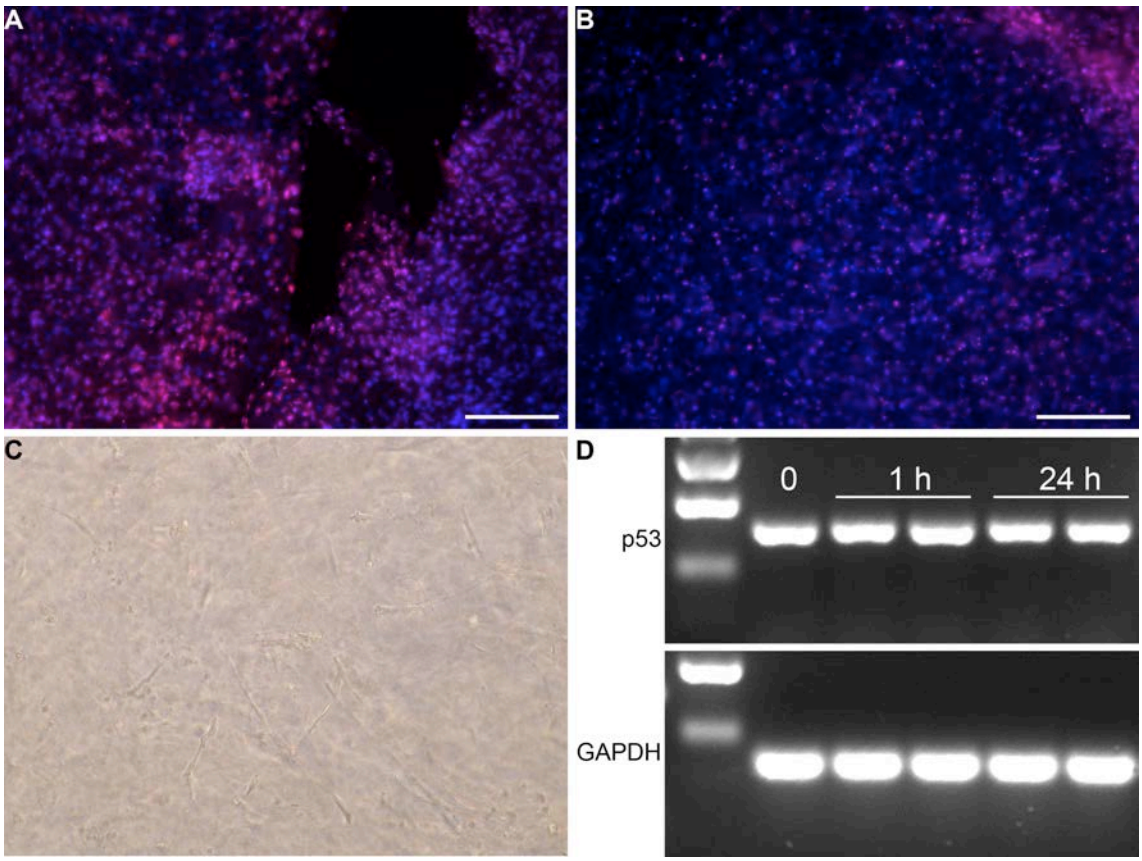

Fig. 24: Representative staining of the viability of human mesenchymal stem cells seeded in a collagen matrix using Hoechst 33342 dye and propidium iodine 1 h (A) and 24 h (B) after seeding. After 24 h, the embedded MSC display a fibroblast-like phenotype (C). p53 remained on the pre-seeding level (D). Calibration bar = 20 µm.

To investigate the cell's osteogenic differentiation potential, they were differentiated into the osteogenic lineage for 21 days. The MSC differentiated into the osteoblast lineage, demonstrated by qualitative staining for alkaline phosphatase and mineral deposition (Fig. 25).

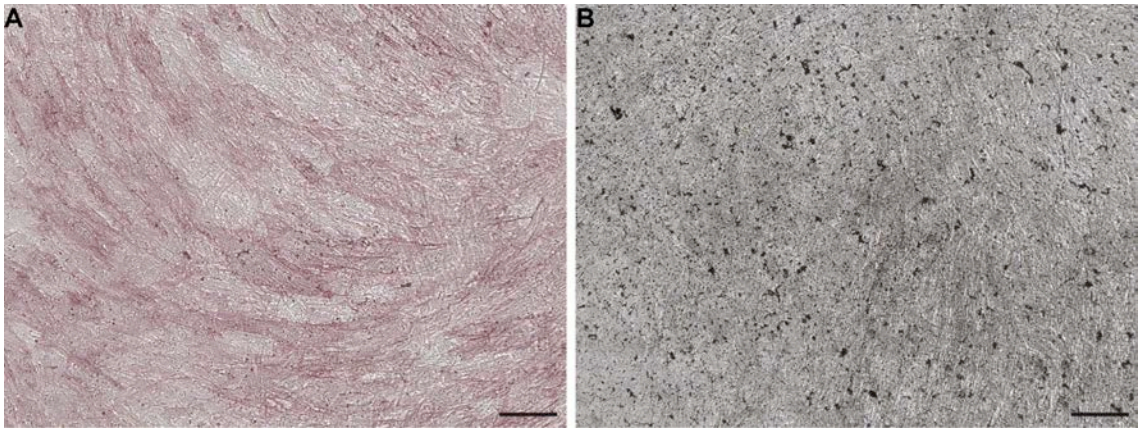

Fig. 25: Qualitative analysis of osteogenic MSC differentiation. After 21 days of cultivation, the cells were stained for alkaline phosphatase (A) and for mineralisation using von Kossa method (B). Calibration bar = 100 µm.

Histomorphometric Assessment of the Defect Region

Histologic and histomorphometric assessment of the defect region from mice with empty defects, defects filled with collagen and the respective cell treatment groups revealed considerable differences in the healing outcome. In animals with untreated defect, the formation of a typical atrophic non-union with closed or almost closed cortical ends showing sings of resorption was found (Fig. 26 A). In defects filled with collagen gel, a larger regenerate with some bone formation was evident but no bridging of the defect (Fig. 26 B). In mice treated with allogeneic MSC, the defect region was predominantly filled with dense fibrous tissue (Fig. 26 C), while defects in animals treated with autogenic MSC were predominantly filled with bone. (Fig. 26 D). Histology also revealed good integration of the regenerated bone in mice treated with autogenic MSC.

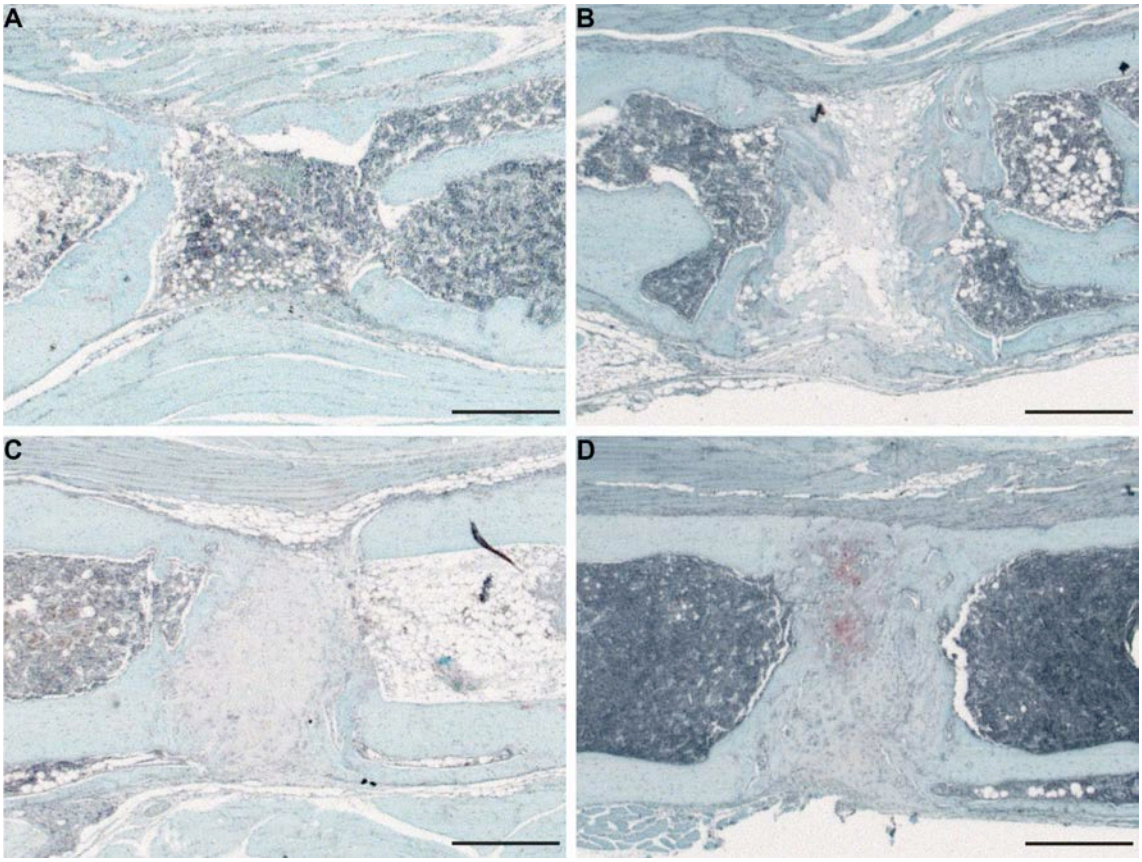

Fig. 26: Safranin-O stained sections of the defect region in animals with empty defect (A), and defects treated filled with collagen gel (B), allogeneic MSC (C) and autogenic MSC (D). Scale bar represents 500 µm.

Quantification of the tissue composition confirmed the visual observation. Implantation of cell-free collagen resulted in a significant larger regenerate area compared to empty defects. In animals treated with autogenic MSC, significantly more bone was detected than in empty defects (+ 200 %, p=0.0002), collagen-filled defects (+ 150 %, p=0.0022) or defects treated with allogeneic MSC (+ 200 %, p=0.0002). There were no significant differences between bone content in empty defects, defects filled with collagen-gel and defects filled with allogeneic MSC-treated defects. In cartilage content, no differences were obvious (Fig. 27). In animals treated with autogenic MSC, significantly less fibrous tissue was detected when compared to the other collagen-gel treated groups.

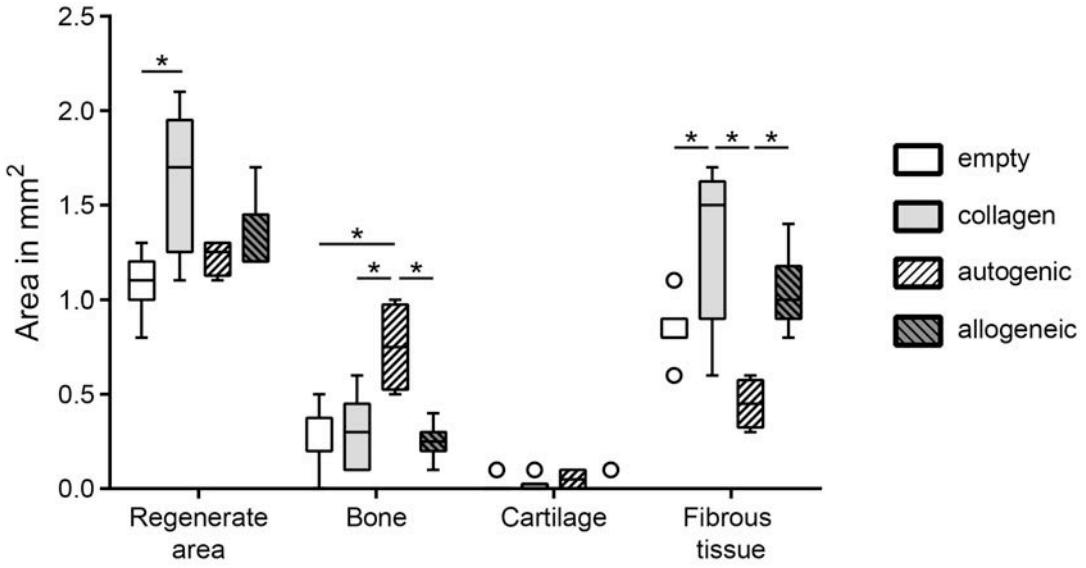

Fig. 27: Histomorphometric analyses of the defect region in animals with empty defect or treated with autogenic and allogeneic MSC, respectively, after 35 days. n =4-8 per group. Asterisk denotes significant differences; $p \leq 0.05$.

µCT Analysis of the Defect Region

Analysis of the defect region using µCT confirmed the data obtained by histomorphometry. Implantation of cell-free collagen gel resulted in a significant increase in TV compared to an empty defect (+ 69 %, p=0.0496). When cell-seeded gels were implanted into the defect, TV was also increased, but the difference did not reach statistical significance. The BV/TV ratio was significantly higher in animals treated with autogenic MSC compared to animals with untreated defects (+ 205 %, p<0.0001), defects treated with cell-free collagen gel (+ 131 %, p=0.0005) or defects of animals that received allogeneic cells (+ 132 %, p=0.0003) (Fig. 28).

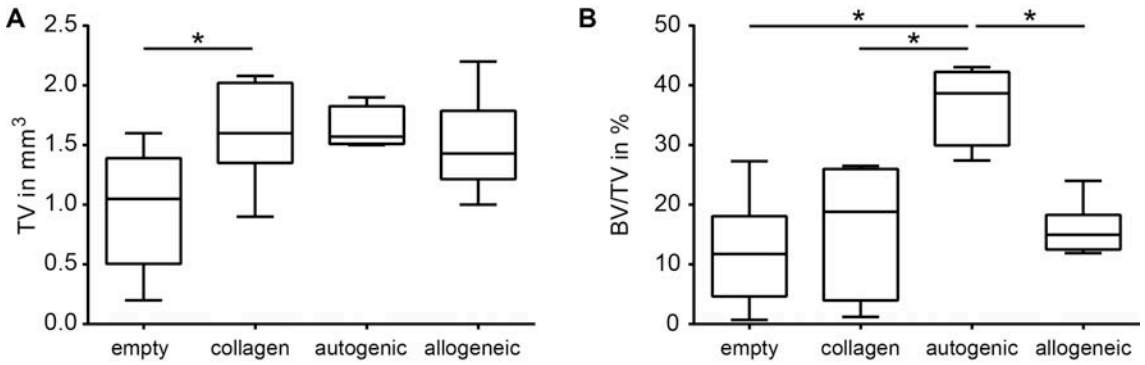

Fig. 28: µCT analyses of the defect region (A) and the bone per tissue volume ratio (B) in animals with empty defects and defects filled with cell-free collagen gel, collagen gel seeded with autogenic cells or collagen gel with allogeneic cells on day 35 after implantation. n = 4-8 per group. Asterisk denotes significance; $p \leq 0.05$.

Immunohistochemic Analyses

In order to investigate the presence of the implanted human MSC, longitudinal sections of femurs were stained for human β2-microglobulin. Three days after implantation, positively stained cells were found in both, the collagen gel seeded with allogeneic cells and the gel seeded with autogenic MSC. Ten days after surgery, positively stained cells could be detected in the collagen matrix of the implanted gels in both groups as well. After 35 days, in the autogenic treated group, human cells were detected in the marrow compartments in the newly formed bone, but the newly formed bone itself was not stained positive for β2-microglobulin. Cartilaginous areas in the defect region were negative for β2-microglobulin, too. In mice treated with allogeneic MSC, there were still elongated cells with fibroblastic phenotype embedded in the collagen matrix, that were stained positive for β2-microglobulin (Fig. 29).

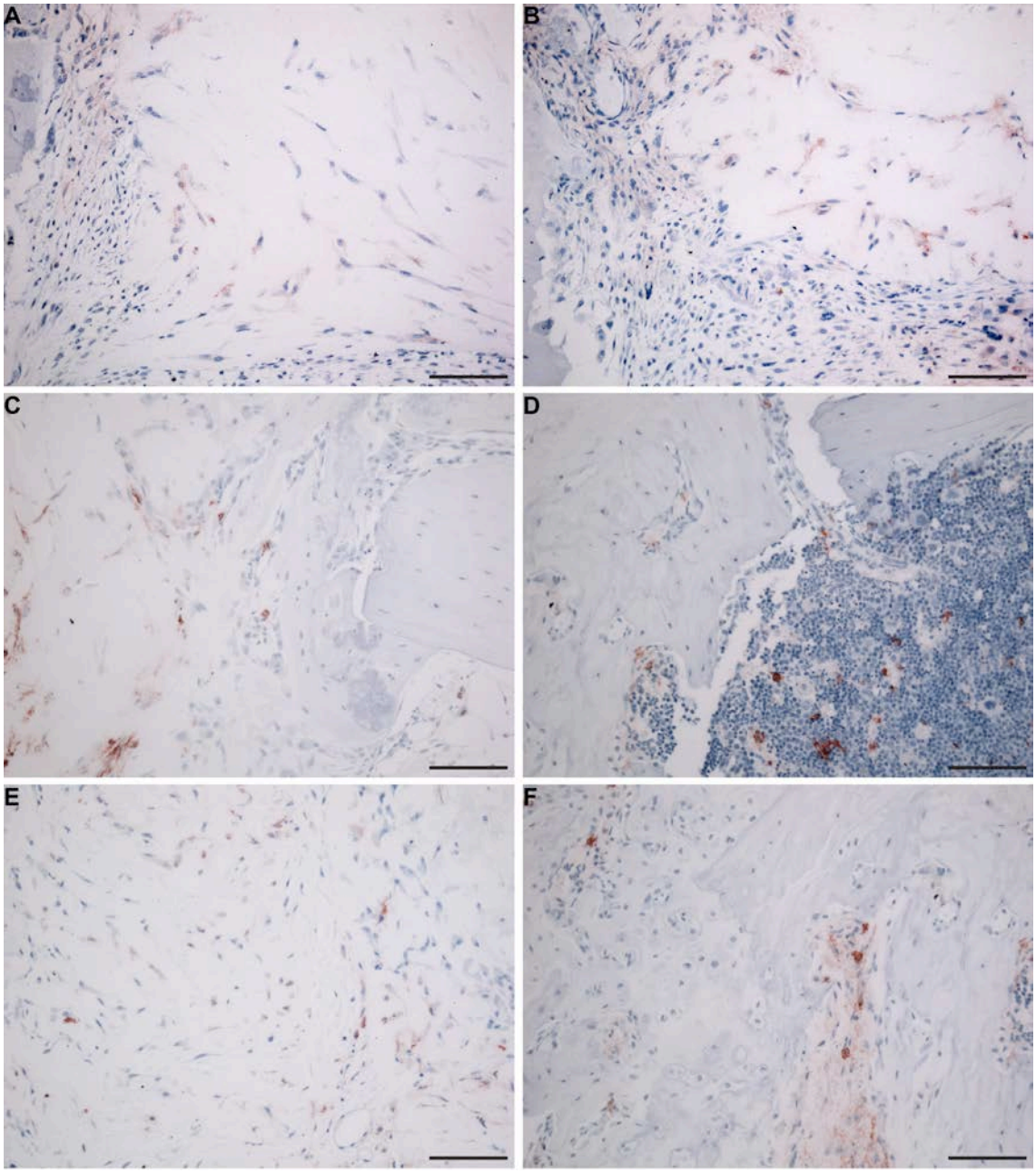

Fig. 29: Immunohistochemical staining for human β2-microglobulin in mice treated with allogeneic (A, C, E) and autogenic (B, D, F) human MSC on day 10 (A, B) and 35 (C-F) after implantation. A-D: interface of bone and collagen gel; E+F: centre of defect/collagen gel. Positive stained cells were found in the gel at all time points. New formed bone did not stain positive for human β2-microglobulin. Calibration bar = 100 µm.

To investigate if an adverse immunoreaction towards the implanted MSC occurred, paraffin-embedded sections were stained for human $CD8^+$ T-cells. On day 3, no positive stained cells were found in mice that received autogenic MSC (Fig. 30 B). In contrast, $CD8^+$ cells were found next to the collagen gel in allogeneic treated mice (Fig. 30 A). Furthermore, in some animals that received

allogeneic cells, massive $CD8^+$ cell influx was detected in the femur distally of the osteotomy.

After 10 days, few positively stained cells were detected in animals treated with allogeneic cells, while there were no positively stained cells evident in animals treated with autogenic cells (Fig. 30 C and D).

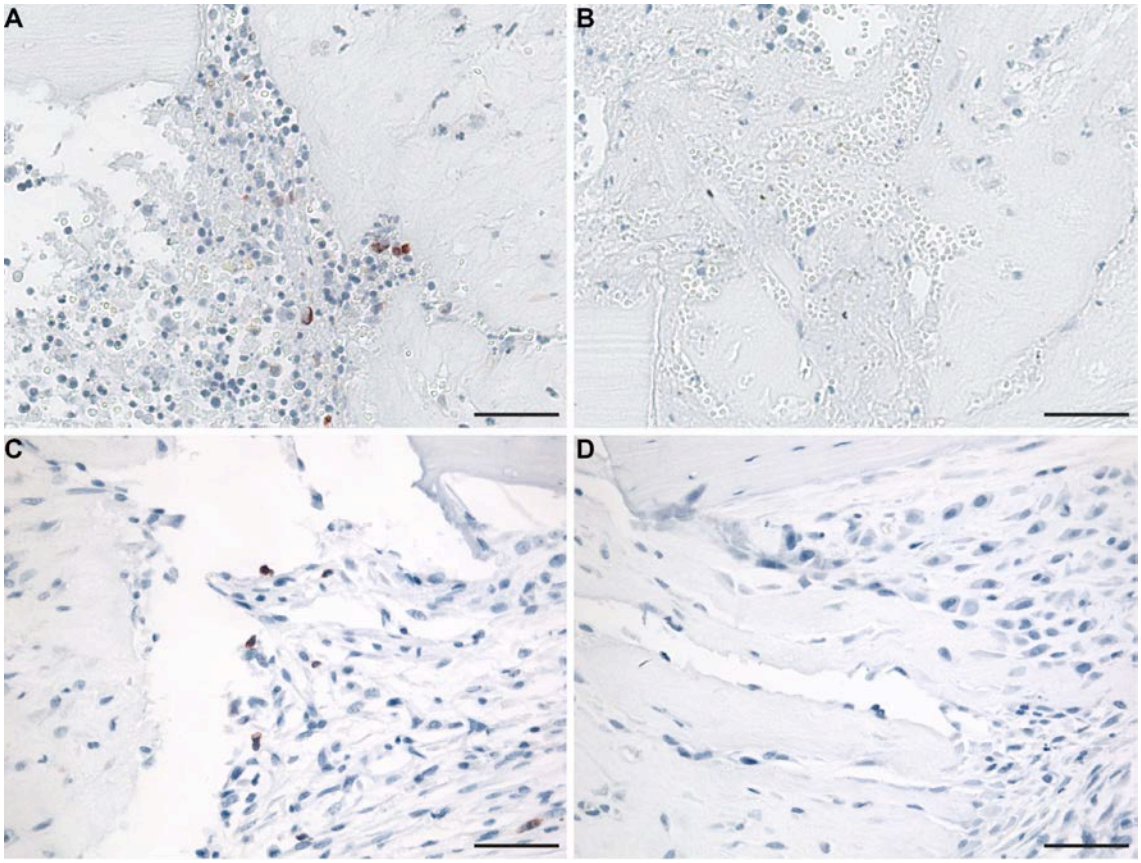

Fig. 30: Staining of human CD8 3 and 10 days after implantation of allogeneic (A, C) and autogenic (B, D) MSC. In allogeneic treated mice, $CD8^+$ cells were detected, while there were no positive stained cells in animals treated with autogenic MSC. Calibration bar = 50 µm.

To determine if there are differences in the formation of blood vessels, sections were stained for CD31 (PECAM), a marker for endothelial cells. After 10 days, positive stained structures were found in the surrounding of the collagen gel in both, mice treated with allogeneic and autogenic MSC (Fig. 31 A and B). There were no obvious differences evident. After 35 days however, more stained structures were detected in mice that received autogenic MSC compared to mice that received allogeneic cells (Fig. 31 C and D). Also the distribution of the vessel-like structures differed between the groups; while they were mainly localized in the

soft tissue in the surrounding of the residual collagen gel in the allogeneic treated group, vessel-like structures were found throughout the whole regenerate in mice that were treated with autogenic MSC (arrowheads in Fig. 31 E and F)

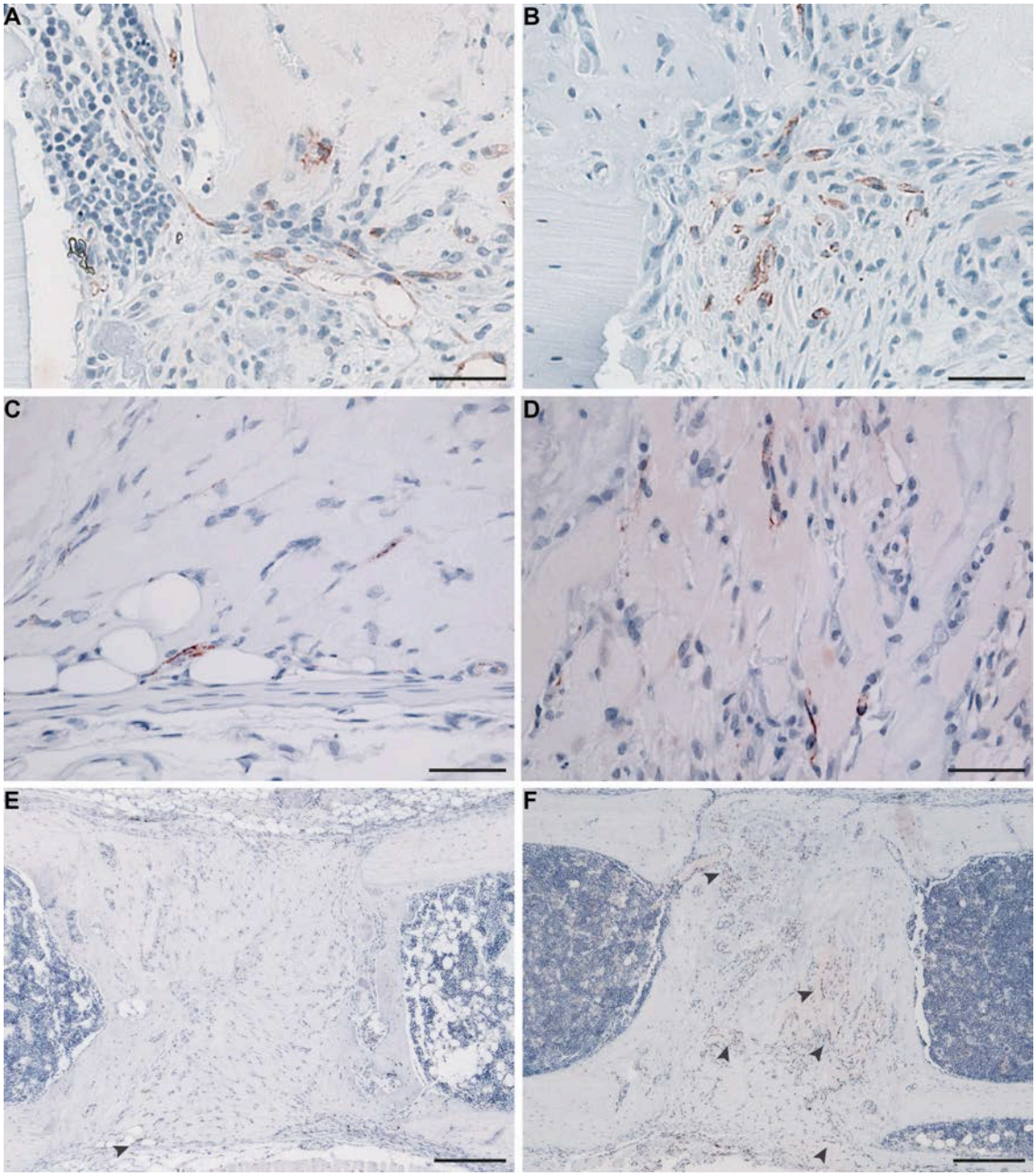

Fig. 31: Immunohistochemical staining for CD31 10 (A, B) and 35 (C - F) days after implantation of allogeneic (A, C, E) or autogenic (B, D, F) MSC. A - D: calibration bar = 50 µm; E+F: calibration bar = 250 µm.

To gain insight into the differences in bone formation, the transcription factor Runx2, an early osteogenic marker, was stained. In mice treated with autogenic

MSC, more Runx2 positive cells were detected in the defect region compared to mice that received allogeneic MSC (Fig. 32).

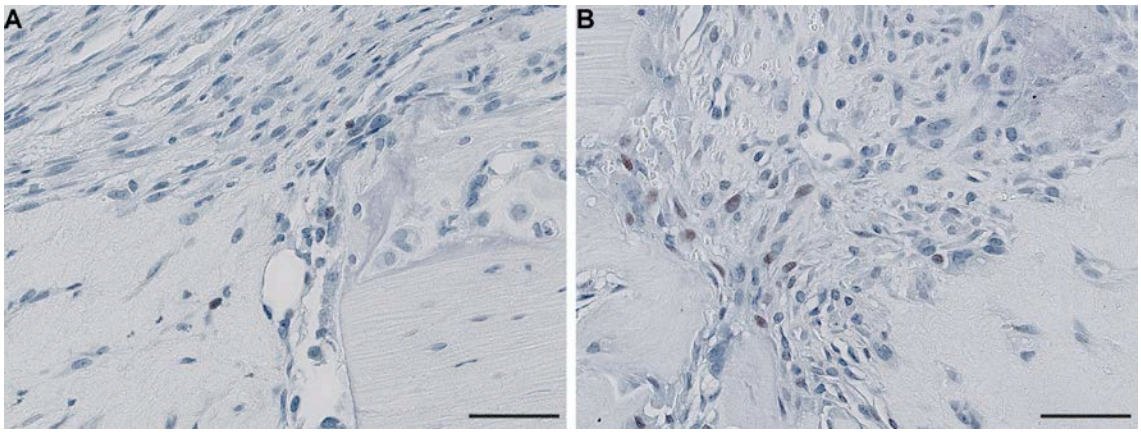

Fig. 32: Immunohistochemical staining for Runx2 in mice treated with allogeneic (A) or autogenic (B) MSC on day 10 after implantation. In mice treated with autogenic MSC, more cells stained positive for Runx2 were found. Calibration bar = 50 µm.

After 35 days, sections were stained for the late osteogenic marker osteocalcin. In both animals treated with autogenic and allogeneic MSC, positive staining for osteocalcin was found in the defect region. As expected, more staining was found in the defect region of the autogenic treated group, as more bone was formed here. In animals treated with allogeneic cells, positively stained cells with elongated, fibroblastic phenotype were found in the residues of the collagen gel (Fig. 33).

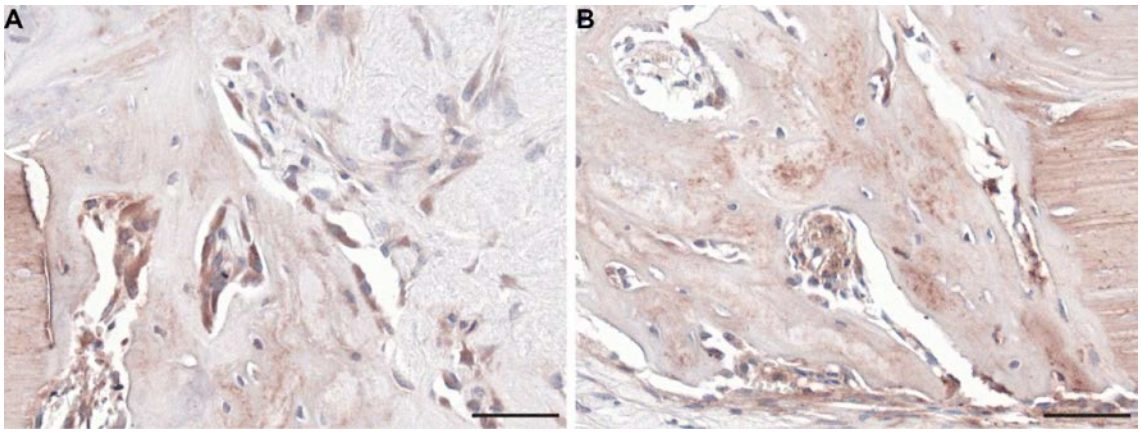

Fig. 33: Immunohistochemic staining for osteocalcin in mice treated with allogeneic (A, C) and autogenic (B, D) MSC. A, B: overview of the defect region; calibration bar = 250 µm. C, D: calibration bar = 100 µm.

4 Discussion

The aim of this study was to investigate, firstly, if systemically administered MSC support bone formation induced either by non-invasive mechanical loading or by bone injury and secondly, if locally implanted autogenic and allogeneic MSC are equally able to consolidate segmental bone defects.

4.1 Contribution of Systemically Administered MSC to Bone Formation in Load-Induced Bone Modelling and Fracture Healing

4.1.1 Contribution of Systemically Administered MSC to Load-Induced Bone Formation

Due to the anticipation, that circulating osteoblast precursors could be recruited into bone remodelling compartments in physiological bone remodelling [54], it was hypothesized that systemically administered MSC are recruited in load induced bone modelling. In contrast to the hypothesis, no engraftment of the injected cells in regions of new bone formation was detected. Apparently, the local stimulus and the subsequent - presumably only local - up-regulation of several chemokines like CCL2, CCL7 or PDGF as it is described in literature is not sufficient to recruit the injected cells [76]. Staining for SDF-1, the factor that is anticipated to be predominantly responsible for stem cell recruitment, revealed positive cells in the stroma of both non-loaded and loaded ulnae in both treatment groups. There were no considerable differences in the staining. Mantila Roosa et al. postulated, that chemokines up-regulated within the first hours after mechanical loading may be active to recruit osteoblasts or their committed precursors to the site of loading. Later in the phase of matrix formation, no additional cells are needed, so chemokines - among them SDF-1 - are rather down-regulated [76]. In the present study, no noticeable regulation of SDF-1 by mechanical loading was evident by immunostaining on day 16 of the loading regimen. Probably, gene expression analysis is more accurate to detect minor regulatory effects.

Independent of further treatment, significant increases in BFR and also in the structural parameters BV, Ct.Wi. and MMIx were detected after loading, as it was to be anticipated form literature [71]. However, there was no further enhancement of bone formation after systemic delivery of MSC. So, the increase in bone formation is rather due to an activation of formerly quiescent bone lining cells that were activated by mechanical stimuli [90] or recruitment of local or perivascular MSC.

4.1.2 Contribution of Systemically Applied Mesenchymal Stem Cells to Fracture Healing

Fracture healing is a complex cascade of cellular processes. One step mandatory for successful healing is recruitment and proliferation of stem- and/or progenitor cells committed to the osteoblast lineage. The importance of this step led to the hypothesis that systemic administration of MSC, the natural progenitor of osteoblasts, might be beneficial for the healing of fractures. Indeed, several studies reported the recruitment of intravenously injected osteoprogenitor cells to sites of bone healing [28, 48, 73]. These studies also demonstrated a participation of the injected MSC on fracture healing; however, the reported effects were rather moderate, ranging from no beneficial effect [28] to enhanced bone formation with [48] or without [73] improvement of biomechanical properties.

Mandatory for progenitor cell recruitment is an appropriate stimulus. During fracture healing, a plethora of cyto- and chemokines is up-regulated, as fracture is associated with a certain degree of inflammation and hypoxia [63, 64]. Some pro-inflammatory cytokines execute chemo-attractive action on progenitor cells of the mesenchymal [20] and presumably also the endothelial lineage. A described previously, CXCR-4/SDF-1 signalling is believed to be the key mechanism of stem cell trafficking and recruitment [21, 61]. Immunohistochemistry revealed strong expression of SDF-1 after osteotomy, so a stimulus for progenitor cell migration and recruitment is present. Recruitment of the MSC to the fracture site seems to be time dependent, as no labelled cells could be detected in or near the osteotomy

on day 3 after surgery but on day 10 and apparently even more on day 21 after surgery. This observation is supported by studies reporting a time-dependent manner of the recruitment of endogenous circulating osteogenic progenitor cells in a parabiosis model and the observations of Granero-Moltó et al. [48], that intravenously injected cells migrate to a fracture site with time, with the first evidence for a fracture-near location 3 days after fracture. However, proliferation of the injected cells and thus increased numbers in later stages of fracture healing cannot be excluded.

To confirm a systemic presence of the injected cells in the mice, lung tissue was analysed for the reporter gene. It was possible to detect the transgene up to 21 days after injection. But in contrast to studies regarding MSC-trafficking after intravenous administration [4], presence of the injected cells in other organs was not consistent.
The retention of intravenous injected cells in the lung shortly after administration is often described; it is anticipated, that intravenous injected cells are initially retained in the lung and re-enter the circulation in a secondary step [39, 43]. This so-called first pass effect is the major drawback that has to be overcome in therapeutic approaches aiming to use intravenous injection of cells [39].

In the present study, recruitment of systemically administered MSC to the site of fracture healing was demonstrated by immuno-localization of EGFP-labelled - and thus injected - MSC at the margins of newly formed bone in the fracture callus at early and later healing time-points. The cells adopted a cuboidal shape that is typical for osteoblasts. The location of the cells as well as their phenotype suggests a partaking at the bone formation process. Interestingly, in transitions zones from cartilage to bone, positively stained cells were detected, but only very few cells were found in the cartilaginous part of the callus. This finding is corroborated by Devine et al. [28]. The reason for the absence of EGFP-positive cells in the cartilaginous part of the callus might be the avascularity of the tissue, but there are also fate decision studies giving hints that cartilage in the fracture callus might primarily be derived from the local periosteal progenitor cells, and thus no or little circulating cells or cells residing in the bone marrow are involved in cartilage formation [25, 26].

To investigate, if systemic administration of MSC improves fracture healing, µCT, biomechanical and histomorphometric analyses were performed. CT analyses revealed a slightly larger callus volume in animals treated with MSC, but this did not reach statistical significant difference. However, a significantly higher bone volume was evident in the osteotomy gap of mice treated with MSC compared to the vehicle-treated control. Both, the larger callus and bone volume are in accordance with literature, but the effects reported seem to be larger [48]. Biomechanical testing revealed no statistical significant differences in callus stiffness comparing MSC- and vehicle-treated animals. Granero-Moltó et al. describe improvement of the biomechanical properties of as early as 14 days after fracture in mice that received MSC in comparison to mice that received PBS only. They report significant increases in toughness and ultimate displacement, while stiffness was not significantly altered [48], as it is the case in this study. Indeed, mean callus stiffness seemed even to be reduced in the study of Granero-Moltó et al. [48].
Histomorphometric analyses revealed no statistically significant differences in callus composition, but 21 days after fracture, there is a trend evident towards more bone in mice treated with MSC, thus confirming µCT data. Discrepancies between data obtained by µCT and histomorphometry result form differences in the dimension. While µCT measures the whole 3-dimensional callus, in histomorphometry, 2-dimensional sections and thus “snap-shots” of the callus composition are assessed.

The immunomodulatroy action of systemically administered MSC reported by others [48] was not found in the present study. However, in house studies demonstrated that an isolated femur-fracture as it was applied here is unable to induce any considerable systemic inflammatory response even 6 h after osteotomy and that the initial inflammatory response is down-regulated to physiological levels within 24 h in rodents. To achieve considerable systemic inflammation, a second trauma is necessary [98]. However, it cannot be fully answered, if the applied MSC have an immunomodulatory effect, as earlier time-points after fracture would be necessary to investigate this.

Besides the use of primary MSC or pluripotent stromal cell lines, the use of more osteogenically primed cell lines like MC3T3-E1 for systemic therapy of bone defects is described [46]. Furthermore, genetically modified MSC that over-express the chemokine receptor CXCR-4 or insuline-like growth factor-1 (IGF-1) have been injected intravenously after fracture. Overexpression of CXCR4 markedly increased homing of the injected MSC to the fracture site; however, the authors did not investigate if the enhanced homing resulted in a better healing outcome compared to native MSC [48]. In comparison to native MSC, IGF-1 transgenic MSC markedly enhanced fracture healing, while application of native MSC did not result in markedly improvement compared to vehicle treatment [49].
Even if the use of pre-osteoblastic cell lines or genetically modified cells is feasible in pre-clinical animal models and allows the investigation of autocrine and paracrine mechanisms of cell action, it is no alternative for treatment of human patients, so other strategies have to be found to enhance fracture healing.

4.2 Local Application of Autogenic and Allogeneic Mesenchymal Stem Cells for Large Bone Defect Regeneration

Despite significant progress in the treatment of large bone defects, there is still the need for new therapeutic approaches. As mentioned in the introduction, autologous bone graft is still the gold standard for treating large bone defects, but the availability of autologous bone material is limited. Use of allogeneic bone material usually leads to inferior results, as allogeneic bone has less intrinsic osteogenic potential [111].
Recent advances were made in the filed of cell therapy. In a clinical study, percutaneous application of concentrated autologous bone marrow was effective in almost 90 % of treated non-unions. Furthermore, a positive correlation between progenitor cell number and outcome was drawn [57]. However, there was only a small cohort included into this study and large, randomized case-control studies on the use of autologous bone marrow or MSC to treat non-unions are missing so far.
In the present study, the efficacy of autologous and allogeneic human MSC to consolidate large bone defects in mice with a humanised immune system was

investigated for the fist time. Generally, MSC - especially human MSC - are described to be immunoprivileged in means of not inducing an adverse immunoreaction or being immunomodulatory [2, 3, 70, 86]. Due to these properties, a safe and effective use of MSC from non-related donors to treat non-healing fractures might be conceivable. The present results, however, indicate a higher efficacy of autologous cells, demonstrated by stronger staining for early osteogenic markers like Runx2 in the defect region and significantly higher amounts of newly formed bone compared to allogeneic cell treatment.
Literature regarding the issue of usability of allogeneic cell for bone regeneration is quite heterogeneous. In accordance with the present findings, allogeneic MSC were found to be inferior to autologous cells regarding bone formation when spray-coated in a fibrin-matrix onto the surface of massive bone tumour prostheses [24]. Furthermore, xenogeneic implantation of human MSC in segmental defects in rabbit radii or sheep tibiae resulted in inferior outcome compared to application of autologous MSC but no evidence for an inflammatory reaction was found [87, 88]. In contrast to these studies, others report equal but only little bone formation when applying autologous and allogeneic ovine MSC on PCL-scaffolds into segmental tibia defects in aged sheep [11]. Moreover, there are reports for an enhancement of bone regeneration by application of allogeneic MSC in critical-sized bone defects in rabbits [126] or in combination with biomaterial in long bone defects in dogs [6].

Staining for human CD8+ cells on day 3 revealed no invasion into the defect region or the cell-loaded collagen gel in autogenic treated mice, while there were positively stained cells at the interface of the surrounding soft tissue and the collagen gel in mice treated with allogeneic MSC. The same observation was true for day 10, where CD8+ cells were detected in the vicinity of the collagen gel after allogeneic treatment. T-cells and IFNγ were associated with inhibition of bone formation induced by allogeneic cells by Dighe et al. [30]. The authors implanted cells of a BALB/c derived bone marrow cell line into mouse models with differing severity of immune deficiency [30]. The cells were able to form bone nodules in immunocompetent syngeneic BALB/c mice or in immunocompromised animals lacking mature T and B cells and natural killer cell cytolytic function, but not in allogeneic immunocompetent C57BL/6 mice. Here, elevated numbers of T- and B-

cells and macrophages as well as higher levels of IFNγ in the implants were reported. Interestingly, the absence of T-cells in NCr nude mice was sufficient to enable bone growth in an otherwise allogeneic organism [30]. However, in the present study, first staining for human IFNγ revealed no positive results, suggesting other mechanisms being responsible for the inferior bone formation.

It is still unclear, how the implanted cells contribute to bone regeneration. On the one hand, they can provide trophic factors that influence host cells in a paracrine way, but on the other hand, a direct action of the locally implanted cells like matrix formation is possible. In the recent study, cells stained positive for human β2-microglobulin were found in the implanted gel in both, gels loaded with allogeneic and autogenic MSC on day 10 after implantation. After 35 days however, in the group that received autogenic MSCs, positively stained cells were only found in the marrow compartments in the regenerated bone, but bone itself did not stain positive for the human marker. In the allogeneic MSC treated group, cells of human origin were detected in the defect region in residues of the collagen gel. Generally, endochondral fracture healing is anticipated to recapitulate embryonic long bone development. Hence, it is anticipated that hypertrophic cartilage undergoes apoptosis and the lacunae are filled with host-derived cells. The absence of bone positive for human marker present here is in line with this hypothesis; however this finding does not exclude the possibility for a direct contribution. In a canine model, transplanted allogeneic cells could be detected in the defect region 4 weeks after implantation, but not after 8 weeks [6]. The authors suggest that the implanted cells differentiate into the osteoblast lineage first, then undergo apoptosis within 8 weeks after implantation and are replaced by host cells. In contrast to the present findings, a recent study using cartilaginous implants for treatment of large bone defects in mice reported trans-differentiation of donor-derived chondrocytes into bone rather than apoptosis of donor cells and replacement by host-derived cells [8]. Others also reported donor-derived bone formation after implanting hMSC-derived cartilage subcutaneously [104, 109]; however, the xenogeneic cartilaginous templates were implanted into immunodeficient mice. As stated previously, the absence of T-cells is sufficient to enable bone formation in a allogeneic setting [30], thus it would be interesting to repeat such a xenogeneic cartilage transplantation in immunocompetent models.

Taken together, the results of the present study demonstrated a beneficial effect of intravenously delivered MSC in fracture healing, shown by a significant increase in bone volume in the MSC-treated group relative to vehicle treatment, but there was no benefit in load-induced bone formation. Questions that remain to be answered regarding a systemic application of MSC include, whether the beneficial effect on fracture healing is a direct effect of the cells themselves or whether the cells secrete trophic factors that foster the potential of resident cells. Furthermore, it has to be addressed, whether the homing potential of MSC is solely dependent on CXCR4 expression or whether other molecules are able to recruit MSC in a similar way.

The results regarding local application of allogeneic or autogenic MSC for treatment of large bone defects or non-unions demonstrate superior action of autogenic MSC, shown by a higher expression of osteogenic markers on day 10 and an increased bone content on day 35 after implantation. Absence of staining for human markers in the regenerated bone suggests indirect action of the implanted MSC on bone formation; however to understand the underlying mechanisms, further studies are needed.

In conclusion, local application of MSC to regenerate bone seems to be more effective than a systemic approach. Local delivery of cells leads to an immediate increase of progenitors cell numbers to a super-physiological level and thus more pronounced cell-based effects are likely, while an increase in the progenitor cell number at the fracture site after systemic injection is unlikely, as the cell recruitment remains at a physiological level.

5 Summary

MSC are in focus for regenerative approaches for several decades now due to their high intrinsic differentiation potential towards the osteoblast lineage. Besides, MSC can secrete a broad spectrum of bioactive substances with regenerative and anti-inflammatory action. Due to these characteristics, MSC might be a interesting tool for treatment of impaired healing fractures or non-unions.

In the study presented here it was investigated whether systemically applied MSC can support bone formation I) under non-inflammatory conditions after mechanical loading and II) after an injury in form of an osteotomy in C57BL/6 wild-type mice. Furthermore, the question was addressed, if human MSC from allogeneic and autogenic sources are equally effective in consolidation of large bone defects in a mouse model with humanised immune system when implanted locally.

The results of the present study demonstrated a moderate beneficial effect of systemically administered MSC on fracture healing, shown by a significant increase in bone volume. The inject ed cells were detected at newly formed bone in the fracture callus on day 10 and 21 after osteotomy, thus confirming recruitment of the cells. In contrast to the finding in fracture healing, no injected cells were detected in newly formed bone after mechanical loading, suggesting lack of an appropriate migratory stimulus. Furthermore, no effect of the administered MSC was detected.

In treatment of non-unions and large bone defects, application of stem cells from allogeneic sources would solve the issue of limited availability of cells from autogenic sources. However, the results obtained in this study indicate an inferior efficacy of allogeneic MSC to regenerate bone in a critical sized bone defect in humanized mice compared to the application of autogenic MSC. In defects treated with autogenic MSC, significantly more bone was evident 35 days after implantation of the cells. There were no signs of fulminant inflammation in mice treated with allogeneic MSC, however more $CD8^+$ T-cells were detected by immunohistochemistry in this cohort.

Taken together, local application of MSC to regenerate bone seems to be more effective than a systemic approach. Local delivery of cells leads to an immediate increase of progenitors cell numbers to a super-physiological level and thus more pronounced cell-based effects are likely while an increase in the progenitor cell number at the fracture site after systemic injection is unlikely, as the cell recruitment remains at a physiological level.

6 References

1. Adams CI, Keating JF, Court-Brown CM: Cigarette smoking and open tibial fractures. Injury 32: 61-65 (2001)
2. Aggarwal S, Pittenger MF: Human mesenchymal stem cells modulate allogeneic immune cell responses. Blood 105: 1815-1822 (2005)
3. Akiyama K, Chen C, Wang D, Xu X, Qu C, Yamaza T, Cai T, Chen W, Sun L, Shi S: Mesenchymal-Stem-Cell-Induced Immunoregulation Involves FAS-Ligand-/FAS-Mediated T Cell Apoptosis. Cell Stem Cell 10: 544-555 (2012)
4. Allers C, Sierralta WD, Neubauer S, Rivera F, Minguell JJ, Conget PA: Dynamic of distribution of human bone marrow-derived mesenchymal stem cells after transplantation into adult unconditioned mice. Transplantation 78: 503-508 (2004)
5. Alm JJ, Koivu HM, Heino TJ, Hentunen TA, Laitinen S, Aro HT: Circulating plastic adherent mesenchymal stem cells in aged hip fracture patients. J Orthop Res 28: 1634-1642 (2010)
6. Arinzeh TL, Peter SJ, Archambault MP, van den Bos C, Gordon S, Kraus K, Smith A, Kadiyala S: Allogeneic Mesenchymal Stem Cells Regenerate Bone in a Critical-Sized Canine Segmental Defect. J Bone Joint Surg Am 85: 1927-1935 (2003)
7. Atesok K, Li R, Stewart DJ, Schemitsch EH: Endothelial progenitor cells promote fracture healing in a segmental bone defect model. J Orthop Res 28: 1007-1014 (2010)
8. Bahney CS, Hu DP, Taylor AJ, Ferro F, Britz HM, Hallgrimsson B, Johnstone B, Miclau T, Marcucio RS: Stem cell-derived endochondral cartilage stimulates bone healing by tissue transformation. J Bone Miner Res 29: 1269-1282 (2014)
9. Belema-Bedada F, Uchida S, Martire A, Kostin S, Braun T: Efficient homing of multipotent adult mesenchymal stem cells depends on FROUNT-mediated clustering of CCR2. Cell Stem Cell 2: 566-575 (2008)
10. Bernardo ME, Fibbe WE: Mesenchymal Stromal Cells: Sensors and Switchers of Inflammation. Cell Stem Cell 13: 392-402 (2013)
11. Berner A, Reichert JC, Woodruff MA, Saifzadeh S, Morris AJ, Epari DR, Nerlich M, Schuetz MA, Hutmacher DW: Autologous vs. allogenic mesenchymal progenitor cells for the reconstruction of critical sized segmental tibial bone defects in aged sheep. Acta Biomater 9: 7874-7884 (2013)
12. Bianco P, Riminucci M, Gronthos S, Robey PG: Bone Marrow Stromal Stem Cells: Nature, Biology, and Potential Applications. Stem Cells 19: 180-192 (2001)
13. Bishop JA, Palanca AA, Bellino MJ, Lowenberg DW: Assessment of compromised fracture healing. J Am Acad Orthop Surg 20: 273-282 (2012)
14. Blair HC: How the OC degrades bone. BioEssays 20: 837-846 (1998)
15. Bonewald LF, Johnson ML: Osteocytes, mechanosensing and Wnt signaling. Bone 42: 606-615 (2008)
16. Canalis E, Giustina A, Bilezikian JP: Mechanisms of anabolic therapies for osteoporosis. N Engl J Med 357: 905-916 (2007)

17. Caplan AI: Adult mesenchymal stem cells for tissue engineering versus regenerative medicine. J Cell Physiol 213: 341-347 (2007)
18. Caplan AI, Correa D: PDGF in bone formation and regeneration: New insights into a novel mechanism involving MSCs. J Orthop Res 29: 1795-1803 (2011)
19. Caplan AI, Correa D: The MSC: an injury drugstore. Cell Stem Cell 9: 11-15 (2011)
20. Carrero R, Cerrada I, Lledo E, Dopazo J, Garcia-Garcia F, Rubio MP, Trigueros C, Dorronsoro A, Ruiz-Sauri A, Montero JA, Sepulveda P: IL1beta induces mesenchymal stem cells migration and leucocyte chemotaxis through NF-kappaB. Stem Cell Rev 8: 905-916 (2012)
21. Ceradini DJ, Kulkarni AR, Callaghan MJ, Tepper OM, Bastidas N, Kleinman ME, Capla JM, Galiano RD, Levine JP, Gurtner GC: Progenitor cell trafficking is regulated by hypoxic gradients through HIF-1 induction of SDF-1. Nat Med 10: 858-864 (2004)
22. Chen JH, Liu C, You L, Simmons CA: Boning up on Wolff's Law: mechanical regulation of the cells that make and maintain bone. J Biomech 43: 108-118 (2010)
23. Claes L, Recknagel S, Ignatius A: Fracture healing under healthy and inflammatory conditions. Nat Rev Rheumatol 8: 133-143 (2012)
24. Coathup MJ, Kalia P, Konan S, Mirza K, Blunn GW: A comparison of allogeneic and autologous mesenchymal stromal cells and osteoprogenitor cells in augmenting bone formation around massive bone tumor prostheses. J Biomed Mater Res A 101: 2210-2218 (2013)
25. Colnot C, Huang S, Helms J: Analyzing the cellular contribution of bone marrow to fracture healing using bone marrow transplantation in mice. Biochem Biophys Res Commun 350: 557-561 (2006)
26. Colnot C: Skeletal cell fate decisions within periosteum and bone marrow during bone regeneration. J Bone Miner Res 24: 274-282 (2009)
27. da Silva Meirelles L, Caplan AI, Beyer Nardi N: In Search of the In Vivo Identity of Mesenchymal Stem Cells. Stem Cells 26: 2287-2299 (2008)
28. Devine MJ, Mierisch CM, Jang E, Anderson PC, Balian G: Transplanted bone marrow cells localize to fracture callus in a mouse model. J Orthop Res 20: 1232-1239 (2002)
29. Di Nicola M, Carlo-Stella C, Magni M, Milanesi M, Longoni PD, Matteucci P, Grisanti S, Gianni AM: Human bone marrow stromal cells suppress T-lymphocyte proliferation induced by cellular or nonspecific mitogenic stimuli. Blood 99: 3838-3843 (2002)
30. Dighe AS, Yang S, Madhu V, Balian G, Cui Q: Interferon gamma and T cells inhibit osteogenesis induced by allogeneic mesenchymal stromal cells. J Orthop Res 31: 227-234 (2013)
31. Dominici M, LeBlance K, Mueller I, Slaper-Cortenbach I, Marini F, Krause D, Deans R, Keating A, Prockop D, Horwitz E: Minimal criteria for defining multipotent mesenchymal stromal cells. The International Society for Cellular Therapy position statement. Cytotherapy 8: 315 - 317 (2006)
32. Duncan RL, Turner CH: Mechanotransduction and the functional response of bone to mechanical strain. Calcif Tissue Int 57: 344-358 (1995)
33. Eghbali-Fatourechi GZ, Lamsam J, Fraser D, Nagel D, Riggs BL, Khosla S: Circulating Osteoblast-Lineage Cells in Humans. N Engl J Med 352: 1959-1966 (2005)

34. Einhorn TA: Enhancement of fracture-healing. J Bone Joint Surg Am 77: 940-956 (1995)
35. Einhorn TA: The Cell and Molecular Biology of Fracture Healing. Clin Orthop Relat Res 355S: S7-S21 (1998)
36. Ezquer FE, Ezquer ME, Parrau DB, Carpio D, Yanez AJ, Conget PA: Systemic administration of multipotent mesenchymal stromal cells reverts hyperglycemia and prevents nephropathy in type 1 diabetic mice. Biol Blood Marrow Transplant 14: 631-640 (2008)
37. Feng X, McDonald JM: Disorders of bone remodeling. Annu Rev Pathol 6: 121-145 (2011)
38. Fiedler J, Etzel N, Brenner RE: To go or not to go: Migration of human mesenchymal progenitor cells stimulated by isoforms of PDGF. J Cell Biochem 93: 990-998 (2004)
39. Fischer UM, Harting MT, Jimenez F, Monzon-Posadas WO, Xue HS, Savitz SI, Laine GA, Cox CS: Pulmonary Passage is a Major Obstacle for Intravenous Stem Cell Delivery: The Pulmonary First-Pass Effect. Stem Cells Dev 18: 683-691 (2009)
40. Fox JM, Chamberlain G, Ashton BA, Middleton J: Recent advances into the understanding of mesenchymal stem cell trafficking. Brit J Haematol 137: 491-502 (2007)
41. Friedenstein AJ, Chailakhjan RK, Lalykina KS: The development of fibroblast colonies in monolayer cultures of guinea-pig bone marrow and spleen cells. Cell Tissue Kinet 3: 393-403 (1970)
42. Friedlaender GE, Perry CR, Cole JD, Cook SD, Cierny G, Muschler GF, Zych GA, Calhoun JH, LaForte AJ, Yin S: Osteogenic protein-1 (bone morphogenetic protein-7) in the treatment of tibial nonunions. J Bone Joint Surg Am 83-A Suppl 1: S151-158 (2001)
43. Gao J, Dennis JE, Muzic RF, Lundberg M, Caplan AI: The Dynamic in vivo Distribution of Bone Marrow-Derived Mesenchymal Stem Cells after Infusion. Cells Tissues Organs 169: 12-20 (2001)
44. Gerstenfeld LC, Cullinane DM, Barnes GL, Graves DT, Einhorn TA: Fracture healing as a post-natal developmental process: molecular, spatial, and temporal aspects of its regulation. J Cell Biochem 88: 873-884 (2003)
45. Giannoudis PV, Einhorn TA, Marsh D: Fracture healing: the diamond concept. Injury 38 Suppl 4: S3-6 (2007)
46. Gibon E, Batke B, Jawad MU, Fritton K, Rao A, Yao ZY, Biswal S, Gambhir SS, Goodman SB: MC3T3-E1 Osteoprogenitor Cells Systemically Migrate to a Bone Defect and Enhance Bone Healing. Tissue Eng Part A 18: 968-973 (2012)
47. Govender S, Csimma C, Genant HK, Valentin-Opran A, Amit Y, Arbel R, Aro H, Atar D, Bishay M, Borner MG, Chiron P, Choong P, Cinats J, Courtenay B, Feibel R, Geulette B, Gravel C, Haas N, Raschke M, Hammacher E, van der Velde D, Hardy P, Holt M, Josten C, Ketterl RL, Lindeque B, Lob G, Mathevon H, McCoy G, Marsh D, Miller R, Munting E, Oevre S, Nordsletten L, Patel A, Pohl A, Rennie W, Reynders P, Rommens PM, Rondia J, Rossouw WC, Daneel PJ, Ruff S, Ruter A, Santavirta S, Schildhauer TA, Gekle C, Schnettler R, Segal D, Seiler H, Snowdowne RB, Stapert J, Taglang G, Verdonk R, Vogels L, Weckbach A, Wentzensen A, Wisniewski T, Group BMPEiSfTTS: Recombinant human bone morphogenetic protein-2 for treatment of open tibial fractures: a

prospective, controlled, randomized study of four hundred and fifty patients. J Bone Joint Surg Am 84-A: 2123-2134 (2002)
48. Granero-Molto F, Weis JA, Miga MI, Landis B, Myers TJ, O'Rear L, Longobardi L, Jansen ED, Mortlock DP, Spagnoli A: Regenerative Effects of Transplanted Mesenchymal Stem Cells in Fracture Healing. Stem Cells 27: 1887-1898 (2009)
49. Granero-Molto F, Myers TJ, Weis JA, Longobardi L, Li T, Yan Y, Case N, Rubin J, Spagnoli A: Mesenchymal stem cells expressing insulin-like growth factor-I (MSCIGF) promote fracture healing and restore new bone formation in Irs1 knockout mice: analyses of MSCIGF autocrine and paracrine regenerative effects. Stem Cells 29: 1537-1548 (2011)
50. Gross TS, Poliachik SL, Prasad J, Bain SD: The effect of muscle dysfunction on bone mass and morphology. J Musculoskelet Neuronal Interact 10: 25-34 (2010)
51. Haapasalo H, Kontulainen S, Sievanen H, Kannus P, Jarvinen M, Vuori I: Exercise-induced bone gain is due to enlargement in bone size without a change in volumetric bone density: a peripheral quantitative computed tomography study of the upper arms of male tennis players. Bone 27: 351-357 (2000)
52. Harada S-i, Rodan GA: Control of osteoblast function and regulation of bone mass. Nature 423: 349 (2003)
53. Hare JM, Traverse JH, Henry TD, Dib N, Strumpf RK, Schulman SP, Gerstenblith G, DeMaria AN, Denktas AE, Gammon RS, Hermiller JB, Jr., Reisman MA, Schaer GL, Sherman W: A randomized, double-blind, placebo-controlled, dose-escalation study of intravenous adult human mesenchymal stem cells (prochymal) after acute myocardial infarction. J Am Coll Cardiol 54: 2277-2286 (2009)
54. Hauge EM, Qvesel D, Eriksen EF, Mosekilde L, Melsen F: Cancellous bone remodeling occurs in specialized compartments lined by cells expressing osteoblastic markers. J Bone Miner Res 16: 1575-1582 (2001)
55. Hayda RA, Brighton CT, Esterhai JL, Jr.: Pathophysiology of delayed healing. Clin Orthop Relat Res S31-40 (1998)
56. Healey JH, Zimmerman PA, McDonnell JM, Lane JM: Percutaneous bone marrow grafting of delayed union and nonunion in cancer patients. Clin Orthop Relat Res 256: 280-285 (1990)
57. Hernigou P, Poignard A, Beaujean F, Rouard H: Percutaneous Autologous Bone-Marrow Grafting for Nonunions. Influence of the Number and Concentration of Progenitor Cells. J Bone Joint Surg Am 87: 1430-1437 (2005)
58. Horwitz EM, Le Blanc K, Dominici M, Mueller I, Slaper-Cortenbach I, Marini FC, Deans RJ, Krause DS, Keating A: Clarification of the nomenclature for MSC: The International Society for Cellular Therapy position statement. Cytotherapy 7: 393-395 (2005)
59. Hosogane N, Huang Z, Rawlins BA, Liu X, Boachie-Adjei O, Boskey AL, Zhu W: Stromal derived factor-1 regulates bone morphogenetic protein 2-induced osteogenic differentiation of primary mesenchymal stem cells. Int J Biochem Cell Biol 42: 1132-1141 (2010)
60. Kebriaei P, Isola L, Bahceci E, Holland K, Rowley S, McGuirk J, Devetten M, Jansen J, Herzig R, Schuster M, Monroy R, Uberti J: Adult human mesenchymal stem cells added to corticosteroid therapy for the treatment

of acute graft-versus-host disease. Biol Blood Marrow Transplant 15: 804-811 (2009)
61. Kitaori T, Ito H, Schwarz EM, Tsutsumi R, Yoshitomi H, Oishi S, Nakano M, Fujii N, Nagasawa T, Nakamura T: Stromal cell-derived factor 1/CXCR4 signaling is critical for the recruitment of mesenchymal stem cells to the fracture site during skeletal repair in a mouse model. Arthritis Rheum 60: 813-823 (2009)
62. Knoferl MW, Liener UC, Seitz DH, Perl M, Bruckner UB, Kinzl L, Gebhard F: Cardiopulmonary, histological, and inflammatory alterations after lung contusion in a novel mouse model of blunt chest trauma. Shock 19: 519-525 (2003)
63. Kolar P, Schmidt-Bleek K, Schell H, Gaber T, Toben D, Schmidmaier G, Perka C, Buttgereit F, Duda GN: The early fracture hematoma and its potential role in fracture healing. Tissue Eng Part B Rev 16: 427-434 (2010)
64. Kolar P, Gaber T, Perka C, Duda GN, Buttgereit F: Human early fracture hematoma is characterized by inflammation and hypoxia. Clin Orthop Relat Res 469: 3118-3126 (2011)
65. Komatsu DE, Hadjiargyrou M: Activation of the transcription factor HIF-1 and its target genes, VEGF, HO-1, iNOS, during fracture repair. Bone 34: 680-688 (2004)
66. Kumagai K, Vasanji A, Drazba JA, Butler RS, Muschler GF: Circulating cells with osteogenic potential are physiologically mobilized into the fracture healing site in the parabiotic mice model. J Orthop Res 26: 165-175 (2008)
67. Kuznetsov SA, Mankani MH, Gronthos S, Satomura K, Bianco P, Robey PG: Circulating skeletal stem cells. J Cell Biol 153: 1133-1140 (2001)
68. LaVelle D: Dealyed union and nonunion of fracture. Mosby, St. Louis, S. (1998)
69. Le Blanc K, Samuelsson H, Gustafsson B, Remberger M, Sundberg B, Arvidson J, Ljungman P, Lonnies H, Nava S, Ringden O: Transplantation of mesenchymal stem cells to enhance engraftment of hematopoietic stem cells. Leukemia 21: 1733-1738 (2007)
70. LeBlanc K, Ringdén O: Immunomodulation by mesenchymal stem cells and clinical experience. J Intern Med 262: 509-525 (2007)
71. Lee KCL, Maxwell A, Lanyon LE: Validation of a Technique for Studying Functional Adaptation of the Mouse Ulna in Response to Mechanical Loading. Bone 31: 407-412 (2002)
72. Lee RH, Pulin AA, Seo MJ, Kota DJ, Ylostalo J, Larson BL, Semprun-Prieto L, Delafontaine P, Prockop DJ: Intravenous hMSCs improve myocardial infarction in mice because cells embolized in lung are activated to secrete the anti-inflammatory protein TSG-6. Cell Stem Cell 5: 54-63 (2009)
73. Lee S-W, Padmanabhan P, Ray P, Gambhir SS, Doyle T, Contag C, Goodman SB, Biswal S: Stem cell-mediated accelerated bone healing observed with in vivo molecular and small animal imaging technologies in a model of skeletal injury. J Orthop Res 27: 295-302 (2009)
74. Lieberman JR, Daluiski A, Einhorn TA: The role of growth factors in the repair of bone. Biology and clinical applications. J Bone Joint Surg Am 84-A: 1032-1044 (2002)
75. Liu Z, Li Y, Zhang ZG, Cui X, Cui Y, Lu M, Savant-Bhonsale S, Chopp M: Bone marrow stromal cells enhance inter- and intracortical axonal

connections after ischemic stroke in adult rats. J Cereb Blood Flow Metab 30: 1288-1295 (2010)
76. Mantila Roosa SM, Liu Y, Turner CH: Gene expression patterns in bone following mechanical loading. J Bone Miner Res 26: 100-112 (2011)
77. Marsell R, Einhorn TA: The biology of fracture healing. Injury 42: 551-555 (2011)
78. Matsuo K, Irie N: Osteoclast-osteoblast communication. Arch Biochem Biophys 473: 201-209 (2008)
79. McKibbin B: The biology of fracture healing in long bones. J Bone Joint Surg Br 60-B: 150-162 (1978)
80. Megas P: Classification of non-union. Injury 36 Suppl 4: S30-37 (2005)
81. Mercurio AD, Motta T, Green E, Noble G, Hart RT, Allen MJ: Effects of extensive circumferential periosteal stripping on the microstructure and mechanical properties of the murine femoral cortex. J Orthop Res 30: 561-568 (2012)
82. Meyerrose TE, De Ugarte DA, Hofling AA, Herrbrich PE, Cordonnier TD, Shultz LD, Eagon JC, Wirthlin L, Sands MS, Hedrick MA, Nolta JA: In vivo distribution of human adipose-derived mesenchymal stem cells in novel xenotransplantation models. Stem Cells 25: 220-227 (2007)
83. Mikuni-Takagaki Y: Mechanical responses and signal transduction pathways in stretched osteocytes. J Bone Miner Metab 17: 57-60 (1999)
84. Morgan EF, Mason ZD, Chien KB, Pfeiffer AJ, Barnes GL, Einhorn TA, Gerstenfeld LC: Micro-computed tomography assessment of fracture healing: relationships among callus structure, composition, and mechanical function. Bone 44: 335-344 (2009)
85. Mountziaris PM, Spicer PP, Kasper FK, Mikos AG: Harnessing and modulating inflammation in strategies for bone regeneration. Tissue Eng Part B Rev 17: 393-402 (2011)
86. Nauta AJ, Fibbe WE: Immunomodulatory properties of mesenchymal stromal cells. Blood 110: 3499-3506 (2007)
87. Niemeyer P, Schonberger TS, Hahn J, Kasten P, Fellenberg J, Suedkamp N, Mehlhorn AT, Milz S, Pearce S: Xenogenic transplantation of human mesenchymal stem cells in a critical size defect of the sheep tibia for bone regeneration. Tissue Eng Part A 16: 33-43 (2010)
88. Niemeyer P, Szalay K, Luginbuhl R, Sudkamp NP, Kasten P: Transplantation of human mesenchymal stem cells in a non-autogenous setting for bone regeneration in a rabbit critical-size defect model. Acta Biomater 6: 900-908 (2010)
89. Otsuru S, Tamai K, Yamazaki T, Yoshikawa H, Kaneda Y: Circulating bone marrow-derived osteoblast progenitor cells are recruited to the bone-forming site by the CXCR4/stromal cell-derived factor-1 pathway. Stem Cells 26: 223-234 (2008)
90. Pead MJ, Skerry TM, Lanyon LE: Direct transformation from quiescence to bone formation in the adult periosteum following a single brief period of bone loading. J Bone Miner Res 3: 647-656 (1988)
91. Phieffer LS, Goulet JA: Delayed unions of the tibia. Instr Course Lect 55: 389-401 (2006)
92. Ponte AL, Marais E, Gallay N, Langonne A, Delorme B, Herault O, Charbord P, Domenech J: The in vitro migration capacity of human bone

marrow mesenchymal stem cells: comparison of chemokine and growth factor chemotactic activities. Stem Cells 25: 1737-1745 (2007)
93. Prasad VK, Lucas KG, Kleiner GI, Talano JA, Jacobsohn D, Broadwater G, Monroy R, Kurtzberg J: Efficacy and safety of ex vivo cultured adult human mesenchymal stem cells (Prochymal) in pediatric patients with severe refractory acute graft-versus-host disease in a compassionate use study. Biol Blood Marrow Transplant 17: 534-541 (2011)
94. Prockop DJ: Two Negative Feedback Loops Place Mesenchymal Stem/Stromal Cells (MSCs) at the Center of Early Regulators of Inflammation. Stem Cells 31: 2042-2046 (2013)
95. Qi S, Wu D: Bone marrow-derived mesenchymal stem cells protect against cisplatin-induced acute kidney injury in rats by inhibiting cell apoptosis. Int J Mol Med 32: 1262-1272 (2013)
96. Raggatt LJ, Partridge NC: Cellular and molecular mechanisms of bone remodeling. J Biol Chem 285: 25103-25108 (2010)
97. Raikin SM, Landsman JC, Alexander VA, Froimson MI, Plaxton NA: Effect of nicotine on the rate and strength of long bone fracture healing. Clin Orthop Relat Res 231-237 (1998)
98. Recknagel S, Bindl R, Kurz J, Wehner T, Ehrnthaller C, Knoferl MW, Gebhard F, Huber-Lang M, Claes L, Ignatius A: Experimental blunt chest trauma impairs fracture healing in rats. J Orthop Res 29: 734-739 (2011)
99. Robling AG, Duijvelaar KM, Geevers JV, Ohashi N, Turner CH: Modulation of appositional and longitudinal bone growth in the rat ulna by applied static and dynamic force. Bone 29: 105-113 (2001)
100. Robling AG, Turner CH: Mechanical signaling for bone modeling and remodeling. Crit Rev Eukaryot Gene Expr 19: 319-338 (2009)
101. Roddy GW, Oh JY, Lee RH, Bartosh TJ, Ylostalo J, Coble K, Rosa RH, Jr., Prockop DJ: Action at a distance: systemically administered adult stem/progenitor cells (MSCs) reduce inflammatory damage to the cornea without engraftment and primarily by secretion of TNF-alpha stimulated gene/protein 6. Stem Cells 29: 1572-1579 (2011)
102. Röntgen V, Blakytny R, Matthys R, Landauer M, Wehner T, Göckelmann M, Jermendy P, Amling M, Schinke T, Claes L, Ignatius A: Fracture healing in mice under controlled rigid and flexible conditions using an adjustable external fixator. J Orthop Res 28: 1456-1462 (2010)
103. Rubin J, Murphy TC, Zhu L, Roy E, Nanes MS, Fan X: Mechanical strain differentially regulates endothelial nitric-oxide synthase and receptor activator of nuclear kappa B ligand expression via ERK1/2 MAPK. J Biol Chem 278: 34018-34025 (2003)
104. Sacchetti B, Funari A, Michienzi S, Di Cesare S, Piersanti S, Saggio I, Tagliafico E, Ferrari S, Robey PG, Riminucci M, Bianco P: Self-renewing osteoprogenitors in bone marrow sinusoids can organize a hematopoietic microenvironment. Cell 131: 324-336 (2007)
105. Santos A, Bakker AD, Klein-Nulend J: The role of osteocytes in bone mechanotransduction. Osteoporos Int 20: 1027-1031 (2009)
106. Sawakami K, Robling AG, Ai M, Pitner ND, Liu D, Warden SJ, Li J, Maye P, Rowe DW, Duncan RL, Warman ML, Turner CH: The Wnt co-receptor LRP5 is essential for skeletal mechanotransduction but not for the anabolic bone response to parathyroid hormone treatment. J Biol Chem 281: 23698-23711 (2006)

107. Schenk S, Mal N, Finan A, Zhang M, Kiedrowski M, Popovic Z, McCarthy PM, Penn MS: Monocyte chemotactic protein-3 is a myocardial mesenchymal stem cell homing factor. Stem Cells 25: 245-251 (2007)
108. Schindeler A, McDonald MM, Bokko P, Little DG: Bone remodeling during fracture repair: The cellular picture. Semin Cell Dev Biol 19: 459-466 (2008)
109. Scotti C, Tonnarelli B, Papadimitropoulos A, Scherberich A, Schaeren S, Schauerte A, Lopez-Rios J, Zeller R, Barbero A, Martin I: Recapitulation of endochondral bone formation using human adult mesenchymal stem cells as a paradigm for developmental engineering. Proc Natl Acad Sci U S A 107: 7251-7256 (2010)
110. Seeman E: Bone modeling and remodeling. Crit Rev Eukaryot Gene Expr 19: 219-233 (2009)
111. Sen MK, Miclau T: Autologous iliac crest bone graft: should it still be the gold standard for treating nonunions? Injury 38 Suppl 1: S75-80 (2007)
112. Shi S, Gronthos S: Perivascular niche of postnatal mesenchymal stem cells in human bone marrow and dental pulp. J Bone Miner Res 18: 696-704 (2003)
113. Shinohara K, Greenfield S, Pan H, Vasanji A, Kumagai K, Midura RJ, Kiedrowski M, Penn MS, Muschler GF: Stromal cell-derived factor-1 and monocyte chemotactic protein-3 improve recruitment of osteogenic cells into sites of musculoskeletal repair. J Orthop Res 29: 1064-1069 (2011)
114. Shoji T, Ii M, Mifune Y, Matsumoto T, Kawamoto A, Kwon SM, Kuroda T, Kuroda R, Kurosaka M, Asahara T: Local transplantation of human multipotent adipose-derived stem cells accelerates fracture healing via enhanced osteogenesis and angiogenesis. Lab Invest 90: 637-649 (2010)
115. Sievanen H: Immobilization and bone structure in humans. Arch Biochem Biophys 503: 146-152 (2010)
116. Starman JS, Bosse MJ, Cates CA, Norton HJ: Recombinant human bone morphogenetic protein-2 use in the off-label treatment of nonunions and acute fractures: A retrospective review. J Trauma Acute Care Surg 72: 676-681 (2012)
117. Steinhausen E, Glombitza M, Bohm HJ, Hax PM, Rixen D: [Non-unions : From diagnosis to healing]. Unfallchirurg 116: 633-649 (2013)
118. Teitelbaum SL: Bone Resorption by Osteoclasts. Science 289: (2000)
119. Thompson WR, Rubin CT, Rubin J: Mechanical regulation of signaling pathways in bone. Gene 503: 179-193 (2012)
120. Tosounidis T, Kontakis G, Nikolaou V, Papathanassopoulos A, Giannoudis PV: Fracture healing and bone repair: an update. Trauma 11: 145-156 (2009)
121. Toupadakis CA, Wong A, Genetos DC, Chung DJ, Murugesh D, Anderson MJ, Loots GG, Christiansen BA, Kapatkin AS, Yellowley CE: Long-term administration of AMD3100, an antagonist of SDF-1/CXCR4 signaling, alters fracture repair. J Orthop Res 30: 1853-1859 (2012)
122. Tuan RS, Boland G, Tuli R: Adult mesenchymal stem cells and cell-based tissue engineering. Arthritis Res Ther 5: 32-45 (2003)
123. Uhthoff HK, Jaworski ZF: Bone loss in response to long-term immobilisation. J Bone Joint Surg Br 60-B: 420-429 (1978)
124. Uhthoff HK, Sekaly G, Jaworski ZF: Effect of long-term nontraumatic immobilization on metaphyseal spongiosa in young adult and old beagle dogs. Clin Orthop Relat Res 278-283 (1985)

125. Visigalli D, Strangio A, Palmieri D, Manduca P: Hind limb unloading of mice modulates gene expression at the protein and mRNA level in mesenchymal bone cells. BMC Musculoskelet Disord 11: 147 (2010)
126. Wan C, He Q, Li G: Allogenic peripheral blood derived mesenchymal stem cells (MSCs) enhance bone regeneration in rabbit ulna critical-sized bone defect model. J Orthop Res 24: 610-618 (2006)
127. Wolff J: Das Gesetz der Transformation der Knochen. August Hirschwald, Berlin, S. (1892)
128. Wynn RF, Hart CA, Corradi-Perini C, O'Neill L, Evans CA, Wraith JE, Fairbairn LJ, Bellantuono I: A small proportion of mesenchymal stem cells strongly expresses functionally active CXCR4 receptor capable of promoting migration to bone marrow. Blood 104: 2643-2645 (2004)
129. Zeidan-Chulia F, Noda M: "Opening" the mesenchymal stem cell tool box. Eur J Dent 3: 240-249 (2009)

Acknowledgments

For reasons of data protection, the acknowledgments are not included in the online version.

Curriculum vitae

For reasons of data protection, the curriculum vitae is not included in the online version.